Durability of Adhesive Joints Subjected To Environmental Stress

by

Emmett P. O'Brien

Dissertation for Doctor of Philosophy

in

Chemical Engineering

Virginia Polytechnic Institute and State University

Blacksburg, Virginia 24060

Committee Chair: Thomas C. Ward

Committee Members:

Dr. Richey Davis

Dr. David Dillard

Dr. Eva Marand

Dr. Ravi Saraf

August 28, 2003

Key Words: polymer, adhesion, environmental degradation, epoxy, water, interface, durability, diffusion, shaft-loaded blister test, sub-critical crack growth, electrochemical impedance spectroscopy (EIS), dielectric spectroscopy, ink

Title: Durability of Adhesive Joints Subjected to Environmental Stress

Author: Emmett P. O'Brien

Abstract

Environmental stresses arising from temperature and moisture changes, and/or other aggressive fluid ingressions can degrade the mechanical properties of the adhesive, as well as the integrity of an adhesive interface with a substrate. Therefore such disruptions can significantly reduce the lifetime and durability of an adhesive joint.[1-4] In this research, the durability of certain epoxy adhesive joints and coatings were characterized using a fracture mechanics approach and also by constant frequency impedance spectroscopy.

The shaft-loaded blister test (SLBT) was utilized to measure the strain energy release rate (G) or adhesive fracture energy of a pressure sensitive adhesive tape. In this study, support for the value of the SLBT fracture mechanics approach was obtained. The SLBT was then used to investigate the effects of relative humidity on a model epoxy bonded to silicon oxide. Lastly, the effects of water and temperature on the adhesion of a commercial filled epoxy bonded to silicon oxide was characterized and interpreted.

A novel impedance sensor for investigating adhesion was developed in a collaborative effort between Virginia Tech and Hewlett-Packard. Utilizing the technique of constant frequency impedance spectroscopy, the distribution and transport of fluids at the interface of adhesive joints was measured. A broad spectrum of adhesives was tested. In addition, the effects of hygroscopic cycling on the durability of adhesive coatings were measured for the commercial filled epoxy using the device. Lastly, recommended modifications of the experimental set-up with the new sensor are proposed to improve the technique.

Acknowledgements

I would like to sincerely thank the following people. You have made the time at Virginia Tech well spent.

Dr. Ward, thank you for all your advice and support throughout the years (personal and professional) and giving me the opportunity to obtain a Ph.D. Thank you for giving our group the intellectual freedom and resources to pursue our own scientific interests. Thank you opportunity to attend numerous conferences, visit interesting places, and meet many important people in industry.

My committee members: Dr. Richey Davis, Dr. David A. Dillard, Dr. Eva Marand and Dr. Ravi Saraf for their tough questions, valuable suggestions and even more valuable time.

I would like to particularly thank David A. Dillard for teaching me about adhesives and adhesives research from a both a practical and fundamental standpoint. Thank you for guiding me through fracture mechanics and giving me the chance to earn a living at breaking things. Thank you also for introducing me to many people in the adhesives industry and for the opportunity to network in places like Yosemite, CA.

Thanks to all my friends and professional colleagues, especially Sandra Case who graduated right before me and showed me the way. Thanks to Amy Eichstadt for keeping my shoes. Thank you Rob Jensen for mentoring me in the embryonic stage of graduate school. Thanks to Dave Porter for teaching me to rig stuff up. Thanks to Taigyoo Park for introducing me to the SLBT. Corey Reed and Jeremy Lizotte for several championships. Thanks to everyone else: Kermit Kwan, Jennifer Robertson, Ojin Kwan, Chitra Subraminiam, Jaime Kalista, Hailing Yang, Kalpana Viswanathan, Ron Defelice, Mitch and Brenda Jackson, Mike Bortner, Eric Scribben, Scott Trenor, Jeremy Lizotte, Lee Williams, The Hunsuckers, Matt O'Sickey, Dave Godshall, Chris Robertson, Martha McCaann, Bradford Carmen, Doug Crowson, Anders DiBiccari, Holly Grammer, and Derek and Kelly.

I would like to thank every one in the Hewlett-Packard project including Dr. John G. Dillard, Dr. James. E. McGrath, Sumitra Subraminian, Johnny Yu, Sankar, Hitendra Singh, Shu Guo, David Xu, and Zuo Sun. I would like to thank the folks at Hewlett-Packard: Thank you Paul Reboa and Thomas Lindner for great project management and the numerous hefe-weizens. Thank you Marshall Field, Dan Pullen, and David Markel for design and production of the impedance sensors. Thank you Jim McKinnel for the numerous tutorials on electrical engineering. Thanks to Josh Smith for his big brain. Despite what people say, you are not really a jackass. Thanks to Brad Benson. Thanks to Ellen Chappell.

Thanks to the Center for Adhesive and Sealant Science: Dr James P. Wightman, Tammy Jo Hiner, and Linda Haney. Thanks to the Adhesive and Sealant Council and all the great people that I have met through the ASC. Great folks like Malinda Armstrong, Wendy Yanis, Dave Jackson, Rick Barry, Robert Lefelar, Jim Sorg, Kay Peters, Norman Pfeifer, Darrel Bryant, Rick Jihnston, Dwight Lynch The guys from Franklin International Adhesives: Mark Vrana, Larry Owen, Larry Gwin, Matt McGreery, Chusk Shuster, Dale and Evan Williams. The folks at Adhesives Research Incorporated: Ranjit Malik and Brian Harkins.

Thank you, Professor J. E. “Big Jim” McGrath for all your help, friendship, and nights at the Karaoke bar. Thanks to Professors Judy Riffle and Alan Esker. Thanks to the friends and folks at TA Instruments: Gary Mann and Steve Aubuchon. Thanks to the following SURPs: Kevin Doyle, Stefan Adreev, and Wes. Thank you Michael Vick and Corey Moore. Thanks to all my undergrad friends: Ray and Tammy, Kirrukk, Kollman, Hinett, Rich, Castello, Sujan, Maharshi, Guarav, Raindeer, Ceasar, Cindy, and Laura. Thanks to Millie Ryan, Laurie Good, and Esther Brann who were always so nice and willing to lend an ear or a cup of coffee. Thanks to Frank Cromer for hanging out and letting me use the sputter coater. Thanks to Jim Coulter for his electrical engineering tutorials and to Travis for helping with computer woes. Thanks to Al Shultz, Dr. Garth Wilkes, Diane Cannaday, Dr. William Conger, and Diane Patty. Thanks to the Physics Machine Shop rednecks: Scott, John, Melvin, Melvin’s cousin and even Fred (O.D.B.). Thanks to Jane for keeping our lab tidy. Thanks to the boys in Boulder, Co. and Aaron

Campbell. Thanks to people in Dart League, early morning tailgaters, and NASCAR people. Thanks to the late Francis VanDamme.

I have saved thanking the most important people in my life for last. I would like to thank my mom, Esperanza R. O'Brien for all her love and support over the years. Mom, I finally got a real job. Thank you, my wife, Kristen W. O'Brien for your love, good times, and improving my writing skills. Thank you to all of Kristen's family for being such great people and raising such a special woman.

Good luck to all the new graduate students, you will need it.

Table of Contents

Table of Figures

Table of Tables

1 INTRODUCTION

The lifetime of adhesive joints, coatings, and polymer composites can be significantly reduced by environmental stresses arising from temperature, moisture, and/or other aggressive fluids effects.[1-3] Although absorbed fluids may plasticize and induce relaxation in the adhesive and swell the adhesive, leading to a loss of mechanical properties, degradation of the *interface* is the primary reason for failure of many adhesive joints.[5] This work, will address one of the most fundamental problems in the adhesive and composite industry- the loss of adhesive bond strength resulting from fluid ingression at, or near, the interface.

Water is regarded by many to be an ubiquitous agent in the degradation process of adhesive bonds.[1-3] Moisture affects nearly all adhesive applications because water is always present in the atmosphere, is readily absorbed and is aggressive toward displacement of physical bonds. The presence of moisture and other aggressive fluids such as solvent and oils are a particular concern in more hostile conditions such as in offshore structures, submersibles, aircrafts, and highway infrastructures.[6] Adhesive bond degradation due to moisture and other fluids is also an enormous concern in the microelectronics components such as those found in ink jet printer cartridges. There are numerous epoxy interfaces found in the microelectronics components of ink jet printer cartridges. These adhesive interfaces lie in contact with aggressive inks at elevated temperatures (~ 60°C) and are also subject to thermal cycling. In general, the primary component of ink is water[7] but may also contain other aggressive agents such as salts, dyes, and surfactants. Moreover, inks can have a wide range of pH values which present special challenges.

Epoxies are also utilized in printed circuit boards (PCB) as the polymer matrix for the layered glass fiber composite structure. They are also used as encapsulates and underfill to increase the durability of the device by acting as both a structural reinforcement and as a sealant, providing a physical barrier to moisture and other fluids. A number of interfaces involving epoxies can be found in a typical ink jet printer, as mentioned above, such as the epoxy/passivation layer, epoxy/silicon dioxide, epoxy/metal, epoxy/PCB, and epoxy/solder interfaces. Over time, environmental factors can lead to failure at these epoxy/substrate interfaces. Adhesive bond degradation can also be accelerated by residual stresses formed by bonding materials with dissimilar coefficients of thermal expansion[8-11] as well as thermal and hygroscopic cycling.[12]

This current research investigates the effects of environmental degradation on adhesion by utilizing a fracture mechanics approach and constant frequency interfacial impedance spectroscopy. The shaft-loaded blister test (SLBT) was used to measure the applied strain energy release rate of a pressure sensitive adhesive and an epoxy adhesive. The SLBT was also modified for measuring the sub-critical fracture behavior of epoxy adhesives. A novel impedance sensor design was developed in a collaborative effort between Virginia Tech and Hewlett-Packard Co. Utilizing the technique of constant frequency impedance spectroscopy, the distribution and transport of fluids at the interface of adhesive joints was measured. We study the diffusion of fluids into several types of adhesives and also use the technique to investigate the effects of hygroscopic cycling.

2 BACKGROUND ON ENVIRONMENTAL DEGRADATION OF ADHESIVE JOINTS AND COATINGS

Water is typically regarded to be ubiquitous in the degradation processes of many adhesive joints and coatings.[1-3,13] Water may plasticize and induce relaxation in the adhesive[14], swell the adhesive, and therefore degrade the mechanical properties of the adhesive. Water can also lead unwanted chemical reactions in the adhesive[15] as well as the formation of cracks and crazes.[16,17] In most incidences, eventual degradation of the interface is the primary reason for failure of an adhesive joint.[5] This literature review surveys the general trends in environmental failure of adhesives but will focus largely on the effects of water, since water is the major component of the environmental exposure of interest here.

2.1 Factors That Influence Water Transport and Subsequent Adhesion Loss

The basic factors which affect the rate of water transport and the corresponding loss of adhesion in coatings are listed by Leidheiser and Funke [18] as:

1. time of exposure
2. effect of the substrate
3. effects of type of coating
4. effect of temperature

From the work of Leidhesiser and Funke and from a survey of the literature regarding environmental degradation of adhesives it is clear that there are some general trends. However, these trends are far from conclusive given the diversity of adhesive systems (adhesive, substrate,

and interface) and exposure conditions (temperature and fluid), and the possible interactions among the parameters.

This above list is incomplete in that the stress level, cyclic loading, cyclic temperature, and cyclic fluid exposure are not included. In addition, if this list is expanded to encompass all relevant fluids, then chemical factors (including but not limited to) such as acidity or basicity, solubility, vapor pressure, and composition should also be of concern.

2.2 General Trends Regarding Loss of Adhesion

In general, the rate of loss of adhesion of thin films to a substrate is dependent upon the rate at which water permeates through the coating to the interface.[18] However, there are many cases where no relationship is observed between the permeation and loss of adhesion. In these instances we would expect the time to failure to be greater than the time for saturation of the adhesive. Gao and Weitsman studied composites exposed to sea water for three years and showed that the time of exposure and durability were related.[19] Under such prolonged conditions it is likely that adhesive degradation is a result of a slowly progressing chemical reaction in the bulk adhesive and/or interface.[6] In this situation, the interfacial chemistry is controlled by the adhesive, substrate, and surface preparation with the latter two playing an important role in the durability of the adhesive joint.[18,20] In general, the substrate has only a nominal effect on the permeation of water. However, there are cases where differences were detected in the permeability, as well as the measured mass uptake, between free-standing non-bonded specimens and adhered films. In general, as the temperature is increased, adhesion loss occurs more rapidly (also see ref 3). There may be cases where evaporative loss and an increase in fracture toughness of the bulk adhesive may offset the effect of temperature. With this brief background in mind, it is clear that there is a broad range of behavior regarding adhesive durability. Furthermore, there

are few generalizations regarding adhesive behavior with the exception that increasing the temperature tends to speeds up adhesion loss.

2.3 Hypothesis and Mechanism for Loss of Adhesion by Water

Leidheiser and Funke have hypothesized that the debonding process occurs by the following: [18]

1. Formation at the substrate/adhesive interface of a continuous or discontinuous water film several to many molecular layers in thickness.

2. Water moving through the adhesive by diffusion through the polymer matrix or through capillaries or pores in the adhesive.

3. A driving force for directional water transport through the coating to the interface by diffusion (under a concentration gradient). Osmotic force, temperature differences and chemisorption or physisorption at the interface lead to accumulation of water or fluids at the interface.

4. Water accumulation at the interface is attributable to the presence of non-bonded areas.

5. Local water volume growing laterally by the continued condensation of water molecules under driving forces outlined in (3). Lateral growth is permitted by the stresses caused by water condensation.

Although the process and mechanisms of adhesive failure by exposure to moisture and temperature are complex, the general hypothesis proposed by Leidheiser and Funke can adequately describe many adhesive failures. Details of each mechanism follow.

2.3.1 Water Accumulation at the Interface

There is a great body of evidence supporting the accumulation of water at the interface/surface.[18] The most convincing are based on absorption studies on metal oxides, where it was noted that

there is strong dependence on the amount of absorbed water and relative humidity. Funke and Haagen noted that coatings absorb more water than non-bonded films due to significant condensation at the interface.[21] Nguyen *et al*. and Linnossier *et al.* observed accumulated water at the interface of coatings bonded to SiO_2-Si substrates utilizing Fourier transform infrared-multiple internal reflection (FTIR-MIR).[3,22] Bowden and Throssell [4] found that on aluminum, iron, and SiO_2 surfaces, these layer can be up to 20 molecular layers thick at ambient temperatures and humidity. Takahashi used ac impedance spectroscopy to show that at a relative humidity of 80% the interfacial capacitance increased abruptly, suggesting the formation of water clusters in the bulk and at the interfacial region.[23,24] Using neutron reflectivity, Wu et al. measured the concentration of D_2O at a polyimide-silicon wafer interface and found that the deuterated water concentration at the interface was 17% (by volume) compared to 2-3% in the bulk polyimide adhesive.[25] Kent et al. used neutron reflectivity to study the absorption of water at a molybdenum/polyurethane interface.[26] They observed a large concentration (> 80%) of deuterated water at the interface attributable to debonding. Kent and co-workers also employed neutron reflectivity to investigate water absorption at the interface between an bisphenol-A epoxy and silicon surface modified with a silane coupling agents (SCA).[27,28] An excess in the concentration of D_2O at the interface compared to the bulk adhesive was noted, as well as a gradient in the moisture content at the interface. They also detected changes in the moisture absorption behavior of the epoxy adhesive associated with the presence of the SCA. The discontinuous distribution of water is evident according to Leidheiser and Funke by the presence of small isolated water-filled blisters and can be attributed to the heterogeneous morphology of the substrate and adhesive (on a local scale.). Blistering will be discussed in greater detail later.

2.3.2 The Heterogeneous Nature of Adhesive Bond: Water Transport and Accumulation

In addition to water transport by diffusion, water can migrate to the interface through pinholes, pores, defects, and local inhomogeneities in the adhesive.[3] Water transport by diffusion is discussed in more detail in Section 2.5. Inhomogeneities or non-bonded areas may be present at the interface. These areas can speed up the transport of water and serve as sites for the accumulation of water.[18] Inhomogeneities have been detected in the crosslink density of coatings using selective resistance and hardness measurements.[29-31] According to DC resistance measurements, the defect size of poor cross-linked areas in composites is in the range of 50-500 nm.[31] Microscopy has shown the presence of regions of high density polymer separated by narrow boundary regions of lower molecular weight material.[32] Macroscopic voids have also been found in epoxy adhesives by Maxwell and Pethrick [33] as well as Kong [34]. The presence of fillers also affects the transport of water. For some adhesive systems, the addition of fillers has reduced the adhesive's affinity for water; in other cases, fillers and pigments provided a transport pathway for water to migrate.[35] Of particular value for adhesives used in microelectronics applications, adding fillers can also improve the bulk properties of the adhesives by reducing the coefficient of thermal expansion, increasing the modulus, and creating a tortuous path for crack propagation.[36]

2.3.3 Osmotic Forces and Lateral Growth by Continued Condensation and Blistering

The rate of transport of water can be increased as the osmotic pressure between the interface and outside environment increases.[18] Osmotic forces are a result in the difference in the chemical potential between the outside liquid media and liquid at the interface, and is the principal

mechansim for blistering in coatings.[3,37] Osmotic pressure and subsequent blistering is promoted by the presence of hydrophilic sites or salts which decreases the equilibrium vapor pressure and promotes condensation.[38] Early work by Kittleberger and Elm showed that water penetration through an alkyd coating was a function of osmotic pressure.[39] Work by Perera and Heertjes, and Kinsella and Mayne showed for a variety of polymer coatings that water diffused by an osmotic pressure gradient. [29,40] Van der Meer-Lerk and Heertjes observed that even if these differences in activity were small, blisters would continue to grow, the implication being that even minute amounts of contaminants at the surface can result in blistering. [41] The formation of water clusters can accelerate the blistering process by absorbing ionic species from the adhesive or substrate, further increasing osmotic pressure.[37]

2.3.4 Physisorption of Water at the Interface

It is accepted that when water reaches the interface between an adhesive and an untreated high-energy substrate, the adhesive bonds attributable to secondary molecular interactions (van der Waals, hydrogen), are disrupted immediately.[3] Furthermore, the work of adhesion between the polymer and a high energy substrate, in the presence of water, is negative. In other words, the force between the two adherends becomes repulsive. However, it should be noted that when covalent bonding, interdiffusion, and/or mechanical interlocking are present, the work of adhesion can not be used to explain adhesive failure.

2.4 Methods to Increase the Lifetime of Adhesive Bonds

From the above evidence, if adhesion forces are attributable to only secondary or van der Waals forces, then adhesion strength will be poor in the presence of water. Moreover, the problem is

exacerbated by temperature. Two general strategies are suggested to improve the durability of adhesive joints:[13]

1. Preventing water from reaching the interface in sufficient quantity
2. Improving the durability of the interface itself

Selection of the appropriate adhesive or chemical modification of the adhesive can reduce the permeability and diffusivity of water into the adhesive joint. Because water transport in the bulk is strongly related to free volume, the absorption of water may be reduced by introducing crystallinity or by increasing the crosslink density, both of which lower free volume. Water permeation can be reduced by decreasing the polymer's affinity for water; for example, by reduction of the number of polar or hydrophilic groups. In addition, water absorption may be reduced by adding fillers to the polymer which may effectively act as a barrier to moisture intrusion.

For metals substrates, inhibitors may be added to retard the hydration of oxide layers at the adhesive-substrate interface. For glass and metals, silane coupling agents are used as a primer, forming a hydrophobic poly(siloxane) network on the surface of the substrate.[42] An exceptional review of the role of silane coupling agents on epoxy adhesion can be found in the work of Whittle et al.[43] As referenced earlier, moisture resistance can be improved if covalent bonds, interdiffusion, and/or mechanical interlocking are present at the interface. Surface roughening can also increase the surface energy of the substrate, providing a longer path of diffusion for the water to travel along the interface, and promoting mechanical interlocking in some cases. Following the arguments of Leidheiser and Funke, to improve adhesive durability, a suitable strategy would be to reduce the number of non-bonded areas, which may act as a nucleus for further debonding. This is supported by a conversation with Professor Henry

Shreiber.[44] He suggested that to improve adhesive durability, the number of covalent bonds at the interface should be increased. This would effectively reduce the space at the interface for water to reside, as well as require a hydrolysis reaction for debonding. Limiting the presence of water at the interface slows down the process of corrosion, hydrolysis, and other mechanisms of joint degradation. Therefore we might expect a correlation between dry adhesion and the durability of adhesive joints in aggressive environments.

2.5 Diffusion in Polymers and Adhesive Joints

2.5.1 Fickian Diffusion

The diffusion of a penetrant (either a fluid or gas) through many materials can be modeled using Fick's second law of diffusion (typically referred to as simply Fick's Law):

Equation 2-1
$$\frac{\partial C}{\partial t} = D\frac{\partial^2 C}{\partial x^2}$$

where C is the concentration (g cm^{-3}) of penetrant or absorbed fluid, t is time (seconds) and x is position (cm) and D is the diffusion coefficient or diffusivity of the penetrant in the polymer.[45] The diffusion coefficient is characteristic of the rate of a penetrant transport for a specific penetrant-host material combination. Fickian diffusion is an ideal case that assumes the absorption process is independent of concentration and temperature. The diffusion takes place by random jumps (or random walk) of the penetrant molecule in the polymer with little interaction with the polymer matrix. In this case, the rate of relaxation of the polymer matrix is faster than the rate of penetrant diffusion. Fickian diffusion is more common in rubbery materials that have flexibility and mobility, larger free volumes, and have relatively fast relaxation times. In glassy materials the rate of relaxation of the host matrix is much slower than the absorption process. In

this case, deviation from ideal Fickian diffusion, or even "non-Fickian" diffusion (see below) may occur and Fick's second law is no longer applicable.

The most common method for characterizing absorption processes and calculating the diffusion coefficient is by a mass-uptake experiment. In most mass-uptake experiments, the mass-gain of penetrant as a function of exposure time of a thin free-standing film is measured using a mass balance. These data can then be fit to Fick's second law provided an equilibrium mass-uptake value is reached. Leidheiser and Funke [18] and Nguyen *et al.* [3] point out that for coatings and composite materials, more relevant mass-uptake results should use the coating or composite itself, rather than a free-standing film of the same material.

For a free polymer film of thickness $2L$ with a uniform initial concentration (C_0) and the surface is kept at a uniform concentration (C_S), the solution to Fick's Law in terms of concentration is [45]:

Equation 2-2
$$\frac{C(x,t)-C_0}{C_S-C_0}=1-\frac{4}{\pi}\sum_{n=0}^{\infty}\frac{(-1)^n}{2n+1}\exp\left[-\frac{D(2n+1)^2\pi^2 t}{4L^2}\right]\cos\left(\frac{(2n+1)\pi x}{2L}\right)$$

where $C(x,t)$ is the concentration of penetrant in the polymer at any time t and distance x. The solution to Fick's Law can be put in terms of the average mass of the substance diffusing in the polymer by integrating Equation 2-2 across the thickness $2L$ of the free polymer film.[46] Note that the expression for the concentration as a function time and distance for diffusion in a bilayer film can be found in the work of McKnight and Gillespie.[47]

The relative mass uptake M_t/M_∞ can be expressed as:

Equation 2-3
$$\frac{M_t}{M_\infty}=1-\frac{8}{\pi^2}\sum_{n=0}^{\infty}\frac{1}{(2n+1)^2}\exp\left[-\frac{D(2n+1)^2\pi^2 t}{4L^2}\right]$$

Where M_t is the mass of absorbed fluid at any time t and M_∞ is the equilibrium or final mass of absorbed fluid. The relative mass uptake is the scaled average water concentration; a fraction ranging from zero at $t = 0$, to one at $t = \infty$.

2.5.2 Non-Fickian Diffusion

It is not unexpected to observe non-Fickian behavior with glassy polymers. A prominent feature of non-Fickian diffusion is that there is no characteristic equilibrium (long time) mass-uptake value (M_∞). There are two general cases of non-Fickian diffusion: two-stage absorption and Case II diffusion. Two-stage absorption is typical for polymers that exhibit structural relaxation induced by the adsorption of the penetrant.[48] In this case, the relative mass uptake curve is composed of two stages, an initial fast Fickian absorption, followed by a slow non-Fickian absorption that on the typical time scale of an experiment, never asymptotes. In some cases, such as in epoxies and other polymers, water will absorb in two stages, but for different reasons than mentioned previously: the first stage entails an interaction with a specific binding site (sometimes referred to as bound water), followed by a second stage association in a liquid like structure (sometimes referred to as non-bound water).[49] Case II is another form of non-Fickian diffusion characterized by a step-like concentration profile with a sharp diffusion front. In this model, the diffusion occurs faster in the swollen material and the relative mass uptake appears linear with time. Note that for Fickian diffusion, the relative mass uptake appears linear with the square-root of time. Solutions of the relative mass uptake as a function of time for two-stage absorption [48,50,51] as well as Case II [52] can be found in the literature.

If however, dramatic changes in the relative mass uptake are observed, then this indicative of damage to the adhesive. A large mass loss may often be attributable to leaching of

the adhesive. A large mass gain in composites or adhesive coatings would be indicative of fluid accumulation at the interface of the matrix, the filler or between the adhesive and substrate.

Although Fickian behavior is not typically observed in glassy materials, there are cases where glassy polymers behave like porous materials and take on Fickian behavior - diffusion of penetrant into free spaces in the polymer being responsible.[46] Two stage absorption has also been observed in epoxies presumably due to the formation of microcracks and crazes.[1,2]

2.5.3 Interfacial Diffusion and Diffusion in Adhesive Joints

A review of the available literature on interfacial diffusion reveals that, in general, the rate of interfacial diffusion, or the presence of fluid at the interface becomes more critical to the lifetime of the adhesive joint as the strength of the adhesive interface decreases. For adhesives bonded to high energy substrates, and in the presence of water, this is especially true. For "weak" interfaces, where secondary bonds forces dominate the adhesion, failure occurs almost immediately as water contacts the interface. It is possible for water to be present in the bulk and interface of the adhesive yet the integrity of the adhesive bond can be preserved if the interface is "strong". This is the case where covalent bonds are present. For strong interfaces, the role of interfacial diffusion becomes less important and the rate limiting step for failure becomes the chemical reaction at the interface. Davis *et al*., utilizing the technique of electrochemical impedance spectroscopy, observed this behavior in epoxies bonded to aluminum with surface preparations that resulted in either a weak or strong interface.[18,20] They observed that the rate of crack growth was slow for strong interfaces, but for weak interfaces crack growth was detected almost immediately as moisture appeared at the interface and resulted in a fast rate of crack growth.

Diffusion into adhesive joints was studied by Zanni-Deffarges and Shanahan by comparing the calculated diffusion rates between non-bonded adhesive specimens and bonded adhesive joints.[53] They observed that the diffusion coefficient of the adhesive joint was greater than that of the bulk adhesive. They conclude that the diffusion rate at the interface was greater than in the bulk adhesive and hypothesize the phenomena of "capillary diffusion" where (at the diffusion front) the higher surface energy of the dry adhesive effectively "pulls" moisture along the interface. Furthermore, they mention the effect of adhesive shrinkage at a constrained interface may result in dilation of the adhesive near the interface.

Nyugen *et al*. [54] and Linossier *et al*. [22] have also compared diffusion rates between bulk specimens and adhesive joints using Fourier transform infrared spectroscopy in the multiple internal reflection mode (FTIR-MIR). They detected significant diffusion at the interface for poorly adhered adhesive systems where adhesion forces are governed by secondary interactions.

Vine *et al*. [55] studied the moisture uptake of an epoxy bonded to aluminum adherends with various surface treatments. They observed faster diffusion in three-layer sandwich specimens than predicted, based on mass-uptake experiments performed on bulk diffusion specimens. They attributed this behavior to the presence of micro-cavities in the adhesive layer and site work by Nyugen *et al*., Zanni-Deffarges and Shanahan, and Linnosier *et al*. as evidence for diffusion at the interface as possibly faster than in the bulk.

The label "interfacial impedance spectroscopy" was coined by Takahashi and Sullivan to refer to impedance measurements made at the surface or interfacial region of a coated substrate.[23,24] They detected changes in the frequency dependent complex impedance (Z^*) associated with the accumulation of moisture at the interface resulting from adhesive debonding.

They estimate that the size of the aqueous film to be at least 1 nm thick. However, from their studies, information about the rate of moisture absorption at the interface was very limited.

2.5.4 Diffusion in Epoxies

2.5.4.1 Moisture Diffusion in Epoxies

Moisture diffusion in epoxies and other polymers is associated to the availability of molecular-sized holes within the polymer and the polymer-water affinity.[56] Water molecules in epoxies and polymers can also be classified as either unbound or bound as discussed above.[56] Unbound water resides in the free-volume of the polymer and this does not cause dimensional changes in the polymer. Bound water interacts with the polymer via hydrogen bonding and can result in swelling and plasticization of the polymer. Therefore, unbound water is associated with the first stage of two-step diffusion and bound water is associated with the non-Fickian second stage of two-step diffusion.

It is generally accepted that moisture diffusion in many polymers is strongly correlated to the free volume.[57,58] This appears to not be the case in epoxies. Soles and coworkers found in amine cured resins no correlation between the topology (nanovoid size and total volume of nanovoids) and moisture transport.[59] Although they found that moisture traveled through the epoxy and gained access to hydrogen bonds via the nanovoids, it appears the nanopores do not appear to be rate limiting. They point to local scale motions in the glassy state associated with the β–relaxation as the rate-limiting step for moisture transport.

2.5.4.2 Water as a Plasticizer

A great deal of information has been accumulated on the role of water in epoxies, specifically the diglycidyl ether of bisphenol A (DGEBA). In general, water can be viewed as “an efficient

homogeneous plasticizer that depresses the glass transition of the polymer".[60] However, given the highly polar nature of water, plasticization of water can not be treated as a simple superposition of the individual response of the polymer matrix and diluent. Controversy surrounds the nature of site specific interactions between the absorbed water and the hydrogen bonds of the host epoxy matrix. Banks and Ellis proposed that plasticization is attributable to an increase in segmental motion and the disruption of hydrogen bonding network in the epoxy.[61] Jelinski *et al*. have shown the contrary using NMR; while recognizing site specific interactions, at room temperature there is likely no disruption of the hydrogen-bonding network, and that water acts simply as a plasticizer.[62] Furthermore, at ambient temperatures and above the average thermal energy of the system can exceed the energy due to local polarization, reducing the likelihood of site-specific interactions.[60] Recently, additional NMR work by Luo and co-workers have shown that, although moisture reduces the glass transition temperature of epoxies, the presence of moisture has no effect on polymer mobility at temperatures below the glass transition temperature.[63]

3 ADHESIVE STUDIES USING THE SHAFT-LOADED BLISTER TEST

3.1 Introduction

The shaft-loaded blister test (SLBT) was used to characterize the strain energy release rate (also commonly referred to as the adhesive fracture energy), G, of adhesive coatings. This research is divided into the following sections:

1. Measuring the applied strain energy release rate of a pressure sensitive adhesive tape and investigating the fracture mechanics model.[64]

2. Measuring the applied strain energy release rate of a model epoxy[36] bonded to quartz as function of relative humidity.

3. Adapting the SLBT for sub-critical fracture testing. The sub-critical fracture behavior of the model epoxy bonded to silicon wafers substrates as a function of relative humidity was measured. The sub-critical fracture behavior of a commercial filled epoxy (L4) bonded to silicon wafers in water as a function of temperature was also investigated.

3.2 Strain Energy Release Rates of a Pressure Sensitive Adhesive Tape Measured by the Shaft-Loaded Blister Test

(*The Journal of Adhesion*, 79: 69-97, 2003)

3.2.1 Abstract

The elastic solution to the shaft-loaded blister test (SLBT) was adopted to measure the applied strain energy release rate (G) of Kapton® pressure sensitive adhesive (PSA) tape bonded to a rigid substrate. The substrates used were either aluminum or Teflon®, a high-energy surface and low-energy surface, respectively. The values of G were calculated from three different equations: (1) load-based, (2) hybrid, and (3) displacement-based. An experimental compliance calibration was utilized to measure the film's effective tensile rigidity $(Eh)_{\text{eff}}$, the results of which are presented in an appendix. Plastic deformation at the contact area of the shaft tip and adhesive results in an overestimated displacement (w_0) (relative to the elastic model) leading to disagreement among the values of G calculated. Estimation of the effective membrane stress in the film, (N_{eff}), as well as the reasonable agreement between the value of (Eh) determined from a stress-strain experiment and the compliance calibration suggest that, in spite of the plastic deformation, the assumption of linear elasticity in the crack growth region, and hence the validity of the model, is reasonable. The compliance calibration has been shown to improve the agreement among the values of G calculated from the three equations. Using the load-based equation, the assumed "correct" value of G may be obtained for a thin adhesive coating independent of the film's stiffness even in the presence of plastic deformation at the shaft tip. Comparing the value of G obtained by a pull-off test and the 90° peel test for a single ply indicates that the value of G obtained by the SLBT is of reasonable magnitude, being less than

that obtained by the more firmly established pull-off test, and also that undesirable plastic deformation is reduced relative to the 90° peel test. An experimental configuration for studying the effects of liquids on the fracture energy has been demonstrated for the SLBT. This study indicates that the SLBT is an attractive and convenient test method for measuring the strain energy release rate of adhesive films, because of the insensitivity of the load-based equation to the coating stiffness, plus the independence of the value of *G* on the plastic deformation at the shaft tip, and the reduced plastic deformation at the crack front relative to the 90° peel.

Key words: strain energy release rate, pressure sensitive adhesive tapes, shaft-loaded blister test, pull-off test, peel test, plastic deformation, environmental degradation, Kapton®

3.2.2 Introduction to Adhesive Testing of Thin Coatings

3.2.2.1 The Peel Test and Pull-off Test

Measuring the adhesion of many important thin coatings is difficult given their small load-bearing capacity, associated with the thinness, and their relatively strong adhesion.[65] These conditions often lead to the film rupturing before debonding can occur. Even if film rupturing is absent and delamination is successful, significant film plastic deformation may result. In this case, calculations of the fracture toughness of the adhesive bond, or the applied strain energy release rate (*G*), may not reflect the intrinsic adhesion strength due to the additional energy consumed by the bending and stretching of the adhesive coating. For example, Kim *et al* has reported that measured peel forces may be one hundred times greater than the actual adhesion strength.[66]

Thin adhesive coatings are commonly and conveniently tested using the peel test. For a linear elastic coating of large tensile stiffness and small bending stiffness, the strain energy release rate can be expressed as follows [67]:

Equation 3-1
$$G = \frac{P}{b}(1 - \cos\theta)$$

where b is the width of the film, P is the load, and θ is the angle between the peel arm and the substrate. In practice, the peel force also depends on plastic dissipation within the coating, which is a function of the angle (or geometry) and stiffness and/or thickness of the peel arm along with the resulting stresses generated during bending and stretching the film. As a consequence, Equation 3-1 has no utility beyond comparing the adhesion of nominally identical films loaded in identical fashion.[68] Gent and Kaang have observed higher strain energy release rates obtained from the 180° peel test relative to the 90° peel test due to larger bending stresses.[69] Conversely, at small peel angles significant energy is stored due to the tensile stresses and stretching of the film. Gent and Kaang suggest using an angle of 45° and limiting the tensile strain to below 10-15%; under their conditions, less than a 20% increase in the peel force resulted compared to the extrapolated intrinsic adhesive strength.

Film rupture during peel testing can occur not only from the high stresses generated but also from the use of mechanical grips. A typical solution is to employ a backing or reinforcement layer to strengthen the adhesive coating; however, the additional reinforcement can change the stiffness of the peel arm and the subsequent peel force. Gent and Hamed showed that for very thin films of Mylar®, which yield substantially during peeling, as the adhesive coating thickness increased, the peel force also rises due to an increase in the strain energy.[70] However, a further increase in the thickness showed that the peel forces were reduced as the stiffness of the film

increased. This latter effect was attributable to an increase in film yield stress, and a reduction in bending stresses, which is consistent with what was shown by Kim *et al*.[66] A critical thickness was observed beyond which no further change in the peel force was observed as the thickness was increased.

Given that the peel force and corresponding value of *G* depend on the energy consumed during plastic deformation of the adhesive, efforts have been made to determine an intrinsic adhesive fracture energy by considering the energy dissipated during tensile deformation and bending of the peel arm, in addition to the energy stored in the peel arm. Kinloch *et al*. utilized this approach to calculate G_a, a 'geometry independent' parameter, independent of the peel angle and thickness of the adhesive.[71] Moidu *et al*. developed an analytic approach to determine the plastic deformation in the adhesive and also studied the effects of adhesive constitutive properties and peel angle. [72,73]

Ideally, for thin coatings an adhesion test should reduce the above discussed misleading effects of the angle and stiffness of the peel arm, reduce plastic deformation, and eliminate the use of mechanical grips. In addition, a procedure for reinforcing the film without significantly affecting the measured peel force would be beneficial. A test that, in general, meets these requirements is the pull-off test [74], or V-peel test [75], illustrated in Figure 3-1. In this experiment, to initiate debonding, a force is applied by a pin placed perpendicular to and in the center of a strip of coating. From the peel force and angle of debond the strain energy release rate can be determined from Equation 3-2.

Equation 3-2
$$G = \frac{3}{8}\frac{P\theta}{b}$$

Gent and Kaang showed that the value of G_c obtained from the pull-off test was independent of the film stiffness.[74] The value of G_c was also significantly less than that obtained by the 90° peel test due to the small angle of deflection between the peel arm and substrate (< 25°), which led to a decrease in the plastic deformation arising to bending stresses.

3.2.2.2 Blister Tests

Another broad category of tests that eliminates the use of grips and reduces plastic deformation due to bending (due to the small angle between the peel arm and substrate) are the blister tests. Blister specimens consist of a thin film adhered to a substrate that has a hole in its center. The development of the first blister test is credited to Dannenburg.[76] However, not until the work of Williams was the circular blister geometry adopted.[77] In the standard or pressurized circular blister test, either a liquid or gas is pressurized through the hole against the underside of the coating until a blister crack is formed. The strain energy release rate can be calculated from the relationship between the pressure, blister radius, and blister height. Similar to the pull-off test, it has been shown that the strain energy release rate for the blister test is independent of the stiffness of the film and specimen geometry.[78] However, a disadvantage of the standard blister is that the strain energy release rate increases as the blister radius increases, which could lead to uncontrolled catastrophic debonding.[79] To circumvent the problem of uncontrolled failure, a constant strain energy release rate test, the "constrained blister" was proposed by Napolitano *et al*. [80] and Chang *et al*. [81]. Allen and Senturia proposed an island blister test to reduce stresses on the film, enabling high strain energy release rates at relatively low pressures; however, a drawback of the island blister is that uncontrolled debonding can still occur.[82,83] Dillard and Bao extended this to an additional constant strain energy release rate test, the peninsula blister.[84] Wan

also developed a blister test that eliminates catastrophic debonding by utilizing a fixed amount of the pressurizing gas, where the increase in pressure is driven thermally.[85,86]

3.2.2.3 Blister Tests for Environmental Studies

The blister test geometry also has a number of advantages when used for testing adhesives subjected to environmental stress (time, temperature, and fluid). Specimens where the adhesive is sandwiched between two impermeable adherends expose only an edge to the environment, increasing the time necessary to saturate the adhesive and degrade the interface. Open face specimens such as peel specimens can considerably reduce the exposure time before deleterious effects of the environment are observed.[87,88] However, the interfacial degradation may be more pronounced at the sample edge, which can produce misleading results. For such environmental degradation tests, blister specimens have several advantages: 1) the pressurizing medium can be the degrading fluid of choice, 2) the blister axisymmetric geometry eliminates edge effects, and 3) direct exposure or diffusion of the fluid occurs perpendicular to the debond front.

3.2.2.4 Shaft-Loaded Blister Test

In this research, we explore the shaft-loaded blister test (SLBT), which utilizes the controlled displacement of a spherically capped shaft, driven by a universal testing machine (UTM), as an alternative to applying fluid or gas media. Malyshev [89] was the first to explore this test geometry and derived the strain energy release rate for a pure bending plate boundary condition. Wan and Mai developed an analytic solution to derive the strain energy release rate for a pure stretching elastic film in a conical geometry and provided additional analysis that accounts for plastic yielding at the contact area of the shaft tip.[90] This elastic solution was adopted to measure the adhesion of nylon to aluminum.[91] Wan analyzed the transition from a bending plate to a

stretching membrane condition in the shaft-loaded blister test geometry.[92] Wan and Liao adopted the shaft-loaded blister test for measuring the constitutive properties of thin films from the load vs. displacement data prior to debonding.[93] In addition, delamination under cyclic loading conditions was studied using the shaft-loaded blister test.[94]

Utilizing the elastic analytic model proposed by Wan and Mai[90], we have adopted the shaft-loaded blister test in order to investigate the adhesion of Kapton® pressure sensitive adhesive tape bonded to a rigid substrate. The substrates reported here is either a low-energy surface (Teflon®), or a substrate with a high-energy surface (aluminum). The model was tested and the effects of film plastic deformation were probed by examining the value of G calculated from three different equations, which will be termed: (1) load-based, (2) hybrid, and (3) displacement-based. The effect of changing the stiffness of the coating while keeping the actual interfacial adhesion constant was investigated by varying the number of plies of PSA tape bonded to the aluminum substrate. The strain energy release rates obtained by the SLBT for a single ply film are compared to the more conventional pull-off test and 90° peel test. An experimental compliance calibration method for in-situ measurement of the film mechanical properties was also obtained based upon blister crack growth data, and in order to preserve the continuity of the paper, is discussed in an appendix. The great utility of the shaft-loaded blister test in environmental exposure testing was demonstrated for several fluids and described below.

3.2.3 Shaft-Loaded Blister Test Theory

In this proposal, we explore the shaft-loaded blister test shown in Figure 3-2. The analytical solution to the shaft-loaded blister by Wan and Mai[90] is based largely on three assumptions: 1) that the film undergoes pure elastic stretching in the radial and tangential directions, or in other words, no that there is no contribution to the stiffness from bending, 2) the load is approximated

as a point load, which results in a conical blister profile, and 3) the angle between the adhesive and substrate is shallow (less than 25°). Based on these assumptions Wan and Mai first arrive at the following relation:

Equation 3-3
$$Pa^2 = \left(\frac{\pi (Eh)_{\text{eff}}}{4} \right) w_0^{\ 3}$$

where a is the radius of debonding, w_0 is the central shaft displacement, P is the load, E is the Young's tensile modulus, and h is the thickness of the backing. Collectively, (Eh) is commonly referred to as the film's tensile rigidity, which defines the film stiffness. $(Eh)_{\text{eff}}$ is the effective tensile rigidity determined from a compliance calibration. Equation 3-3 is modified from the original work of Wan and Mai- we take the liberty of replacing (Eh) with $(Eh)_{\text{eff}}$, and also utilize equation 3 to carry out a compliance calibration. The results from application of Equation 3-3 are presented and discussed in the Appendix of this section.

Utilizing Equation 3-3 and an energy balance derived from linear elastic fracture mechanics, Wan and Mai arrive at the following three expressions for the strain energy release rate:

Equation 3-4
$$G = \left(\frac{1}{16\pi^4 Eh} \right)^{1/3} \left(\frac{P}{a} \right)^{4/3}$$

Equation 3-5
$$G = \frac{1}{\pi^2 Eh} \left(\frac{P}{w_0} \right)^2$$

Equation 3-6
$$G = \frac{Eh}{16} \left(\frac{w_0}{a} \right)^4$$

During stable crack growth a, w_0, and P are predicted to increase linearly. From the slope of either P vs. a, P vs. w_0, or w_0 vs. a, the value of G can be calculated from Equation 3-4, Equation 3-5, and Equation 3-6 respectively. Examination of these three equations reveals that the value of G calculated from Equation 3-4 depends strongly on the measured load (P), and the G calculated from Equation 3-6 depends strongly on the measured displacement (w_0). The debond radius (a) is eliminated from Equation 3-5 a hybrid form involving both load and displacement. As a consequence Equation 3-4, Equation 3-5, and Equation 3-6 are referred to as the load-based, hybrid, and displacement-based equations, respectively.

The film tensile rigidity (Eh) can be determined from either an independent stress-strain experiment or from a compliance calibration with the SLBT fixture. The initial linear relationship of the stress–strain experiment yields the Young's modulus, E. For the PSA tape used in our research, the area and stress are calculated based only on the thickness of the backing (Kapton®), not the soft adhesive layer. The tensile rigidity calculated as described from the stress-strain data is denoted as $(Eh)_{\mathrm{UTM}}$. On the other hand, if the adhesive system closely follows the assumptions of the analytic model, then fitting the experimental data to Equation 3-3 allows a compliance calibration which will then independently determine the effective film tensile rigidity $(Eh)_{\mathrm{eff}}$. We note that a plot of $P\,a^2$ vs. w_0^3 should yield a straight line with a slope equal to $\pi\,(Eh)_{\mathrm{eff}} / 4$. For several reasons this effective tensile rigidity $(Eh)_{\mathrm{eff}}$ may be more representative of the adhesive film's mechanical properties than the film tensile rigidity determined from the Young's modulus and the film thickness, $(Eh)_{\mathrm{UTM}}$. Most importantly, the effective tensile rigidity $(Eh)_{\mathrm{eff}}$ can account for such effects as the difference in loading between the uniaxial stress-strain experiment and the biaxial stress the film experiences in the actual blister test configuration. In addition, the effects of the Poisson ratio, shear loading, anisotropy,

as well as the co-existence of bending and stretching stresses may be significant and could be accounted for by the $(Eh)_{\text{eff}}$ method. Overall, this technique is similar to the compliance method often adopted for the double cantilever beam specimen.[95]

To estimate the stress in the adhesive film, the effective membrane stress (N_{eff}), is given by Wan and Mai as:

Equation 3-7
$$N_{\text{eff}} = (GEh)^{1/2}\left[\left(\log\frac{a}{r}\right)^2 + \frac{3}{4}\right]^{1/2}$$

where r is the radial distance from the center of the blister. Membrane stress is defined as the stress multiplied by the film thickness, therefore N_{eff} is not a "true" stress in the strict sense (load per unit cross sectional area), but rather a force per unit width. N_{eff} is composed only of the radial and tangential stress components of the film, and ignores stresses due to bending, which may or may not be significant. If $N_{\text{eff}} \geq \sigma_y h$, where σ_y is the adhesive yield strength, then membrane yielding is predicted to occur. Examination of Equation 3-7 reveals that in the limit of $r \to 0$, the effective stress approaches infinity; thus, in the center of the blister we expect deviations from simple elastic response. However, application of Equation 3-4, Equation 3-5, and Equation 3-6 requires that the assumption of linear elasticity hold true at the crack front, where $r = a$ and $N_{\text{eff}} = (3G(Eh) / 4)^{1/2}$. In the event that $N_{\text{eff}} \geq \sigma_y h$ at the crack front, the elastic blister equations are invalid. The solution for the case of a thin film experiencing plastic deformation in an inner annulus and an elastic outer annulus has been developed also by Wan and Mai, but is not discussed here.

3.2.4 Experimental

3.2.4.1 Materials

The PSA tape utilized in the experiments is Kapton® polyimide film tape with a total thickness of 63.5 μm (2.5 mils). The PSA tape is a bilayer system consisting of a Kapton® backing, which has a thickness of 25.4 μm (1 mil), and a pressure sensitive silicone-based thermosetting adhesive, which has a thickness of 38.1 μm (1.5 mils). The base polymer used in silicone-based PSAs is polydimethylsiloxane (PDMS)[96] which has a glass transition at –125°C. The PSA tape was bonded to either aluminum or Teflon®, a high energy and low energy surface, respectively. The surface energies of Al_2O_3 and Teflon® are 574 and 19.1 mJ/m^2, respectively.[97] The aluminum surface was treated with a caustic solution and rinsed with acetone prior to application of the PSA tape. The Teflon® surface was also rinsed with acetone prior to application of the PSA tape. The tensile modulus (E) of the Kapton® tape, calculated from ASTM D-882-91 using the sample cross-sectional area based on the backing thickness, is roughly 3.05 +/- 0.06 GPa. The stress-strain curve for the PSA tape is shown in Figure 3-3, and the yield strength σ_y was calculated as 120 +/- 6 MPa using a bimoduli approximation.

3.2.4.2 Technique

A 0.8 cm diameter hole was bored into the aluminum and Teflon® substrates. The PSA tape dimensions were 2.54 x 2.54 cm square. A ball-bearing 0.7 cm in diameter is mounted on the shaft tip. The bonded PSA tape was attached face down in a rigid fixture. During the experiment, a mirror and a transparent ruler were used to observe the debond radius with a video camera. To account for the parallax error, a small correction was necessary. A schematic of the visual image as seen through the video camera is shown in Figure 3-5. The load (P) and displacement (w_0)

were recorded by the UTM and the shaft displacement rate was 0.1 mm/sec. The tests were conducted at room temperature. This experiment is mechanically much simpler than the pressurized blister test since the mechanically driven shaft eliminates the use of a pump, pressure gauge, and valves. For the aluminum substrate, samples consisted of stacked, bonded, Kapton® PSA tape either 1, 2, or 4 plies thick. The number of stacked films is designated as n. As a result, the film thickness (h), based on the backing, is equal to 25.4 μm multiplied by n. A single ply only was tested for the Teflon® substrate. The only criterion each sample must meet for acceptable analysis is that the debond must occur roughly axisymmetrically. For comparison, the strain energy release rate for a single ply of Kapton® PSA tape was also measured by the pull-off test and the 90° peel test. For the pull-off test, G was calculated from Equation 3-2. For the 90° peel test, G was calculated from equation 1, which in this case simplifies to Equation 3-8.

Equation 3-8
$$G = \frac{P}{b}$$

3.2.5 Results and Discussion

3.2.5.1 Aluminum Substrate

3.2.5.1.1 Shaft-Loaded Blister Test

The load (P) vs. shaft displacement (w_0) curves obtained directly from the UTM are shown in Figure 3-6 for n = 1, 2, and 4. There are three regions of interest: Region I, the pre-debonding region at the beginning of the test where the blister begins to form, Region II, the stable crack growth region where the crack begins to propagate once a critical load is reached (P*) and the slope of P vs. w_0 becomes linear, and Region III, where edge effects occur and the load begins to decrease as the film debonds completely from the substrate. From the slope of P vs. w_0 in the

stable crack growth Region II, the value of G may be determined using the hybrid equation (Equation 3-5).

The debond radius (a) vs. shaft displacement (w_0) data are shown in Figure 3-7 for n = 1, 2, and 4. From the slope of these lines, G may be determined using the displacement-based equation (equation 6). During stable crack growth the relationship of the load (P) and crack length (a) is also linear, but is not shown. From the slope of the load (P) vs. debond radius (a) plot, G may be determined using the load-based equation (equation 4). As mentioned by Wan and Mai, the non-zero intercept observed in Figure 3-6 and Figure 3-7 is a result of the finite contact area between the shaft tip and adhesive film.

For n = 1, 9 samples were tested. For the n = 2 and 4 specimens we tested 4 and 3 samples, respectively, because fewer samples met the criteria of axisymmetric debonding. We noted that as the thickness increased, the debond radius tended to be less symmetric and the blister shape became roughly square, probably due to anisotropy in the film and to the increase in the stiffness of the film. This effect was most noticeable in the n = 4 case. Evidence for the anisotropy of the Kapton® backing can be found in an article by Park *et al*.[98]

Utilizing $(Eh)_{\mathrm{UTM}}$, the resulting calculated average values of G, determined from the load-based, hybrid, and displacement-based equations, are presented in Table 3-1 for n = 1, 2, and 4. For the load-based equation, the calculated values of G for different plies are in good agreement. The hybrid and displacement-based equation both show good agreement when n = 1 and 2 but not for n = 4. G values from the displacement-based calculation are significantly larger than those obtained by either the load-based or hybrid equation.

Table 3-1 Applied strain energy release rates (J/m^2) for n = 1, 2, and 4 on aluminum calculated from the load, hybrid, and displacement equations and $(Eh)_{UTM}$

n	*Load (P/a)*	*Hybrid (P/w_0)*	*Displacement (w_0/a)*
1	33.4 +/- 3.6	31.9 +/- 3.1	45.8 +/- 10.4
2	35.0 +/- 7.7	33.9 +/- 5.2	44.8 +/- 9.6
4	31.0 +/- 2.2	24.2 +/- 1.5	62.4 +/- 11.1

The discrepancy between the values of G calculated by either the load-based, hybrid equation, or displacement-based equation is largely associated with the (visible) plastic deformation at the contact zone between the shaft tip and PSA tape, where the stresses are highest. Equations 3-6 are based on an elastic, conical blister profile (Figure 3-2); however, the actual blister shape resembles that shown in Figure 3-8. As a result, the measured w_0 is larger than the theoretical, elastic, w_0. This difference is especially significant in the displacement-based equation where w_0 is in the numerator and is raised to the 4^{th} power. Error in w_0 is less significant in the hybrid equation where w_0 is in the denominator and is raised to the 2^{nd} power. As a consequence, the value of G determined from the displacement-based equation is significantly larger than the value of G calculated from the load-based or hybrid equation. In contrast, the value of G obtained by the load-based equation, having no w_0 term, is independent of plastic deformation of the film around the shaft tip.

A visible dimple remaining in the PSA tape at the contact region of the shaft tip after testing is evidence that significant localized plastic deformation or permanent set has occurred during testing. Additional evidence that significant permanent set has occurred was also gathered from the loading and unloading cycles, which were repeated six times. The area of contact

between the shaft tip and adhesive film was coated with chalk to reduce effects of the adhesive film adhering to shaft tip. The substrate used for this experiment was polished aluminum, which is different than the aluminum treated with caustic solution that was used in the previous experiments. Although the adhesion strength is larger (≈71 J/m^2) for this substrate than that of the caustic solution treated aluminum surfaces (≈35 J/m^2), the salient features of the loading and unloading cycles are most probably similar. Figure 3-9displays the resulting graph of the load (P) vs. displacement (w_0) for each cycle. Each cycle displays an initial loading region (Region I) followed by a brief zone of crack propagation (Region II) where the blister radius increased approximately 0.5 – 1 mm. For each cycle, the characteristic signature of plastic deformation is evident where the displacement does not immediately return to the origin once the load is removed. Examination of Figure 3-9 shows that with each cycle, there is a progressive increase in the amount of permanent set. The critical displacement (w_0), where the load first begins to rise, corresponding to the point where the shaft tip contacts the film, increases with each subsequent cycle. However, during unloading when the shaft tip returns to zero displacement, the PSA tape may partially re-adhere to the substrate. This can result in the load increasing prematurely. It is therefore more meaningful to look at the value of displacement when the load is completely removed as an indication of the permanent set that occurs. The final and maximum load (P_{Max}) of each cycle vs. the displacement when the load is completely removed is shown in Figure 3-10. Figure 3-10 also shows that net amount of film yielding increases, which each subsequent loading cycle; however, the rate at which yielding increases slows. Taken collectively, the debonding regions (Region II) of each cycle appear to overlap in the same fashion as expected for a single P vs. w_0 curve in which a specimen is loaded in a typical fashion.

The inaccurate value of w_0 (relative to the pure elastic case) and the resulting disagreement between the values of G, obtained by Equation 3-4, Equation 3-5, and Equation 3-6, may raise questions about the validity of the basic assumption of linear elasticity for the SLBT. To examine this, plots of N_{eff} vs. r for different values of a were constructed as suggested by Equation 3-7for n = 1, 2, and 4. As an example, the resulting plot for n = 1 is shown in Figure 3-11. We assume that if $N_{\text{eff}} \geq \sigma_p h$ then plastic deformation occurs. The resulting plots reveals that plastic deformation is predicted solely at the contact zone of the shaft tip ($r \leq 0.1$ mm for n = 1), and that no plastic deformation (attributable to radial and tangential stresses) is predicted to occur at the crack front ($r = a$). These results suggest that the assumption of linear elasticity is valid, if bending stresses are ignored.

Evidence of the adhesive-substrate system deviating from the assumptions of the model is observed for the multiple stacked tape, where n = 4. As shown earlier, the effects of plastic deformation here seem to be more pronounced; the value of G is either smaller or larger when calculated from the hybrid and displacement based equation, respectively. This is unexpected, given that the stiffer film should plastically deform the least, therefore plastic deformation is probably not the most significant reason for the discrepancy. An alternative explanation is that for n = 4 the adhesive system does not follow the assumptions of the model as closely as in the n = 1 and 2 case. The thicker structure should result in the adhesive behaving more like a bending plate and less like a stretching membrane. In addition, significant shear forces between the stacked plies are possibly playing a role. This shear effect may contribute significantly given that the four layered structure of Kapton® is interspersed with the soft PSA, and would reduce the effective stiffness of the film. As mentioned earlier, the deviation from the model is supported by the visual observation that increasing the film stiffness and anisotropy may cause the blister to be

less circular and adopt a square or non-symmetric debond pattern. However, when employing the load-based equation, the similarity between the n = 4 case and the model is close enough to obtain values of G close to those for to n = 1 and 2.

Rearrangement of the load-based, hybrid and displacement-based equations shows that the slopes of (P / a), (P / w_0) and (a / w_0) plots should linearly scale with the variables $h^{1/4}$, $h^{1/2}$, and $h^{1/4}$ or $n^{1/4}$, $n^{1/2}$, and $n^{1/4}$ respectively. Plots of such graphs using average slopes obtained from the group of samples are shown in Figure 3-12. The error bars represent one standard deviation. For the load-based equation, the predicted scaling behavior is followed, albeit the relationship is not perfect. For the hybrid and displacement-based equation, the graphs show that for n = 4 the scaling law fails, a result which may be attributable to reasons outlined previously.

The assumption of linear elasticity and hence the validity of the model is supported by calculations of N_{eff}. In addition, the agreement among the values of G obtained from the load-based equation for n = 1, 2, and 4 (independent of the film stiffness) is further evidence supporting the approach of Wan and Mai. It is not unexpected that the value of G obtained by hybrid and displacement based equations do not agree with that obtained by the load based equation given the plastic deformation at the shaft tip, unaccounted for by the elastic solution. If we accept that plastic deformation is confined to the area at the shaft tip, and linear elasticity is a valid assumption at the crack front (r = a), then we can assume that the load and blister radius are in equilibrium and that the value of G obtained by the load-based equation is independent of film yielding near the shaft tip and provides good values of G. This is confirmed by the consistency of the values of G calculated using this method.

3.2.5.1.2 Alternative test geometries

The values of G for a single ply (n = 1) PSA tape which were obtained from alternative test geometries (the pull-off test and the 90° peel test) are shown in Table 3-2. The tests were performed at the identical crack propagation rate as that of the SLBT (10 mm/minute) in order to reduce the viscoelastic differences at the crack tip. The value of G determined from the pull-off test was of the same order of magnitude as that obtained using the SLBT when employing the hybrid equation. The value of G determined from the 90° peel test was an order of magnitude greater than these, probably due to plastic deformation of the tape, which may originate from the bending stresses associated with the large angle of deflection between the peel arm and substrate. These observations support our contention that the value of G obtained by the SLBT is valid, and an especially attractive alternative to the 90° peel test. Similar to other low angle adhesion tests, the SLBT may produce values of G that more closely reflect the intrinsic adhesion strength of an adhesive system than do the high angle 90° and 180° peel counterparts. Both the pull-off test and SLBT share similar angles of debonding (for n = 1), roughly 14° and 16° (estimated from $\theta = \arctan(w_0 / a)$), respectively, and so large differences in the localized stress at the crack front are not expected. Although there may also be significant bending stresses associated with the SLBT, given the similar angle of debonding between the SLBT and pull-off test, any bending stresses if they are significant, may be similar in magnitude. Given the similarity between the pull-off test and SLBT, and how well established the pull-off test is, further supports the utility of the SLBT.

Table 3-2 Applied strain energy release rates (J/m^2) calculated from alternative test geometries (n = 1).

Load based SLBT	*Pull-off Test*	*90° Peel Test*
33 +/- 4	45 +/- 1	141 +/- 7

The assumption that the angle of debonding be less than 25°, used to derive the SLBT model, is satisfied. Furthermore, this angle appears to be constant given the linear relationship between the displacement (w_0) and debond radius (a). It is also of interest to mention that the SLBT, peel test, and pull-off test are all constant angle adhesion tests, and so they share the characteristic of self-similarity, and a value of G that is independent of the crack length or length of the peel arm.

3.2.5.2 Teflon® Substrate

3.2.5.2.1 Shaft-loaded blister test

Load (P) vs. displacement (w_0), and crack length (a) vs. displacement curves (w_0) were also generated for a single ply (n = 1) of the PSA adhering to a low surface energy Teflon® substrate, shown in Figure 3-13. Seven samples were tested. The resulting average values of G are listed in Table 3-3; there, as expected for such a low surface energy substrate, the values are low. Utilizing $(Eh)_{UTM}$, the effects of plastic deformation are notable in this adhesive system; the average values of G obtained by the hybrid and displacement-based equations were smaller and larger, respectively, relative to the load-based equation. However, the value of G calculated by the load-based and the hybrid equation agree within one standard deviation.

Table 3-3 Applied strain energy release rates (J/m^2) for Kapton® PSA tape bonded to Teflon®, $n = 1$, calculated from the load, hybrid, and displacement equations and $(Eh)_{UTM}$

Load (P/a)	*Hybrid (P/w_0)*	*Displacement (w_0/a)*
17.6 +/- 3.4	15.5 +/- 1.5	21.8 +/- 4.2

3.2.5.2.2 Alternative Test Geometries

The value of G obtained from the pull-off and 90° peel tests from Teflon®, with equal crack propagation rates, were approximately 60% greater than those found by the SLBT, see Table 3-4. The agreement between the pull-off and 90° peel test is excellent. These results in conjunction with the values of G obtained by the pull-off test for aluminum, suggest that the fracture energies obtained by the SLBT, will be slightly less than obtained by the pull-off test. The agreement between the pull-off and 90° peel suggests that plastic deformation of the peel arm due to bending is reduced for the Teflon® - Kapton® combination. In sharp contrast, if the PSA tape is adhered strongly (e.g., the aluminum substrate), the bending of the peel arm causes significant plastic deformation when using the 90° peel geometry. Similar results were observed by Gent and Kaang [74] for adhesives with weak interfacial adhesion. More significant discrepancy could result as the film yield strength decreased or as the interfacial adhesion strength increased.

Table 3-4 Applied strain energy release rates (J/m^2) for Kapton® PSA tape bonded to Teflon®, $n = 1$, using alternative test geometries

Load based SLBT	*Pull-off Test*	*90° Peel Test*
18 +/- 3	27 +/- 1	26 +/- 3

3.2.6 Effects of Fluids at the Interface

The effect of fluid added directly to the interfacial region during crack propagation was investigated and is reported in terms of changes in of the applied strain energy release rate. For these experiments, the reservoir between the PSA tape and aluminum substrate was filled with a mixture of methanol and water, and the load was immediately applied. The reservoir eliminates experimental difficulties associated with the complete fluid submersion of an adhesive specimen. The methanol concentration was varied from 0, 40, 60, 80, to 100 wt. %. Tests were conducted at room temperature. A schematic of the experimental configuration is shown in Figure 3-14. The load (P) vs. displacement (w_0) curves are shown in Figure 3-15. Table 3-5 lists the G values, calculated using the hybrid equation and the $(Eh)_{UTM}$, and P^* for the respective methanol concentrations. Good agreement between the value of G calculated from load-based and hybrid equations and $(Eh)_{UTM}$, for n = 1 and 2 bonded to aluminum, was noted. The presence of water (0 % methanol concentration) increased the value of G, or at least within reasonable error did not have any measurable effect on the value of G. Furthermore, as the concentration of methanol increases, the critical load where debonding begins (P^*), and the slope of the P vs. w_0 plot decreases.

Table 3-5 Applied strain energy release rates (J/m^2) calculated from hybrid equation for Kapton® PSA tape (n = 1) with various concentrations of methanol in water (0, 40, 60, 80, 100 wt. %) and $(Eh)_{UTM}$

methanol concentration	*G (J/m^2)*	*P* (N)*
dry	36	9.6
0 %	38.3	8.7
40 %	31.6	8.7
60 %	29.3	6.7
80 %	27.8	5.2
100 %	6.9	0.1

Our results are similar to those obtained by Chaudhury and Whitesides for the adhesion of PDMS surfaces in contact with mixtures of methanol and water.[99] Utilizing the JKR model and Young's equation, they observed that the adhesion of PDMS surfaces in the presence of a high surface energy fluid (γ = 72.94 at 20°C [100]), water, was higher than in air. The work of adhesion for PDMS was determined to be 43.6 mJ/m^2 and 74 mJ/m^2 in air and in water, respectively. In the presence of a low surface energy fluid (γ = 22.5 at 20°C [100]), methanol, the adhesion of PDMS surfaces decreased to 6 mJ/m^2. The observed reduction in adhesion strength is attributable to the absorption of fluids on the surface; therefore, the lower the surface energy of the fluid, the more readily the fluid can wet the surface and disrupt the bonds between the adhesive and substrate.

3.2.7 Conclusions

We investigated the SLBT for its applicability in determining adhesive fracture energy of tapes adhering to rigid substrates. Plastic deformation at the contact area of the shaft tip resulted in an overestimated displacement, w_0 (relative to the elastic model), resulting in discrepancy among the values of G calculated by the load-based, hybrid, and displacement-based equations. Estimation of the effective membrane stress (N_{eff}) in the film suggests that, in spite of the plastic deformation, the assumption of linear elasticity in the crack growth region, and hence the validity of the model, seem reasonable.

As discussed in the appendix, a compliance calibration has been adopted to measure $(Eh)_{\text{eff}}$, which agrees reasonably well with $(Eh)_{\text{UTM}}$ in cases of one or two plies of tape. For more layers of tape, the disagreement between $(Eh)_{\text{eff}}$ and $(Eh)_{\text{UTM}}$ is roughly 20%, but is not unexpected given the large stiffness and multi-layered structure. The compliance calibration has been shown to improve the agreement between the value of G among the load-based, hybrid, and displacement-based equations, however this appears to be an artifact of the error in w_0.

Using the load-based equation accurate values of G were obtained for a thin adhesive coating independent of the film's stiffness, even with plastic deformation at the shaft tip. The insensitivity of this load-based equation to the film stiffness suggests the compliance calibration is unnecessary. Comparing the value of G also obtained by a pull-off test and a 90° peel test for a single ply suggests that our value of G obtained by the SLBT, although of reasonable magnitude, is smaller than that obtained by the more firmly established pull-off test, and also that the plastic deformation is reduced relative to the 90° peel test, presumably due to the low angle of deflection between the peel arm and substrate. An experimental configuration for studying the effects of liquids on the fracture energy has been demonstrated. This study indicates that the

SLBT, because of the insensitivity of the load-based equation to the coating stiffness, the independence of the value of G on the plastic deformation at the shaft tip, and the reduced plastic deformation at the crack front relative to the 90° peel is an attractive and convenient test method for measuring the strain energy release rate of adhesive films. Because the value of G is independent of the film stiffness, the SLBT could be advantageous for testing fragile thin films that could benefit from the addition of a reinforcement layer.

3.2.8 Appendix: Experimental compliance calibration

3.2.8.1 Aluminum Substrate

An experimental compliance calibration was performed by fitting the experimental data to equation 3. As predicted, the relation between $P\,a^2$ vs. w_0^3 (Figure 3-16) was linear and, from the slope of the line, the effective film tensile rigidity $(Eh)_{\text{eff}}$ was calculated. A comparison of this average $(Eh)_{\text{eff}}$ and the independently obtained $(Eh)_{\text{UTM}}$ is shown in Table 3-6. In all cases (n = 1, 2, and 4) the average $(Eh)_{\text{eff}}$ is less than the $(Eh)_{\text{UTM}}$. For n = 1 the average $(Eh)_{\text{eff}}$ is about 9% less than $(Eh)_{\text{UTM}}$. The agreement is best for n = 2, the difference between the average $(Eh)_{\text{eff}}$ and $(Eh)_{\text{UTM}}$ is 3%. The disagreement between $(Eh)_{\text{UTM}}$ and $(Eh)_{\text{eff}}$ for n = 4, about 20%, is not unreasonable given the departure from the assumptions of the Wan's model, attributable to reasons discussed earlier: increased stiffness, anisotropy, and the multi-layered structure.

Table 3-6 Film tensile rigidity determined from ASTM D-882-91: $(Eh)_{UTM}$, and from equation 3: $(Eh)_{eff}$, as well as the number of samples tested

n	$(Eh)_{UTM}$ *N/m*	$(Eh)_{eff}$ *N/m*
1	77,500	70,600+/-6,300
2	154,900	150,800+/-11,600
4	309,800	252,100+/-17,200

Utilizing $(Eh)_{eff}$, the average values of G, determined from the load-based, hybrid, and displacement-based equations were calculated and are listed in Table 3-7 for n = 1, 2, and 4. Using $(Eh)_{eff}$, we note good agreement of G values between the load-based and hybrid equation (Table III) irrespective of the number of plies. The disagreement observed when utilizing the displacement-based equation is attributed to the plastic deformation and was discussed earlier. A comparison of Table 3-1 and Table 3-7 reveals no significant difference between the values of G measured using $(Eh)_{UTM}$ and $(Eh)_{eff}$. However, more consistency was obtained when the compliance calibration was utilized. When a compliance calibration was carried out for n = 2 virtually no difference in G values was observed, because of the small difference between $(Eh)_{UTM}$ and $(Eh)_{eff}$.

Table 3-7 Applied strain energy release rates (J/m^2) for n = 1, 2, and 4 on aluminum calculated from the load, hybrid, and displacement equations and the effective tensile rigidity: $(Eh)_{eff}$

n	*Load (P/a)*	*Hybrid (P/w_0)*	*Displacement (w_0/a)*
1	34.7 +/- 4.2	35.1 +/- 4.5	40.7 +/- 6.9
2	35.3 +/- 7.7	34.7 +/- 2.9	43.5 +/- 9.3
4	33.3 +/- 2.9	29.8 +/- 2.7	50.3 +/- 5.4

A larger value of w_0, relative to the pure elastic case, will effect the value of $(Eh)_{eff}$, obtained by fitting the experimental data to Equation 3-3. Examination of Equation 3-3 reveals that $(Eh)_{eff} \propto w_0^{-3}$. Therefore, the displacement, w_0, which is overestimated if there is plastic deformation would result in a calculated $(Eh)_{eff}$ which is less than that predicted in the case of a purely elastic response. However, the effects of plastic deformation and the multi-layered structure of the PSA tape would also effectively reduce the stiffness of the film and contribute to the observation that $(Eh)_{eff}$ is less than $(Eh)_{UTM}$. The ambiguities associated with the discrepancy in w_0 are also exacerbated by the similar and strong dependence of the value of G on both w_0 and (Eh) in the hybrid and displacement-based equations. Examination of the hybrid equation and displacement-based equation reveals that $G \propto (Eh)^{-1} w_0^{-2}$, and $G \propto (Eh) w_0^{4}$, respectively. The load-based equation is less sensitive to the value of (Eh) relative to the hybrid and displacement-based equation because $G \propto (Eh)^{-1/3}$. Because of the relative difference between the values of $(Eh)_{eff}$ and $(Eh)_{UTM}$, utilizing $(Eh)_{eff}$ rather than $(Eh)_{UTM}$ resulted in increasing the value of G obtained by the hybrid equation and decreasing the value of G obtained by displacement-based equation. The net effect is that the apparent results of plastic deformation are offset by a corresponding reduction in the value of (Eh). This produced more consistent results when $(Eh)_{eff}$

was incorporated into the calculations. This might lead to the conclusion that $(Eh)_{eff}$ better describes the stiffness of the film and more closely reflects the mechanical propeties of the film in the SLBT loading conditions as compared to $(Eh)_{UTM}$. However, given the dependency on the overestimated displacement, it is unlikely that the value of $(Eh)_{eff}$ truly reflects the mechanical properties of the film loaded in the SLBT geometry, but is an artifact of the error in w_0. In any case, the linear fit of the experimental data to Equation 3-3, and the reasonable agreement between $(Eh)_{eff}$ and $(Eh)_{UTM}$ (especially for $n = 2$) support the validity of Wan's model and the assumption of linear elasticity.

3.2.8.2 Teflon® Substrate

By fitting the experimental data to Equation 3-3an average $(Eh)_{eff}$ was calculated as 64,700 ± 7,100 N/m, approximately 17% less than $(Eh)_{UTM}$. Using the experimental compliance calibration, the average value of G was in good agreement among all three equations (Table 3-8). Again, this is probably a result of the strong dependence of G on both (Eh) and w_0 for the hybrid and displacement equation, or it could be that $(Eh)_{eff}$ more closely reflects the mechanical properties of the adhesive loaded in the SLBT conditions. If indeed $(Eh)_{eff}$ is reasonable, the good agreement would not be unexpected given that the Teflon-PSA tape system complies well with the assumptions of the model: namely, 1) the reduced bending stresses attributable to the small thickness (single ply), and 2) the reduced interfacial adhesion strength, which reduces stress and/or plastic deformation in the adhesive.

Table 3-8 Applied strain energy release rates (J/m^2) for Kapton® PSA tape bonded to Teflon®, n = 1, calculated from the load, hybrid, and displacement equations and the effective modulus: $(Eh)_{eff}$

Load (P/a)	*Hybrid (P/w_0)*	*Displacement (w_0/a)*
18.7 +/- 3.6	18.6 +/- 1.5	18.2 +/- 4.2

3.2.9 Figures

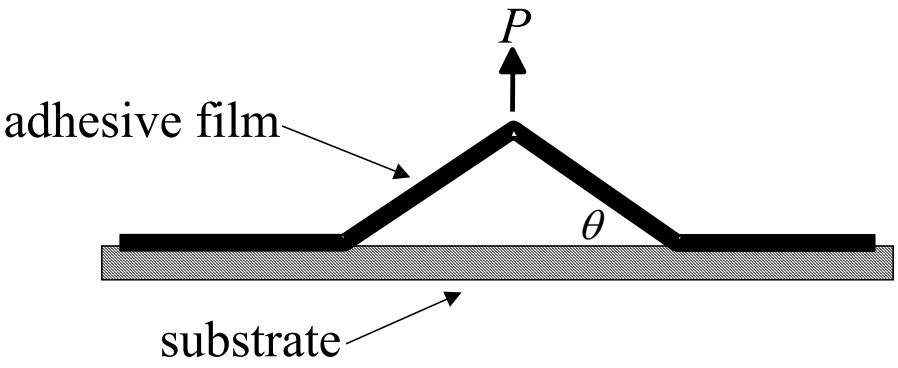

Figure 3-1 Schematic of the pull-off test

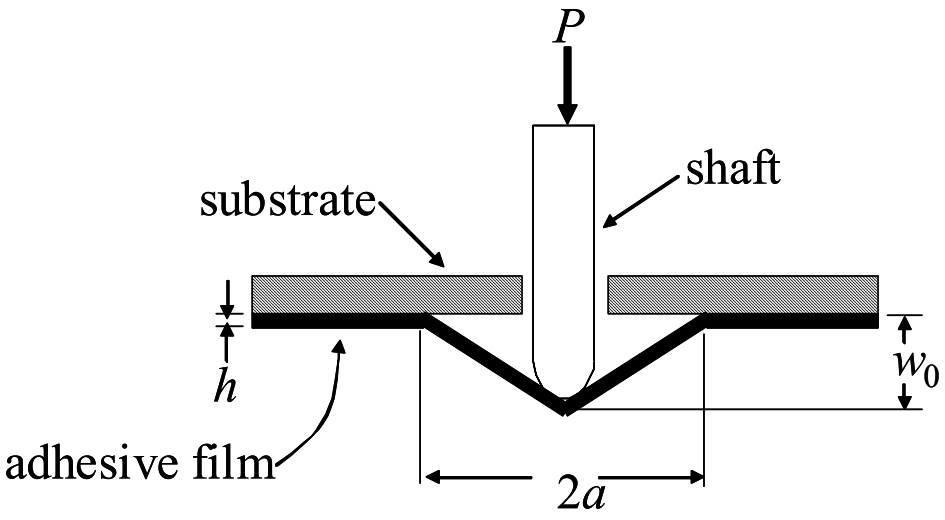

Figure 3-2 Schematic of the shaft-loaded blister test

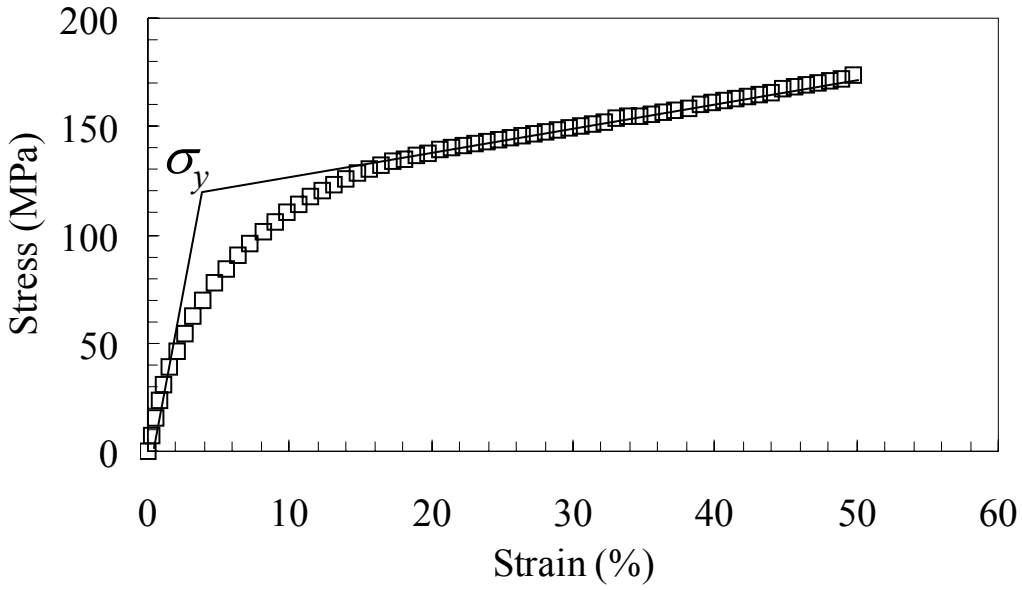

Figure 3-3 Stress-strain curve for Kapton® PSA

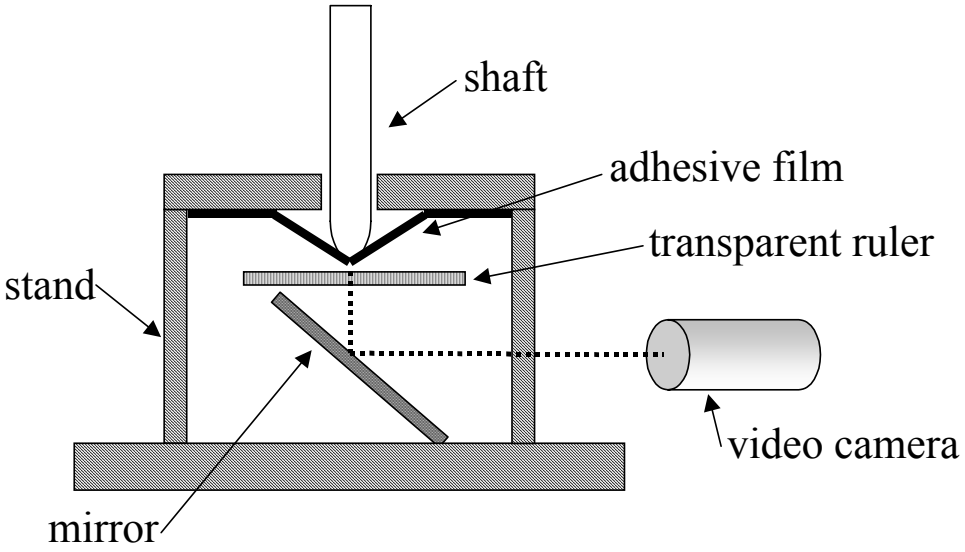

Figure 3-4 Schematic of the experimental set-up of the shaft loaded blister test

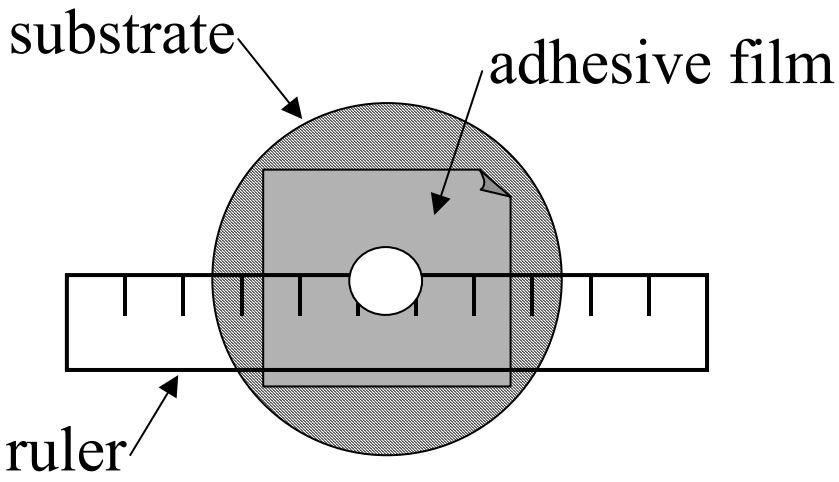

Figure 3-5 Schematic of view of blister radius propagation

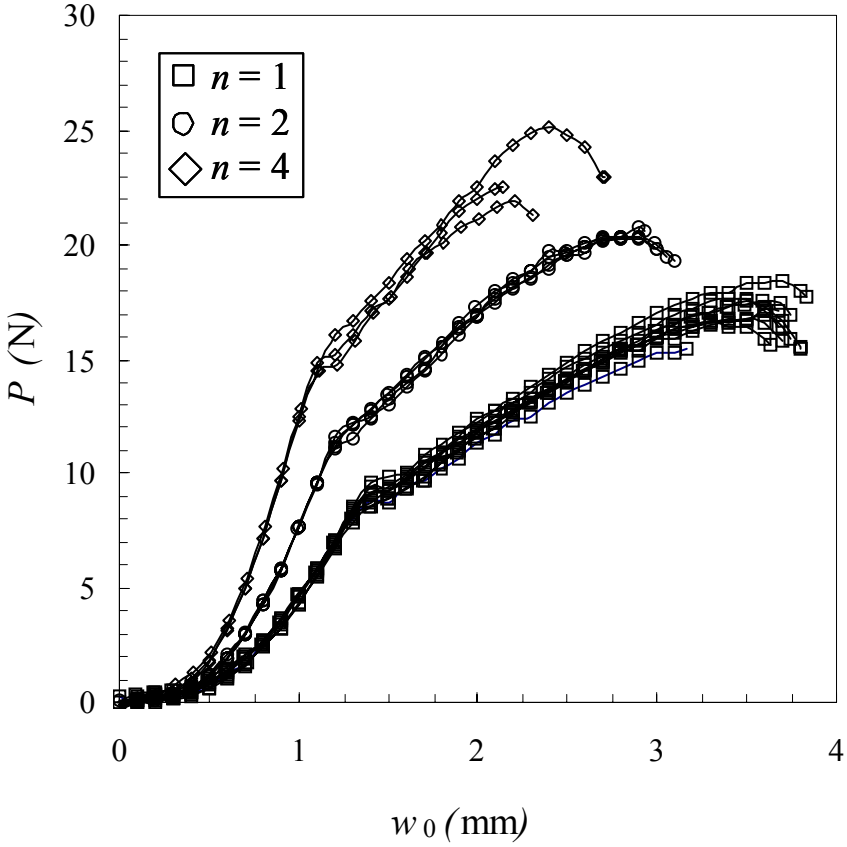

Figure 3-6 Load (P) vs. central shaft displacement (w_0) for n = 1, 2 and 4

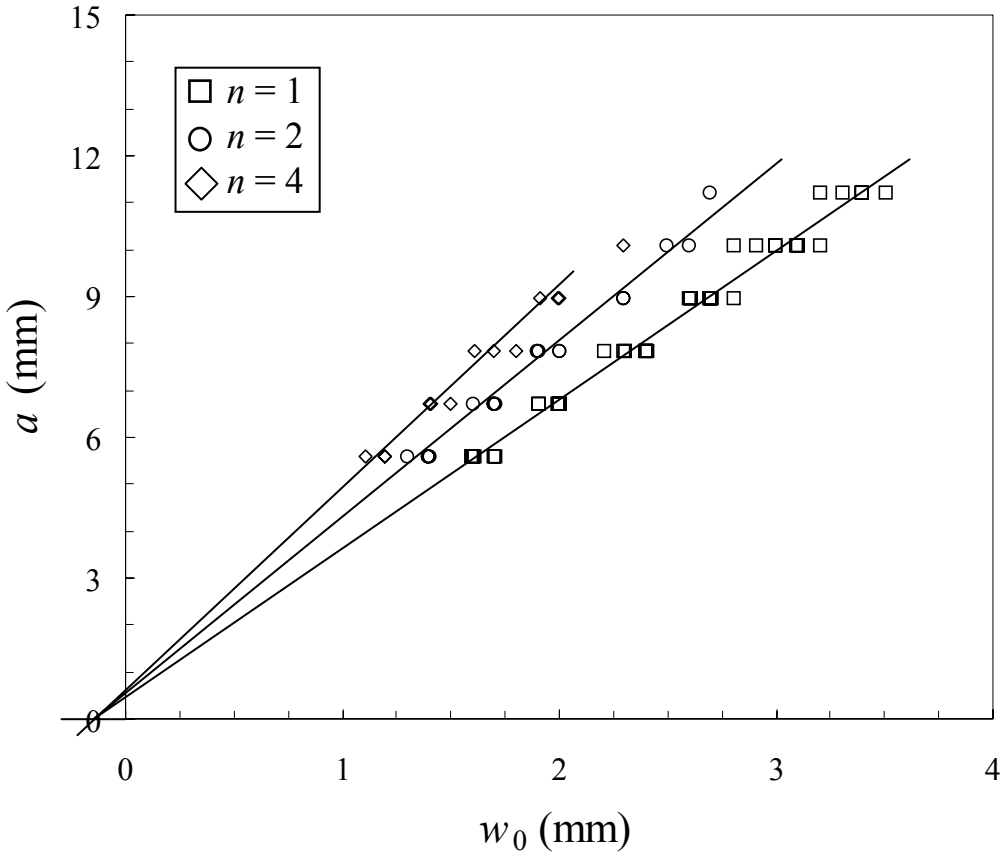

Figure 3-7 Debonding radius (a) vs. central shaft displacement (w_0) for n = 1, 2 and 4

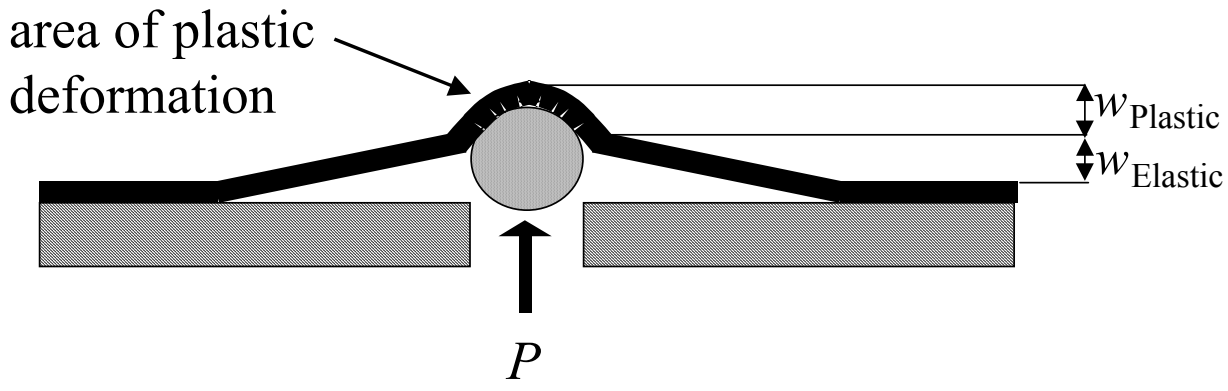

Figure 3-8 Schematic of the actual blister profile

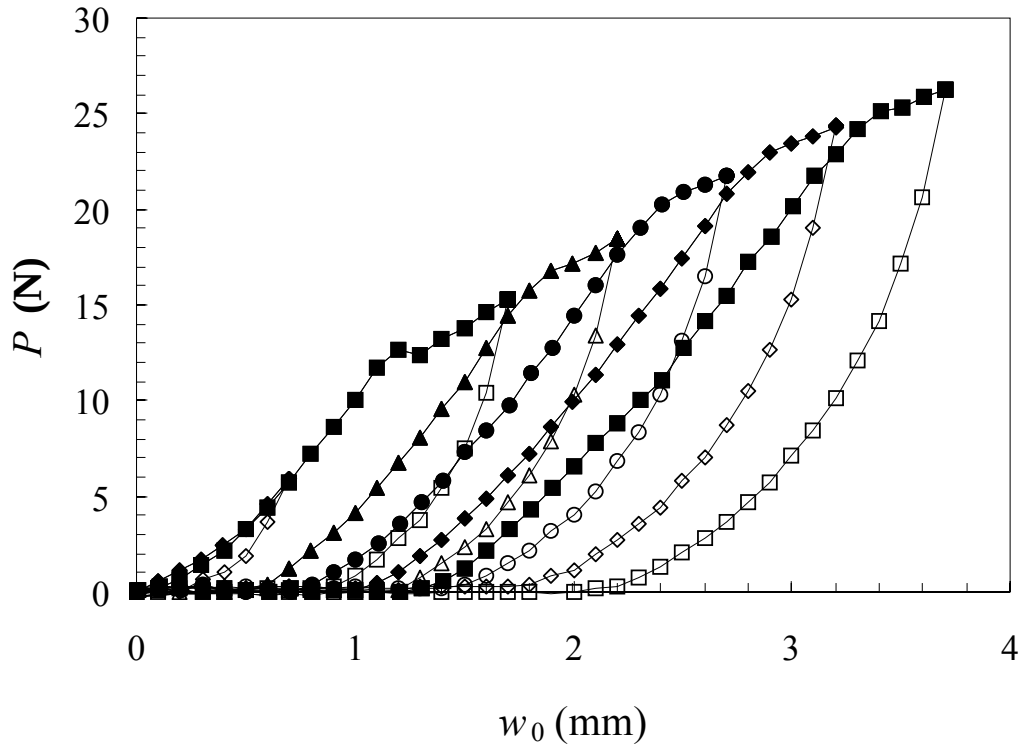

Figure 3-9 Loading and unloading cycles for Kapton® PSA tape bonded to polished aluminum. The loading portion of the curve is shown in filled symbols and the unloading portion is shown in unfilled symbols.

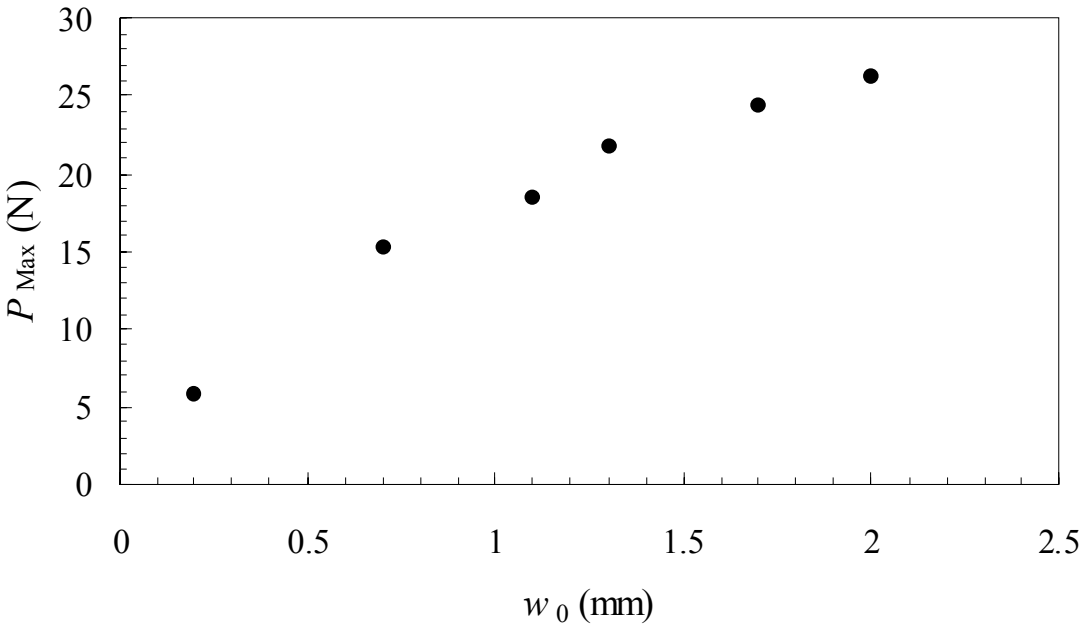

Figure 3-10 Plot of the final load P_{Max} of each cycle vs. w_0 for Kapton® PSA tape bonded to polished aluminum.

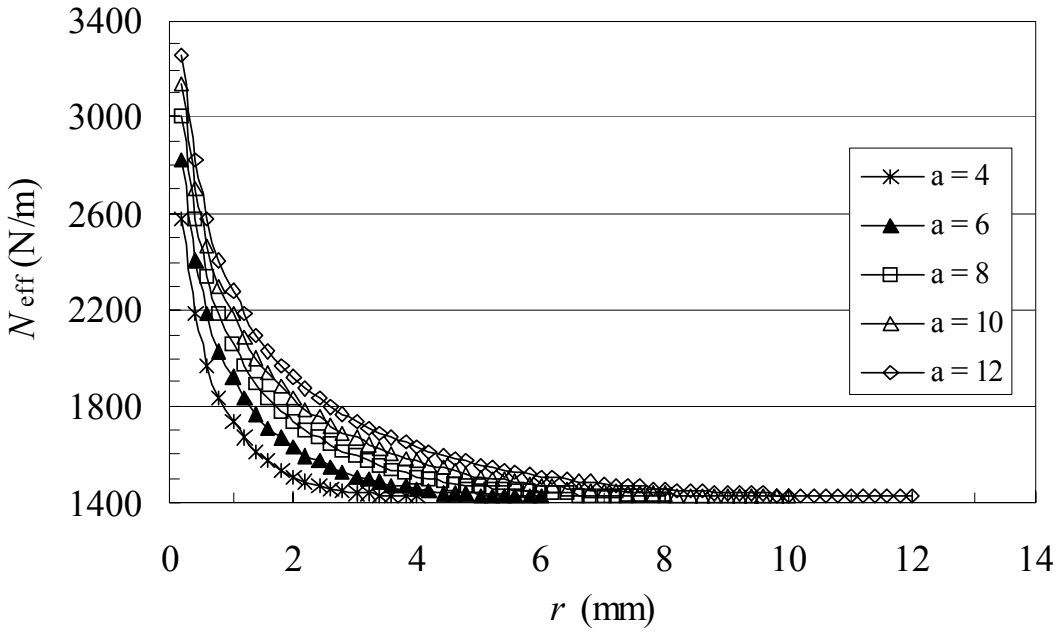

Figure 3-11 Plot of effective membrane stress as a function of crack length (a) and r

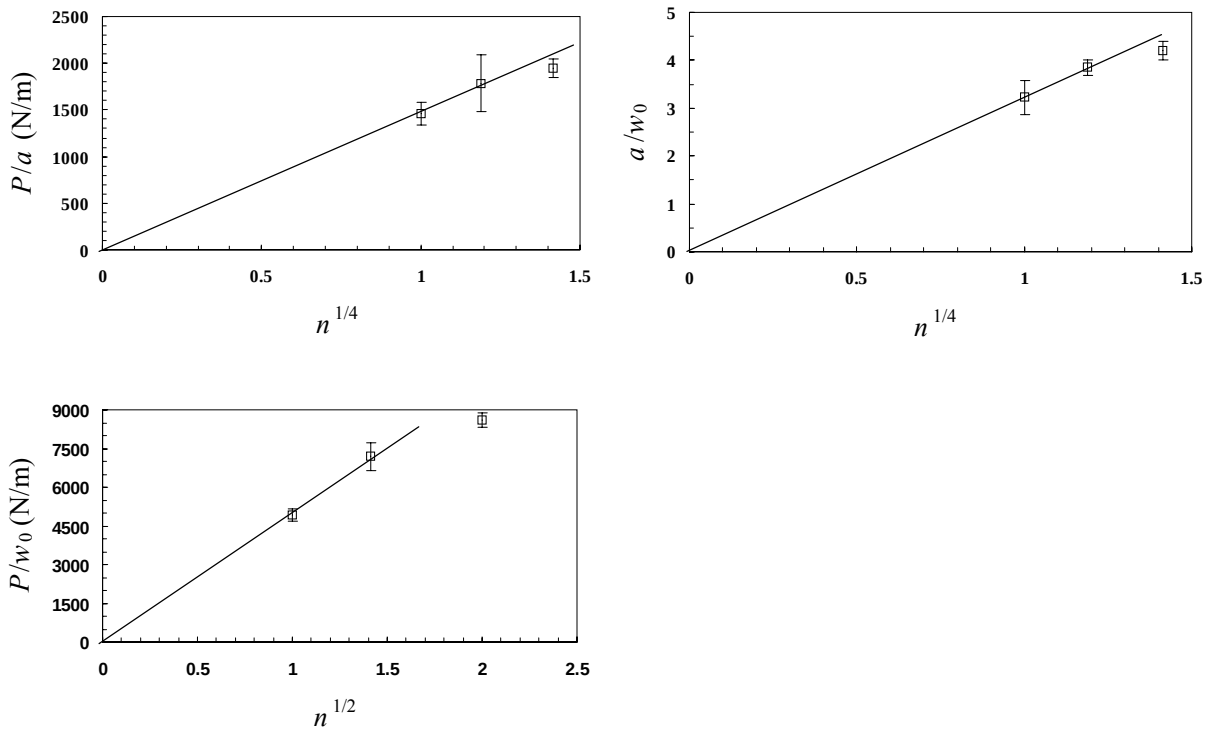

Figure 3-12 Plots of predicted scaling laws based on load, hybrid, and displacement equations

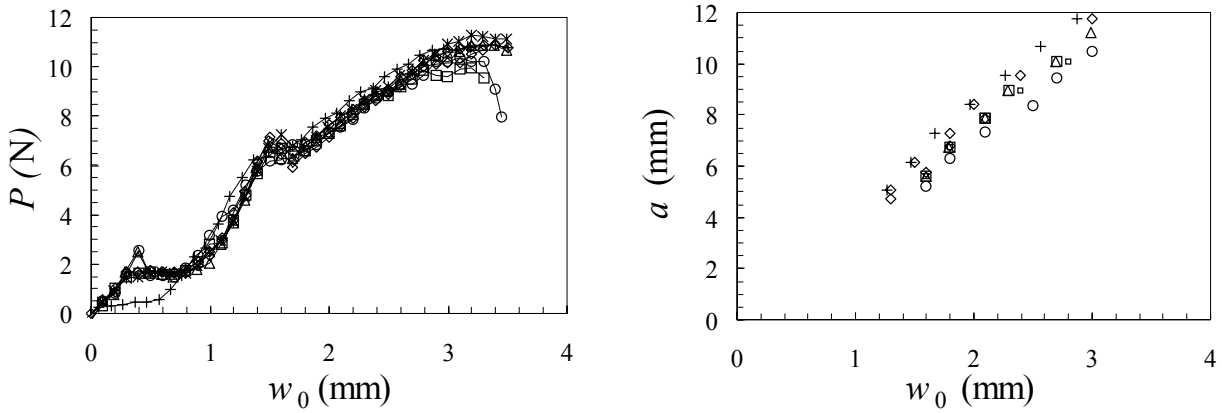

Figure 3-13 Load (P) vs. central shaft displacement (w_0), and crack length (a) vs. central shaft displacement curves (w_0), for Kapton® PSA tape bonded to Teflon (n = 1)

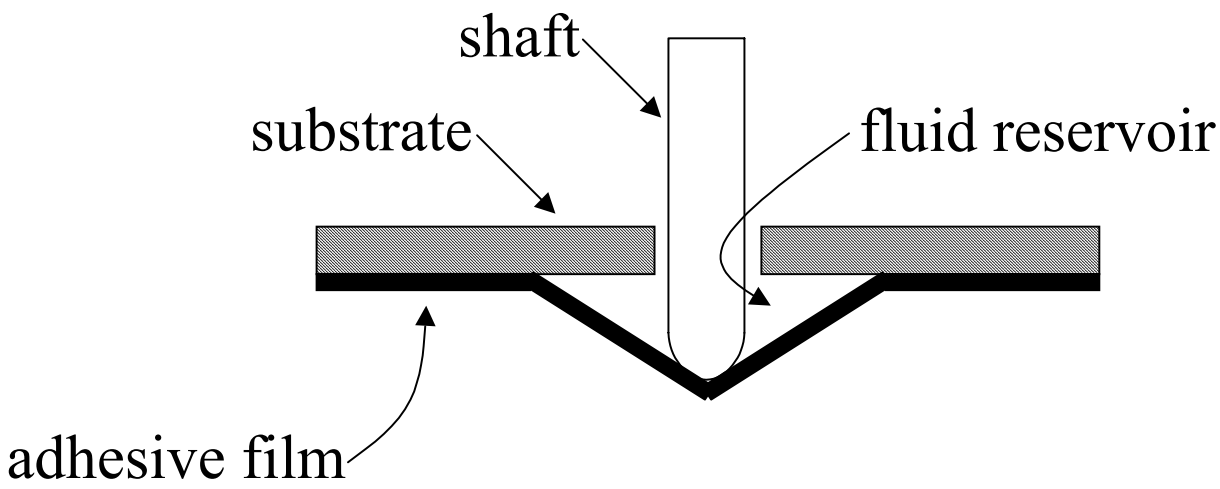

Figure 3-14 Schematic of the experimental set-up used to make in-situ measure of liquid influence the strain energy release rate

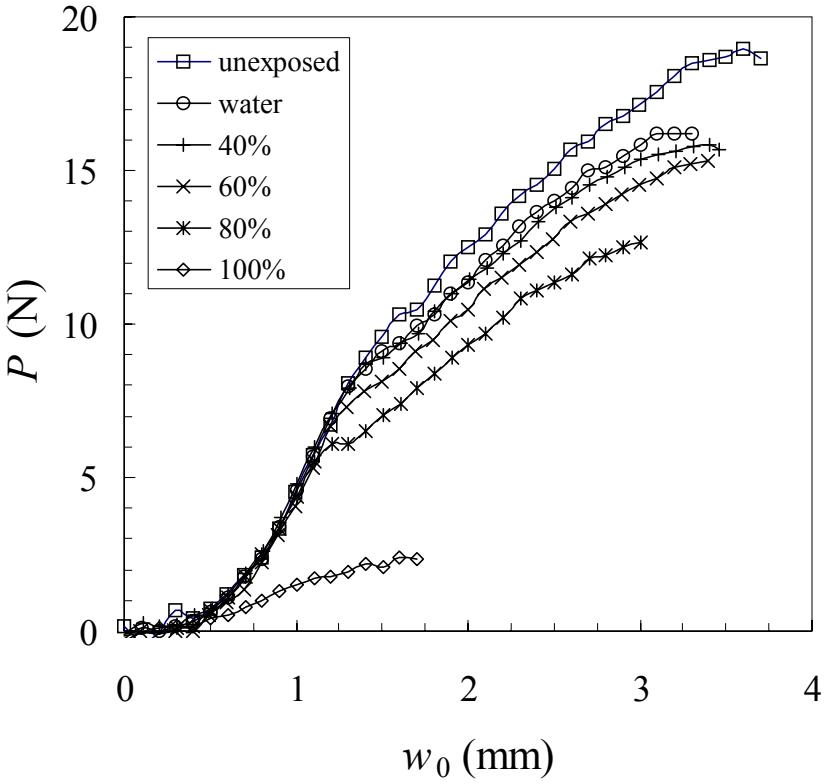

Figure 3-15 Load (P) vs. central shaft displacement (w_0) for various concentrations of methanol in water (0, 40, 60, 80, 100 wt. %)

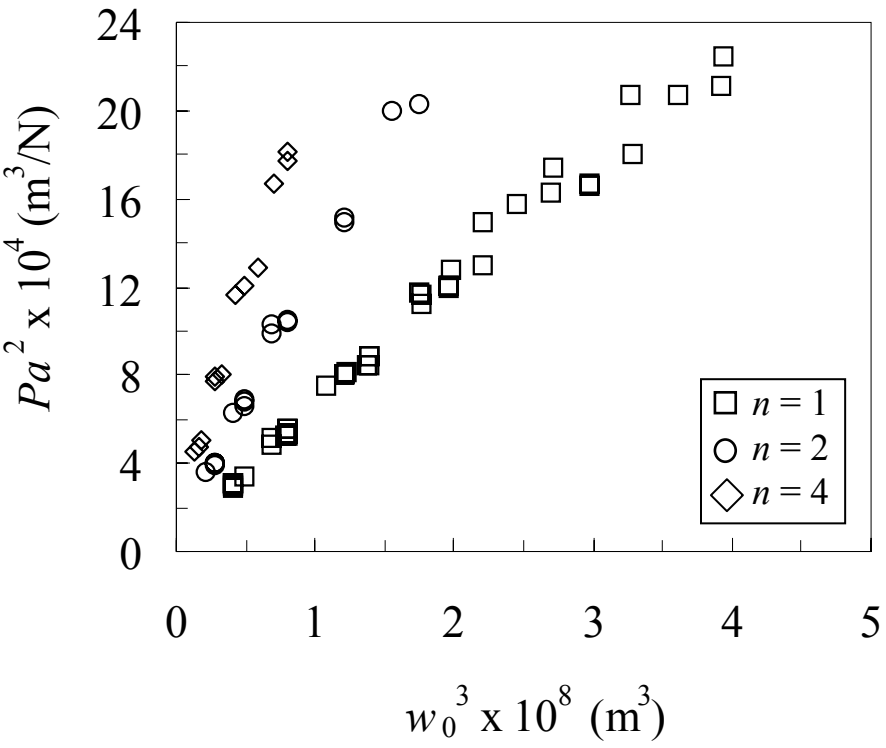

Figure 3-16 Linearized plot of equation 7, $P\,a^2$ vs. $w_0{}^3$ for n = 1(□), 2 (o), and 4 (◊)

3.3 Moisture Degradation of Epoxy Adhesive Bonds Measured by the Shaft-Loaded Blister Test

3.3.1 Abstract

In this study, the shaft-loaded blister test was determined to be a relatively simple and convenient method for characterizing the degradation of adhesive bonds due to moisture exposure. An experimental sample for this shaft-loaded blister test was developed using reinforcing layers of Kapton® film. Moreover, the procedure for measuring the blister radius and corresponding adhesive fracture energy has been greatly simplified by eliminating the need for a video image recording system. The advantages and disadvantages of the shaft-loaded blister test (SLBT) were illustrated by studying the effect of relative humidity on the adhesion between a model epoxy and a quartz substrate. This work has provided further evidence of a critical relative humidity level for adhesion loss that has been observed in many epoxy systems.

3.3.2 Introduction

3.3.2.1 Critical Relative Humidity for Adhesion Loss

Water is often regarded as the primary agent in the reduction of service life and reliability of adhesive joints and composites.[1-3,101-103] Moisture affects nearly all adhesives performance because water is ubiquitous in the atmosphere and has a substantial affinity for both organic and inorganic materials. A class of adhesives that is particularly sensitive to moisture includes the epoxies. Characteristic of many epoxy – substrate systems is a dramatic loss of adhesion strength during environmental exposure above a critical relative humidity level.[102-111] A typical value of

this critical relative humidity level is near 70%, thus limiting the number of applications for these adhesives.

The mechanism of adhesion loss at a critical relative humidity is the subject of much speculation. The dramatic reduction in adhesion strength has been attributed to both physical and chemical changes resulting from moisture absorption in either the bulk of the adhesive or at the interface between the adhesive and substrate. Brewis et al.[108] and Cognard et al.[111] proposed that degradation of the interface is the basic cause for loss of adhesion strength. They suggest that bonds attributable to secondary forces at the interface are broken up by moisture, hydration of the oxide surface, and/or water condensation due to lowering of the vapor pressure by the presence of salt impurities at the interface. Lefebvre and coworkers present the most recent and detailed study of the critical relative humidity for adhesion loss.[102,109] In contrast to Brewis et al. and Cognard et al., Lefebvre and coworkers conclude that the changes in the bulk properties of the epoxy adhesive are responsible for the observed onset of adhesion loss at a critical relative humidity. They reported that the solubility, or mass of absorbed water, as a function of relative humidity increased abruptly at the critical relative humidity. Similar results led Gledhill et al.[103] to propose a critical water concentration in the bulk adhesive for adhesion loss to occur. Furthermore, the work of Lefebvre and coworkers suggests that capillary condensation, water condensation on water-soluble impurities, and the depression of the glass transition, are not responsible for the observed adhesion loss. They proposed that inter-chain hydrogen bonds are broken by absorption of water. Molecular simulations supported their hypothesis that water displaced the hydrogen bond network. However, results obtained by Karasz and co-workers[60] contradict the hypothesis that inter-chain hydrogen bonds are broken by absorption of water. Using nuclear magnetic resonance, Karasz and co-workers have shown in epoxies based on the

diglycidyl ether of bisphenol A (DGEBA) that no disruption of the hydrogen-bonding network occurs at room temperature in the hydrated epoxy resin.

3.3.2.2 Research Goal

In this research we explore the shaft-loaded blister test (SLBT).[64,90,93,112-114] The experiment utilizes the controlled displacement of a spherically capped shaft driven by a universal testing machine (UTM) as an alternative to driving blister growth by applying a fluid or gas media (Figure 3-17). As discussed in Section 3.2.2 the shaft-loaded blister test has a number of advantages for environmental testing of adhesives. The advantages and disadvantages of the SLBT will be highlighted by studying the effect of relative humidity on the adhesion between a model epoxy and a quartz substrate. This work also provides further evidence of a critical relative humidity level for adhesion loss that is observed in many epoxy systems.

3.3.3 Experimental

3.3.3.1 Materials

The model epoxy system is Epon 862 bisphenol-f resin (Shell Chemical Corporation) mixed with 10 parts hundred resin (phr) of 1,4-butanediol (added to increase the solubility of the curing agent) and cured with 3 phr of 4-methyl-2-phenylimidazole.[115] The model epoxy was cured for one hour at 130°C. More details can be found in the dissertation of Case.[36] The model epoxy was bonded to a quartz substrate approximately 3.6 x 3.6 cm^2 (1.5 x 1.5 inches square) with a 0.8 cm (0.31") diameter hole drilled in the center.

3.3.3.2 Blister Test Specimen Preparation

The quartz substrates were boiled in 98 M sulfuric acid for one hour at approximately 150°C to remove any organic contaminants on the surface. The substrates were then rinsed in deionized water to remove any trace of sulfuric acid on the surface. A pre-crack was fabricated by placing a 3/8" diameter piece of Kapton® PSA tape (acrylic PSA) over the hole in the center of the quartz substrate. The Kapton® PSA tape consists of a 25 micron (1 mil) thick Kapton® backing and a 37.5 micron (1.5 mil) thick acrylic pressure sensitive adhesive. The Kapton® PSA tape also provided additional mechanical reinforcement to the thin epoxy film at the highly stresses contact area between the coating and shaft-tip. The un-cured model epoxy was coated on to the quartz substrate. A 50 micron (2 mil) thick piece of Kapton® film was then placed on top of the epoxy coating. The Kapton® film acts as a mechanical reinforcing layer for the epoxy coating. The resulting adhesive coating is therefore a composite of the model epoxy, Kapton® PSA tape and Kapton® film. A schematic of the test specimen is shown in Figure 3-18. The sample was then cured in a convection oven. The resulting epoxy film was between 50 and 100 microns (2 and 4 mils) thick. Samples were conditioned at constant relative humidity (8, 29, 42, 71, or 98%) for 3 days at room temperature; long enough for the adhesive to be saturated. The relative humidity was controlled using saturated salt solutions.[116] After environmental exposure the samples were immediately tested at room temperature at ambient relative humidity (~50%). Three samples were tested for each relative humidity.

3.3.3.3 Determination of the Adhesive Fracture Energy

The adhesive fracture energy, G, can be calculated from the relationship between the blister radius, a, and load, P, using Equation 3-9.[90]

Equation 3-9

$$G = \left(\frac{1}{16\pi^4 Eh}\right)^{1/3}\left(\frac{P}{a}\right)^{4/3}$$

where E is the Young's tensile modulus, and h is the thickness of the adhesive coating. The advantage of Equation 3-9 is that it is a load-based equation and is independent of any plastic deformation in the adhesive which will be located at the contact area between the shaft-tip and adhesive coating.

To determine the crack length as a function of load, samples were tested by loading and unloading cycles, which were repeated up to seven times. As an example, the load as a function of the central shaft displacement for repeated cycles is shown in Figure 3-19. In this test procedure, the film was loaded and the crack was allowed to propagate a few millimeters. The load was then removed and the blister radius was measured using calipers. This procedure is different from the typical blister radius measurement. Usually, the crack is allowed to propagate continuously and is measured simultaneously with a video camera. An example of a typical load as a function of blister radius curve is shown in Figure 3-20. Utilizing loading and unloading cycles, considerable work involving measuring the blister radius with a video camera has been eliminated.

From the slope of the line shown in Figure 3-20 or from each individual point the fracture energy can be calculated using Equation 3-9 provided that the modulus of the coating is known. The modulus of the coating for the bi-layer film (Kapton® and epoxy) can be estimated from a simple rule of mixtures:

Equation 3-10

$$E_{\text{composite}} = v_{\text{Kapton®}}\, E_{\text{Kapton®}} + v_{\text{Model}}\, E_{\text{Model}}$$

Where $E_{\text{composite}}$ is the modulus of the composite, $v_{\text{Kapton®}}$ and v_{Model} are the volume fractions of the Kapton® backing and model epoxy, respectively, and $E_{\text{Kapton®}}$ and E_{Model} are the moduli of

the Kapton® backing and model epoxy, respectively. The Kapton® PSA tape is ignored because it is used only during crack initiation. The modulus of Kapton® is approximately 6 GPa.[117] The modulus of the model epoxy is approximately 2.5 GPa. An additional advantage of Equation 3-9 is that it is fairly insensitive to the value of the modulus of the film. Note the modulus of the film is lies in the denominator and is raised to the 1/3 power in Equation 3-9. This also reduces any error introduced by not knowing the change in modulus as a function relative humidity.

3.3.4 Results and Discussion

The resulting adhesive fracture energies calculated from the load-based equation as a function of relative humidity are shown in Figure 3-21. At 8, 29, and 42% relative humidity the film ruptures before debond growth occurs according to Figure 3-21. Also at 71% and 98% relative humidity, the adhesive interface is degraded sufficiently for crack propagation to occur. The resulting strain energy release rates were 163 +/- 27 and 111 +/- 27 J/m^2 for 71% and 98% relative humidity respectively. Although the average strain energy release rate of the 98% humidity sample is less than the 71% as expected, the difference is not substantial if the standard deviation is considered. These results, which show a dramatic loss of adhesion at 70% relative humidity, are consistent with a critical relative humidity level for adhesion loss.[102-111]

Despite the axisymmetric geometry, short saturation time, and relatively simple sample preparation and test procedure, the shaft-loaded blister test has some shortcomings. As illustrated in this study, the adhesive film can rupture before debonding can occur. This is attributable to the large stresses generated within the film near the contact area between the film and shaft tip. Significant, visible plastic deformation at the contact area may still arise even if film rupture does not occur and crack propagation takes place. However, if plastic deformation is confined solely to the center of the blister and not at the crack tip, the fracture mechanics analysis remains

valid.[64] Plastic deformation and film rupture is a common problem of many adhesive coating test methods, and is associated with their small load-bearing capacity, their thinness, and their relatively strong adhesion.[79] For these reasons the SLBT is most suitable to environmental testing where the adhesive interface has been substantially degraded. A decrease in interface toughness reduces the applied stresses on the adhesive coating during the fracture process. Utilizing a higher strength material for the backing, such as a metal, could provide enough reinforcement to produce crack growth at lower values of relative humidity, rather than film rupture. An alternative means for preventing film rupture would be to reduce the applied load, and therefore the stress on the film. This strategy is employed in sub-critical fracture experiments which are discussed in detail in Section 3.4.

3.3.5 Conclusion

The SLBT was demonstrated to be a simple and informative method for characterizing the degradation of adhesive bonds due to environmental stress. These results illustrate the benefits and shortcomings of the SLBT, suggesting that this test method is most suitable to environmental testing of specimens where the adhesive fracture energy has been substantially reduced. Moreover, this study has also provided an additional example of a critical relative humidity for adhesion loss which has been previously observed in many epoxy systems.

3.3.6 Figures

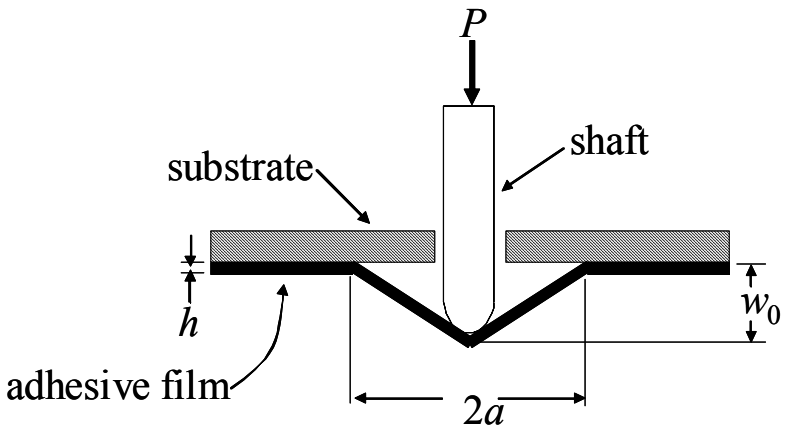

Figure 3-17.Schematic of the shaft-loaded blister test

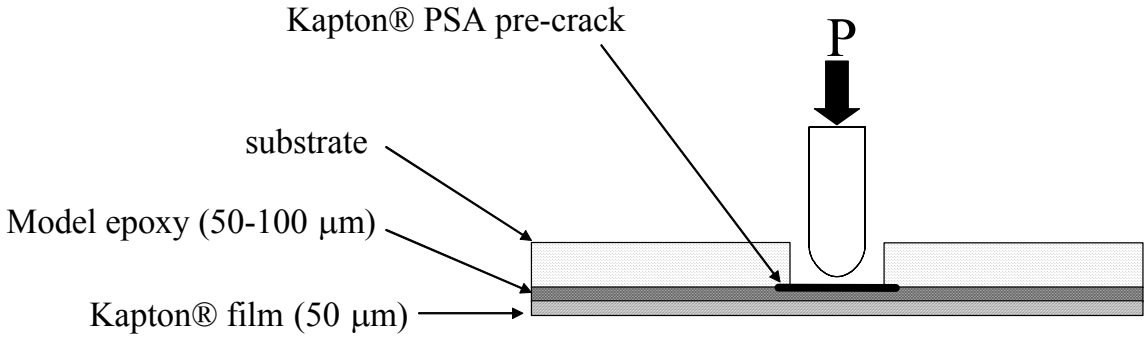

Figure 3-18 Schematic of shaft-loaded blister test specimen

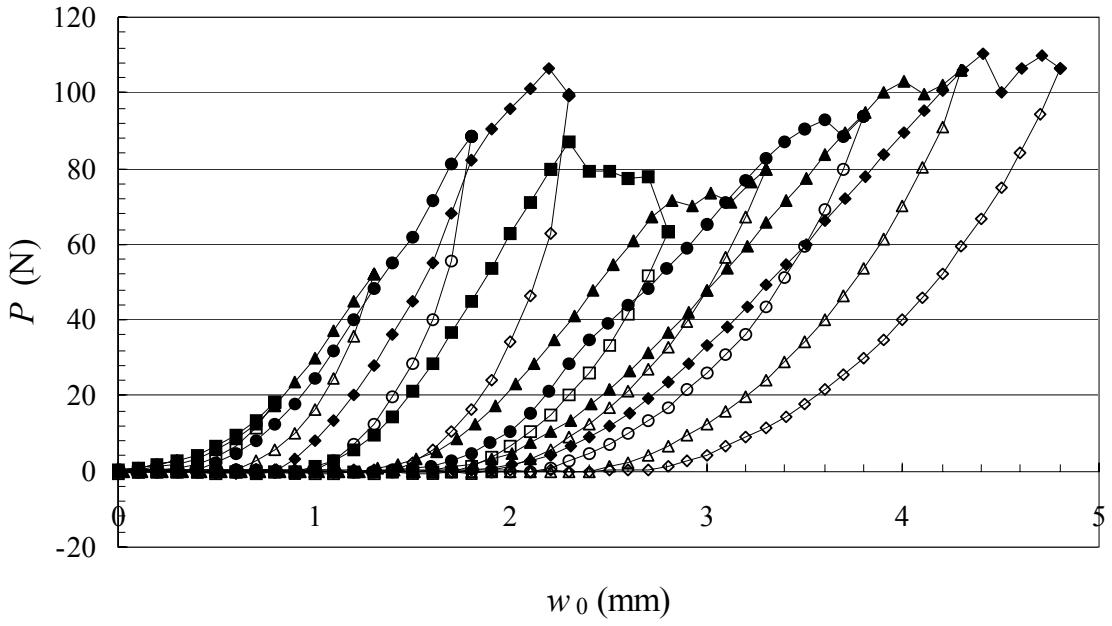

Figure 3-19 Successive load as a function of central shaft displacement curves for 98% relative humidity. The filled in symbols are the loading curves and the unfilled symbols are the unloading curves.

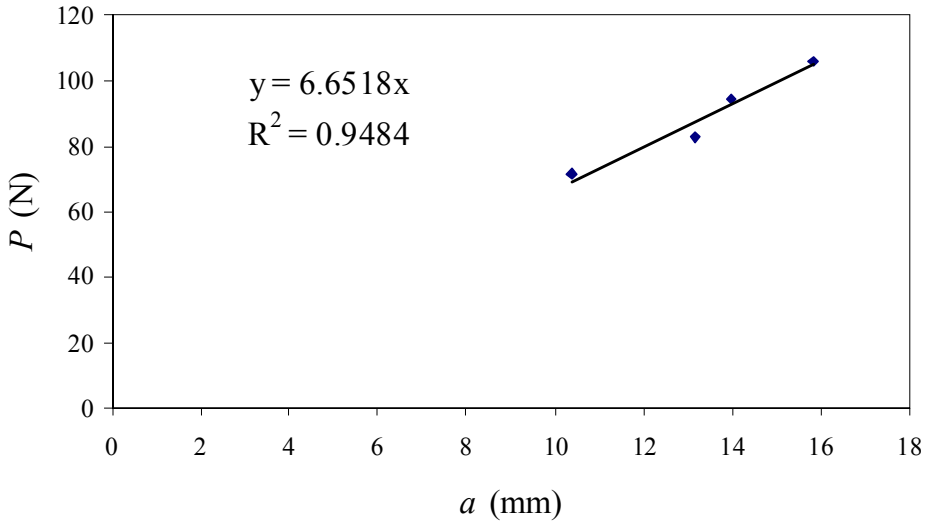

Figure 3-20. Load vs. blister radius for 98% relative humidity

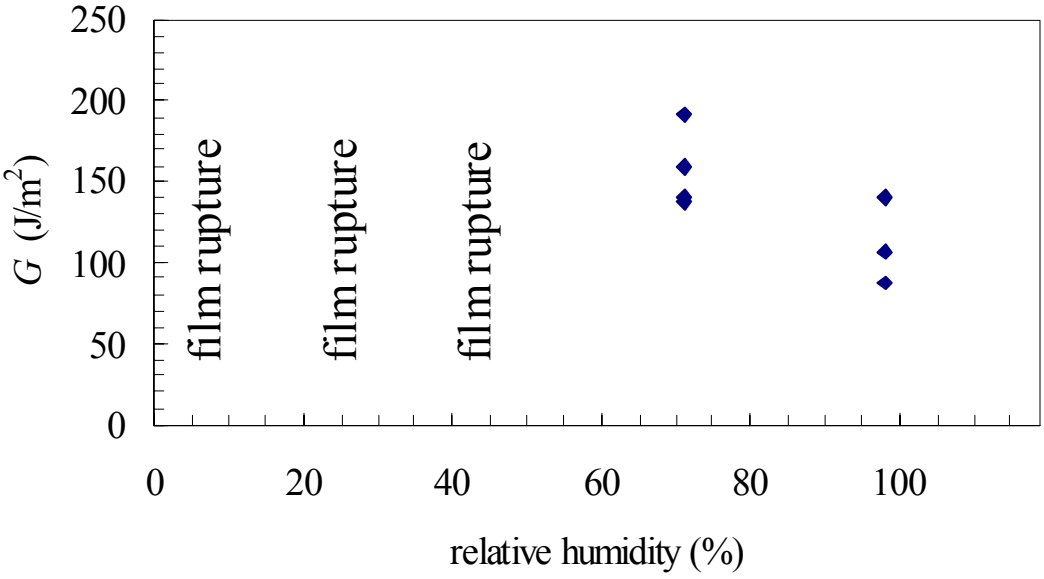

Figure 3-21. Summary of strain energy release rates G (J/m^2) vs. relative humidity for critical SLBT

3.4 Environmental Studies of Adhesive Bonds Using the Sub-critical Shaft-Loaded Blister Test

3.4.1 Abstract

The shaft-loaded blister test has been adopted for sub-critical fracture testing. Two different epoxy adhesives and environments were investigated. In both cases, the epoxy adhesive was bonded to a silicon wafer which had a silicon oxide surface. The adhesion of a model epoxy as a function of relative humidity (42, 71, and 98%) at room temperature was investigated. In addition, the sub-critical fracture behavior of a commercial filled epoxy, designated as L4, and exposed to water as function of temperature (60, 70, and 80°C), was also investigated. These results were correlated to the bulk (non-bonded) adhesive diffusion behavior. This research suggests that the constant-load sub-critical shaft-loaded blister test is a new and valuable technique for studying the effects of the environmental degradation on adhesive joints and coatings. Given the great difficulty in testing thin, strongly adhered coatings and films, this technique is particularly attractive.

3.4.2 Introduction

3.4.2.1 Sub-Critical Adhesion Testing

Sub-critical adhesion testing is of practical interest to engineers because it explores adhesive debonding in a range of crack velocities and applied strain energy release rates, G, which are significantly less than required for catastrophic failure. Sub-critical adhesion testing therefore more closely resembles the failures observed in the actual application or service of the adhesive. In these more realistic situations, degradation and failure takes place over long periods of time.

In such cases, crack growth can be driven by small applied loads generated by residual stresses, thermomechanical cycling, and mechanical or vibrational loading.[8] Furthermore, sub-critical testing reduces the ambiguity associated with the measured adhesion energy dependence in crack velocity, which is associated with viscoelastic effects at the crack tip.

Sub-critical adhesion measurements can be carried out at any temperature and in the presence or absence of moisture or other environmental fluid. The results are typically presented in the form of the average crack velocity, v (da/dt) (m/s), as a function of the applied strain energy release rate (G) or crack driving energy (J/m^2). A schematic of a typical v-G curve is shown in Figure 3-22 (taken from Gurumurthy *et al* [118]). When comparing different environmental conditions and adhesive systems at a constant velocity, the applied crack driving energy decreases as the aggressiveness of the environment or chemical activity increases. Figure 3-22 illustrates three regions typically found in a v-G curve, where changes in slope indicate a change in the rate limiting step for crack advancement.[8,119,120] Region III is associated with critical fracture events and for classic fracture of bulk glasses is independent of the environment. Region II depends strongly on the environment, little on the crack driving energy, and is characteristic of fracture where diffusion of the penetrant or environmental fluid to the crack tip is the rate limiting step to crack advance. Region I is characteristic of low crack velocities and low applied crack driving energies. For bulk fracture of glasses in Region I, crack growth was found to be controlled by bond rupture and healing, the ratio of the two governed by the crack driving energy.[121] Furthermore, the crack velocity in Region I is also controlled by the stress-activated chemical reaction of the penetrant with the bonds at the crack tip.[118] At crack velocities below Region I there exists a threshold value of crack driving energy, G_{Th}, below which no crack propagation is observed.

The *v*-*G* curve can adopt several different shapes that are characteristic of the mechanism of interfacial degradation. Lane et al. observed two characteristic shapes of the *v*-*G* curve as the temperature is increased or as the chemical activity increases, shown in Figure 3-23 [121]. In the first case (left graph of Figure 3-23), as the chemical activity is increased, G_{Th} and region II shift to smaller applied crack driving energies, which Lane et al attribute to a stress-dependent chemical reaction at the crack debond tip. In the second case (right graph of Figure 3-23), as the chemical activity is increased the plateau region (region II and corresponding value of v*) increases and a decrease in the G_{Th} (region I) is not observed. Lane et al indicate that this is consistent with a steric hindrance mechanism where the crack tip is less than a size of the penetrant species.

Gurumurthy *et al*. [118] observed for an epoxy-polyimide interface, as the moisture content was kept constant and the temperature increased, there was an decrease in both v^* and G_{Th}, which is consistent with a stress and temperature dependent chemical reaction at the crack tip. Although not shown, alternatively, the *v*-*G* curve may also take on the shape of a backwards letter "C" where the applied crack driving energy goes through a maximum. This behavior is attributable to viscoelastic effects.

Sub-critical fracture testing can be used to predict the durability of adhesive joints. Curley et al made theoretical predictions of the fatigue lifetime of adhesive joints based on mechanical fatigue data.[122] Fatigue data measures the rate of crack growth per cycle (da/dN), rather than rate of growth per second (da/dt), as a function of crack driving energy. The approaches developed in fatigue (da/dN) can therefore be extended to *v*-*G* experiments (da/dt). In the approach of Curley et al, lifetime predictions were made by modeling the (da/dN) vs. *G*

curve and then calculating the number of cycles until failure based on an initial flaw size and the applied stress in the joint.

Traditionally, sub-critical fracture tests specimens have been the laminated beam type where the adhesive is bonded to rectangular rigid adherends. Examples of the laminated beam type experiments are the double cleavage drilled compression specimen[123], four-point flexure samples[124], double cantilever beam wedge test[106], and the asymmetric double cantilever beam test[118]. The advantages of laminated beam type specimens are: 1) the adhesive is loaded elastically away from the crack tip, 2) high strain energy release rates are obtainable, 3) the fracture mechanics models are well understood, and 4) the specimens are often self-loading. For the double cantilever beam wedge test, the strain energy release rate decreases as a function of $1/a^4$ yielding a wide range of values of G which can rapidly approach a threshold value. The disadvantages of all these tests are that they may require sophisticated experimental set-up to measure the crack length (video camera, acoustic methods, or electrical). Also the time for fluid saturation of the adhesive may be long because the adhesive is sandwiched between two impermeable substrates and only edge diffusion into the adhesive may occur.

With respect to the laminated beam type specimens, the advantages of the shaft-loaded blister test is that the time to saturation is reduced considerably because it is an open face coating allowing diffusion through the top of the coating rather than edge diffusion. In addition, the specimen geometry is axisymmetric, which reduces any misleading edge effects caused by degradation of the interface away from the crack tip. The disadvantages of the shaft-loaded blister test are that the facture mechanics models have not been studied as extensively as the laminated beam specimens; and, like most coatings tests, the value of the strain energy release rates is limited by the film's mechanical strength. In the case where the film strength is low or if

the intrinsic interfacial toughness is high, film rupture can occur, as was observed in the previous study. Furthermore, the strain energy release rate decreases as a function of $1/a^{1/3}$ yielding a narrow range of values of G that slowly approach a threshold value. Several other disadvantages exist which we will discuss later.

3.4.2.2 Residual Stress Effects in Critical and Sub-Critical Experiments

Residual stresses can affect the fracture energy of an adhesive if, during debonding, these stresses change.[125] For the peel test and blister test tensile residual stresses reduce the energy release rate. Conversely, compressive stresses increase the energy release rate. Note that for dry polymeric adhesives bonded to low coefficient of thermal expansion silicon substrates, these stresses are tensile. However, due to exposure to elevated temperatures and the absorption of water, the state of stress in the SLBT specimens is unknown. Allen and Senturia have pointed out that the energy balance for a blister test does not need to consider residual stress (tensile), because as long as the edges of the film are attached to the substrate the residual stresses are not relieved.[82] This is also the general case for thin-layer laminated beam specimens, where the adhesive remains adhered and the strain energy stored in the layer due to residual stress is not released.[126] Furthermore, Allen and Senturia note that in the pressurized blister test at large pressures the effects of residual stress are overwhelmed by the stresses generated in the film during testing. However, in the pressurized blister test the residual stress effects the load deflection behavior. Thus, when utilizing the critical debond pressure; the value of G was less than expected because of the extra contribution to debonding by residual stresses. Wan and coworkers studied the load-deflection behavior of the blister test and provide a comprehensive list of existing work on residual stresses in blister tests.[127]

3.4.3 Experimental

3.4.3.1 Materials

3.4.3.1.1 L4 commercial filled epoxy

L4 is a commercial, filled (21% by weight) epoxy adhesive manufactured by Loctite and obtained from Hewlett-Packard Co. The L4 epoxy is cured at 140°C for thirty minutes. The glass transition temperature is 110°C. The modulus is approximately 4 GPa. Details of the material properties can be found elsewhere.[36] A coating thickness on average of 100 +/- 20 microns was used for the L4 specimens. Distilled water at temperatures of 60, 70, and 80°C was used as the environmental fluid. Mass uptake experiments were performed also at 60, 70, and 80°C.

3.4.3.1.2 Model Epoxy and Relative Humidity

A description of the model epoxy adhesive can be found in Section 3.3.3.1. Details of the model epoxy can also be found in the work of Case and Ward.[36,115] coating thickness on average of 75 +/- 25 microns was used for the model epoxy specimens. The entire SLBT specimen was paced in a large glass vessel and conditioned at constant relative humidity (42, 71, or 98%) at room temperature. The relative humidity was controlled using saturated salt solutions.[116]

3.4.3.1.3 Silicon Wafer Substrate

The substrate used in this study was a 152.4 mm (6” inch) diameter silicon wafer with a 10 nm thick thermally grown layer of silicon oxide. These wafers were supplied by the Hewlett-Packard Comapny.

3.4.3.2 Sample Preparation of Constant Load Sub-Critical SLBT Specimens

Two types of self-loaded SLBT specimens were used in this study. Specimens were self-loaded by suspending a known mass from the center of the blister. The first type of specimen was used in the model epoxy study where the specimen was completely immersed in the humid environment. The second type of specimen was used in the L4 adhesive study. Although the sample must also be self loaded, the sample is not completely immersed in the fluid environment. In this case, the fluid is confined solely in the fluid reservoir formed by the adhesive and substrate (see Figure 3-24).

3.4.3.2.1 Preparation of Adhesive Coating and Substrate

A hole approximately 12.5 mm in diameter is fabricated in the center of the silicon wafer using a diamond coated drill bit and a Dremel® tool. Extreme care must be taken when drilling the brittle wafers. The wafer is then rinsed with IPA and blown dry with ultra-high purity nitrogen gas. The hole in the wafer is then covered with a 19 mm (3/4 inch) diameter piece of Kapton® PSA tape (acrylic based adhesive). The Kapton® tape serves two purposes: 1) it forms a pre-crack for the crack to initiate and 2) acts as an additional mechanical reinforcement layer for the adhesive in the vicinity where the load is suspended. The wafer is coated with epoxy adhesive using a pneumatically driven doctor blade. A 152.4 x 152.4 mm (6" x 6") square piece of Kapton® (50 microns thick) is carefully applied on the wafer to avoid disrupting the adhesive and the formation of air bubbles. The coated wafer (with Kapton®) is then cured and removed from the oven and is placed in a dessicator to slowly cool down (approximately 30 minutes).

3.4.3.2.2 Preparation of Model Epoxy Self-Loaded SLBT Specimen (No Self-Contained Fluid Environment)

To develop a sub-critical blister test specimen the sample must be self-loading. Also, the integrity of the thin adhesive coating must be maintained and the sample must be exposed to the fluid in this experiment. To fabricate a simple self-loading constant load SLBT specimen a hole is punched in the coating that can accommodate a 2.54 mm (or 4/40") stainless steel machine screw. The machine screw acts as the fastener from which to suspend the load (via a flexible copper wire). The punched hole containing the screw is sealed with a room temperature cure epoxy (Devcon 2-ton Epoxy). A photograph of this type of self loading specimen with the applied adhesive, Kapton® reinforcement layer, and attached screw is shown in Figure 3-26. The entire specimen with the suspended weight was then set in the environmental chamber. The entire adhesive is exposed to the moist environment during testing and is saturated.

3.4.3.2.3 Preparation of L4 Self-Loading SLBT Specimen with Self-Contained Fluid Environment

The L4 adhesive SLBT specimens require a self-contained fluid environment shown schematically in Figure 3-25. The self-contained environment is necessary to minimize the space occupied by the wafers in the convection oven. The self-loaded sample described in the prior section can be modified using a pair of o-rings, a Teflon® sheet, a steel sheet and some clamps. As shown in Figure 3-25 the fluid reservoir is formed by the blister and substrate and sealed with a rigid top-piece sheet of steel or aluminum and two silicon rubber o-rings: a center (smaller) o-ring and an outer (larger) o-ring. Between the o-rings and the steel is a thin piece of Teflon® film which acts as a barrier and curbs any chemical reaction which may occur between the metal

sheet and water. Pressure on the o-ring is achieved using Kant-twist® c-clamps. Given the brittleness of the wafer it is important to use delicate c-clamps to avoid damaging the wafer. The o-rings and Teflon® are cleaned with isopropyl alcohol to provide an excellent seal. To ensure that there is no difference in pressure between the blister and outside environment (a vacuum), a small vent is utilized. The vent is a syringe needle that has been inserted into the outer o-ring creating a passage for gas to travel from the fluid reservoir to the outside atmosphere. The center (smaller) o-ring has a large cut to allow for the free passage of water and gas inside the fluid reservoir. A significant disadvantage of this experimental set-up is the inevitable evaporation and small coating thickness that facilitates fluid loss by permeation. Because of these factors, it is difficult to test volatile fluids such as the ink vehicles supplied by Hewlett-Packard.

3.4.3.3 General Procedure and Analysis for Sub-Critical Blister Testing

3.4.3.3.1 Model Epoxy

As mentioned previously, the loaded model epoxy specimens are placed entirely in a constant relative humidity environment. Samples are removed periodically to measure the blister radius as a function of time. The blister radius is measured with calipers.

3.4.3.3.2 L4 Adhesive

The reservoir is filled with distilled water up to the top level of the o-rings and sealed up. The entire set up can be then placed in the convection oven. A photograph of the L4 specimens in a convection oven is shown in Figure 3-27. Samples are removed periodically to measure the blister radius as a function of time. After measuring the crack length, the fluid reservoir is topped off with water.

3.4.3.3.3 Analysis

Using the load-based equation (Equation 3-11), from the load, P, and blister radius, a, the crack driving energy, G, can be calculated.

Equation 3-11
$$G = \left(\frac{1}{16\pi^4 Eh}\right)^{1/3}\left(\frac{P}{a}\right)^{4/3}$$

The blister radius is measured periodically with a micrometer as function of time. Two or three micrometer measurements are utilized to calculate the average blister radius. These were used to determine the average crack velocity v or (da/dt). The crack velocity is expressed in units of m/s.

The modulus of the coating for the bi-layer film (Kapton® and epoxy adhesive) can be estimated from a simple rule of mixtures:

Equation 3-12
$$E_{\text{composite}} = v_{\text{Kapton®}}\, E_{\text{Kapton®}} + v_{\text{Epoxy}}\, E_{\text{Epoxy}}$$

Where $E_{\text{composite}}$ is the modulus of the composite, $v_{\text{Kapton®}}$ and v_{Epoxy} are the volume fractions of the Kapton® backing and epoxy, respectively, and $E_{\text{Kapton®}}$ and E_{Epoxy} are the moduli of the Kapton® backing and epoxy, respectively. The modulus of Kapton® is approximately 6 GPa.[117] Because the film tensile rigidity (Eh) is in the denominator of equation Equation 3-11 and is also raised to the 1/3 power, the expression for the crack driving energy is relatively insensitive to the value of (Eh). The advantage is that the value of G is insensitive to the numerical values of the modulus and thickness which are a function of the temperature and fluid content.

3.4.3.4 Mass Uptake Experiments

Diffusion coefficients, D, and equilibrium moisture saturation level, M_∞, of water in the L4 adhesive as a function of temperature were obtained by traditional mass uptake experiments. Mass uptake specimens had dimensions of 10 mm x 50 mm x 0.5 mm and were cured in silicone

rubber molds. Molds were sprayed with non stick release agent prior to adding the epoxy. The molds were also preheated to 60°C to reduce the viscosity of the epoxy and bubble formation. Any visible bubbles or defects on the sample surface were smoothed away with sandpaper and a Dremel® tool. Samples were condition in water at the respective temperature and periodically removed, patted dry, and weighed on a balance. Three samples of each temperature were tested. The mass uptake values as a function of time were used to determine the diffusion coefficient using the short time solution to Fick's law. Details of the solutions to Fick's Law can be found in the Appendix (Section 3.4.7). The diffusion coefficient typically follows an Arrhenius relationship defined in Equation 3-13.[56]

Equation 3-13
$$D = D_0 e^{-(Ea/RT)}$$

Where D_0 is a constant coefficient, E_a is the activation energy for diffusion, R is the universal gas constant and T is the temperature in Kelvin.

3.4.4 Results and Discussion

3.4.4.1 Model Epoxy in a Humid Environment (Room Temperature)

The *v*-*G* curves obtained for the model epoxy as a function of relative humidity are shown in Figure 3-28. For the 42% and 71% relative humidity conditioning, 2 samples were tested. For the 98% relative humidity, 3 samples were tested. Each *v*-*G* curve begins at roughly 40 J/m^2 of crack driving energy. All samples exhibited diffusion controlled Region II crack growth behavior with some stress dependence. The average values of the plateau velocity as well as a single standard deviation are listed in Table 3-9. The graph of the plateau velocity as a function of relative humidity is shown in Figure 3-29. The plateau velocity, *v**, did not increase linearly with relative humidity although the velocity at 42% relative humidity was slower than both 71% and 98%

relative humidity. This is in contrast to model proposed by Wiederhorn[128] for Region II crack growth of glass in moist air. Weiderhorn showed that the plateau velocity is linearly dependent on the relative humidity which agrees well with what has been observed in the literature[124,129].

Table 3-9 The plateau velocity, v^*, as a function of relative humidity for the model epoxy-silicon oxide adhesive system

	42 % rh	*71% rh*	*98% rh*
Average v^* (m/s)	1.6×10^{-9}	3.6×10^{-9}	3.3×10^{-9}
Standard Deviation	7.2×10^{-10}	3.0×10^{-10}	1.9×10^{-9}

The average and single standard deviation of the threshold values of G as function of relative humidity are listed in Table 3-10. The results in Table 3-10 show that the threshold values of G are similar for 71% and 98% relative humidity. Moreover, the threshold value of G for 42% relative humidity is significantly higher than either the 71 or 98% relative humidity cases. The independence of the threshold value of G on relative humidity was unexpected. The threshold value of G is theoretically dependent on the partial pressure of water and has been confirmed experimentally.[124,129] The sub-critical SLBT may not be sensitive enough to detect any significant differences between the 71% and 98% relative humidity conditioning. This postulate is plausible, given the similarity between the values of G measured by the traditional SLBT method (Section 3.3) and the experimental uncertainty. The experimental uncertainty is discussed in the next section. In addition, condensation at the crack tip would negate any relative humidity differences and would also lead to similar threshold value of G observed for 71% and 98% relative humidity.

Table 3-10 The threshold value of G as function of relative humidity for the model epoxy-silicon oxide adhesive system.

	42 % rh	*71% rh*	*98% rh*
Average G_{Th} (J/m^2)	25.2	10.2	11.5
Standard Deviation	4.9	2.1	2.6

Error is introduced in the calculation of the values of ,G, and crack velocity ,v, that are associated with measuring the blister radius, a. The error associated with measuring the blister radius with the micrometer is approximately ± 0.2 – 0.3 millimeters. In addition, the blister may not be entirely symmetric. In the most extreme cases, the difference between two measurements of the same blister radius was 0.5 mm. The error attributable to the blister radius measurement depends on the magnitude of the value of G and crack velocity. Values of G that ranged between 20-50 J/m^2 had a small error ranging from ± 1-2 J/m^2. Values of G that ranged between 1 - 20 J/m^2 had an error between ± 0.1 – 0.5 J/m^2. Crack velocities on the order of 10^{-8} and 10^{-9} m/s had errors on the order of a ± 10%, which was much less than the inherent scatter of the experiment. The error was significant for crack velocities approaching 10^{-10} m/s or less; however, at these crack velocities the experimental limit of the measurement is being rapidly approached and these cracks appear to arrest.

The sub-critical results of the model epoxy-silicon oxide wafer adhesive system can be compared to the results of the model epoxy-quartz adhesive system (Section 3.3). The quartz substrate and silicon wafer substrate are expected to have similar surfaces given that they both are silicon oxide. In the model epoxy-quartz experiments, evidence was presented that suggested there was a critical level of relative humidity where adhesion loss occurred. At a relative

humidity of 42%, the reinforced epoxy film ruptured and the adhesive fracture energy was not measured. Utilizing the constant load sub-critical SLBT the adhesive was characterized by its plateau velocity, v^*, and threshold value of G. Therefore, by reducing the applied strain energy release rate and consequently the applied stresses in the adhesive coating, the integrity of the epoxy coating was maintained and adhesive could be debonded. In addition, from the sub-critical SLBT experiments, the evidence of a critical level of relative humidity for adhesion loss was less dramatic. These results suggest the constant-load sub-critical shaft-loaded blister test is promising new technique for studying the effects of the environmental degradation on adhesive joints and coatings. Given the great difficulty in testing thin, strongly adhered coatings and films, this technique is particularly attractive.[65]

3.4.4.2 L4 Adhesive in the Water Environment (60, 70, and 80°C)

3.4.4.2.1 Constant Load Shaft-Loaded Blister Test

The v-G curves obtained for the L4 adhesive in water as a function of temperature are shown in Figure 3-30. The number of specimens tested was three for both 60°C and 80°C, and 4 for the 70°C condition. Each v-G curve begins at an applied crack driving energy of roughly 40 J/m^2. All samples exhibited diffusion controlled Region II crack growth behavior with some stress dependence. As the temperature was increased, the plateau velocity, v^*, was observed to increase and the threshold value of G was observed to decrease. The average values of the plateau velocity obtained at approximately at 30 J/m^2 as well as the standard deviation are listed in Table 3-11. The plateau velocity is expected to follow an Arrhenius dependence similar to that of the diffusion coefficient because both phenomena are believed to share a similar mechanism. Replacing the appropriate terms in Equation 3-13 results in the following expression:

Equation 3-14 $$v^* = v^*_0 \, e^{-(Ea/RT)}$$

where v^*_0 is a constant coefficient, E_a is the activation energy for Region II crack growth, R is the universal gas constant and T is the temperature in Kelvin. An Arrhenius plot is shown in Figure 3-31. Utilizing Equation 3-14 the activation energy was calculated to be 126 kJ/mol.

Table 3-11 The plateau velocity, v^*, as a function of temperature for the L4-silicon oxide adhesive system in water

	60°C	*70°C*	*80°C*
Average v^* (m/s)	2.1×10^{-9}	6.5×10^{-9}	2.8×10^{-8}
Standard Deviation	3.5×10^{-10}	3.9×10^{-9}	8.4×10^{-9}

The average threshold values of G as function of temperature and a single standard deviation are listed in Table 3-12. The threshold values of G were also analyzed in an Arrhenius analysis. Replacing the appropriate terms in Equation 3-13 results yeilds the following expression:

Equation 3-15 $$G_{th} = G_0 e^{-(Ea/RT)}$$

Where G_0 is a constant coefficient, E_a is the activation energy for threshold value of G, R is the universal gas constant and T is the temperature in Kelvin. An Arrhenius plot is shown in Figure 3-32. Utilizing Equation 3-15 the activation energy was calculated to be 222 kJ/mol.

Table 3-12 The threshold value of G as function of temperature for the L4 epoxy-silicon oxide adhesive system exposed to water.

	60°C	*70°C*	*80°C*
Average G_{Th} (J/m^2)	19.5	6	0.2
Standard Deviation	1	1	0.1

3.4.4.2.2 Bulk Diffusion Measurement

The diffusion coefficient, D, and equilibrium moisture saturation level, M_{sat}, of water in the bulk (non-bonded) L4 adhesive as a function of temperature were obtained by mass uptake experiments. The temperature dependence of the absorption behavior and the diffusion controlled Region II behavior of the sub-critical SLBT were compared. These results were also used to predict the moisture content of L4 adhesive joints and coatings used in the impedance studies. A graph of the normalized percent moisture uptake as a function of the square root of time (seconds) normalized by the sample thickness for each temperature is shown Figure 3-33. Only the initial Fickian stage of diffusion is shown in Figure 3-33. The L4 epoxy exhibits two-stage or non-Fickian diffusion at all tested temperatures, which is characteristic of many epoxy systems. The graph of the percent moisture uptake as a function of the square root of time (seconds) normalized by the sample thickness for each temperature is shown in Figure 3-34. Figure 3-34 illustrates the non-Fickian behavior observed for all three temperatures. The diffusion coefficient and equilibrium moisture saturation level as a function of temperature are listed in Table 3-13 and Table 3-14 respectively. As the temperature is increased, the diffusivity

increases. The equilibrium moisture saturation level appears to be independent of the temperature.

Table 3-13 The average diffusion coefficient, D, of water in the L4 epoxy as a function of temperature. A single standard deviation is also listed.

	60°C	*70°C*	*80°C*
Average D (cm^2/s)	1.3×10^{-8}	2.2×10^{-8}	3.8×10^{-8}
Standard Deviation	1.7×10^{-9}	1.9×10^{-10}	8.5×10^{-10}

Table 3-14 The average equilibrium moisture saturation level, M_∞, of water in the L4 epoxy as a function of temperature. A single standard deviation is also listed.

	60°C	*70°C*	*80°C*
Average $\%M_\infty$ (grams)	2.5	2.6	2.5
Standard Deviation	0.1	0.1	0.1

3.4.4.2.3 Discussion of Activation Energies

The Arrhenius plot of the diffusion coefficient is shown in Figure 3-35. The calculated activation energy for the diffusion process is 53 J/mol. This value falls in the expected range of activation energies for moisture diffusion into epoxy adhesives, which typically range between 30 – 50 kJ/mol[59]. The activation energies for the plateau velocity and threshold value of G are 126 J/mol and 222 J/mol, respectively. These values are an order of magnitude greater than the activation energy for diffusion. This is not unexpected given that both the plateau velocity and threshold value of G depend not only on the rate of transport of fluid to the crack tip but also on the

applied stress. The dependence of the Region II crack velocity and threshold value of G on the applied stress is evident from the slope of the v-G curve. The idea that rate limiting step for the Region II crack growth that is not diffusion controlled is supported by the sub-critical SLBT relative humidity study of the model epoxy as well as and preliminary results in 2003 from Singh and Dillard at Virginia Tech.

In the model epoxy adhesive SLBT study, the specimens were stored long term in the moist environment and are therefore entirely saturated with moisture. As a consequence, moisture was always present near the crack tip. Effectively, the process of diffusion of moisture to the crack tip has been "turned off". Nevertheless, Region II diffusion controlled crack growth was observed despite the fact the adhesive was saturated. This suggests that Region II behavior is not solely dependent on diffusion, but depends also on stress. Similar, unpublished, results were obtained by Singh and Dillard (Virginia Tech, 2003) who studied sub-critical fracture of the L4 epoxy in fluid environments using the wedge test. They observed similar v-G curves between samples that were saturated with fluid before testing and samples that were not preconditioned.

.

3.4.5 Summary

The shaft-loaded blister test was adopted for sub-critical fracture testing by applying a self-loading mechanism whereby a mass is suspended from the center of the inverted blister. The adhesion of the model epoxy to silicon oxide as function of relative humidity (42, 71, and 98%) at room temperature was characterized. Notably, the adhesion at low humidity (42%) was measured, where the traditional SLBT was unsatisfactory. An Arrhenius analysis of the L4 epoxy and the sub-critical fracture behavior of the saturated model epoxy adhesive suggest that the Region II behavior is not solely dependent on the diffusion of fluid to the crack tip. These

results suggest the constant-load sub-critical shaft-loaded blister test is promising as a new technique for studying the effects of the environmental degradation on adhesive joints and coatings. In particular, the application of the sub-critical SLBT technique for testing adhesive coatings is promising given their typical experimental difficulties.

3.4.6 Figures

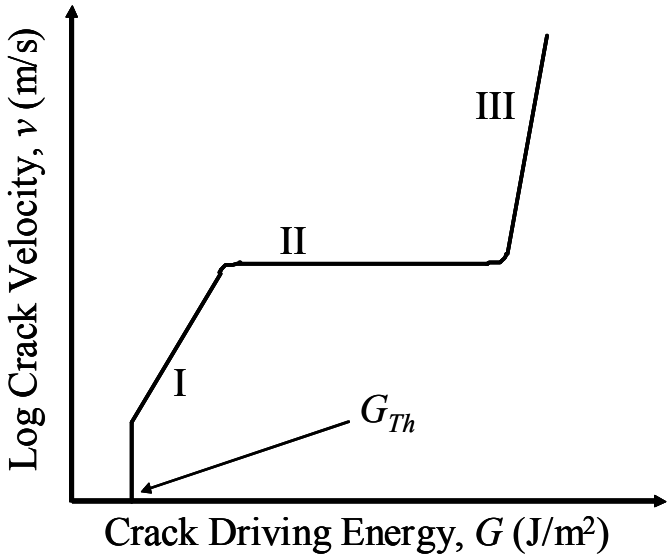

Figure 3-22. Schematic of v-G curve illustrating three region of crack growth

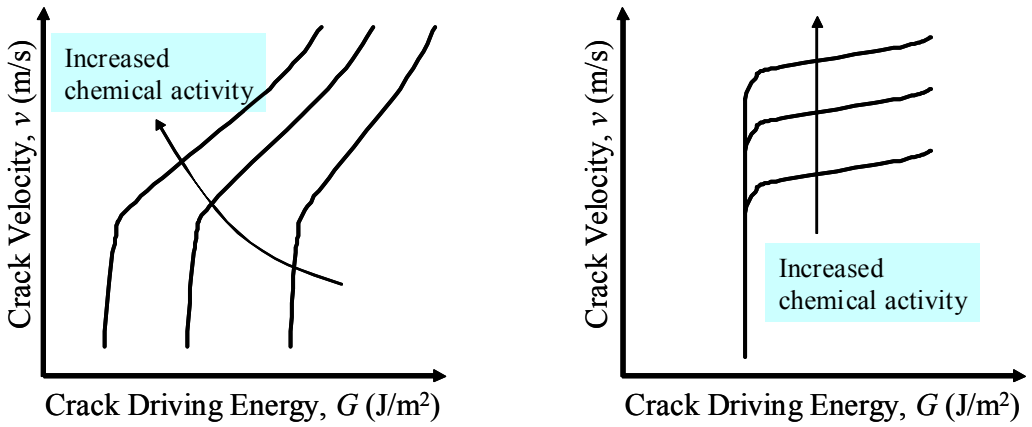

Figure 3-23. Schematic of typical behavior as the chemical activity changes.

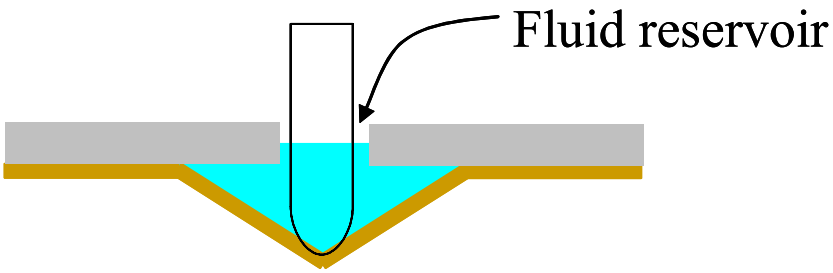

Figure 3-24 Schematic of the fluid reservoir formed between the adhesive membrane and substrate.

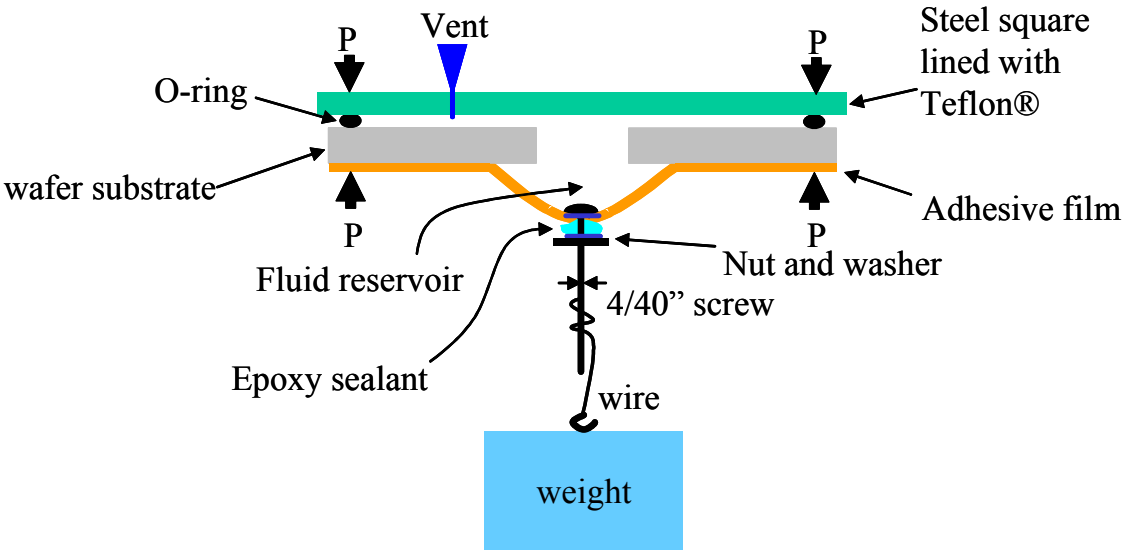

Figure 3-25 Schematic of the sub-critical shaft-loaded blister test specimen.

Figure 3-26 Photograph of L4 adhesive blister specimen.

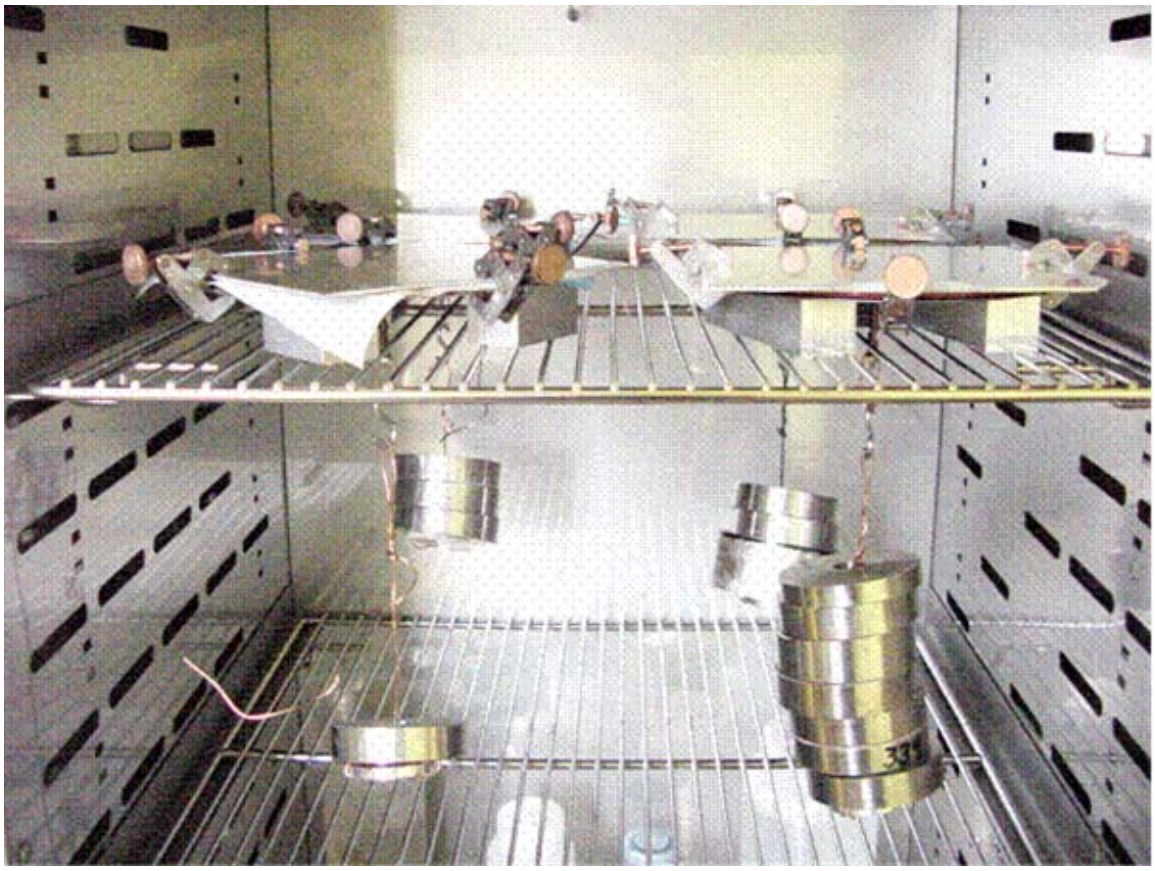

Figure 3-27 Photograph of sub-critical shaft-loaded blister test specimens in oven environment.

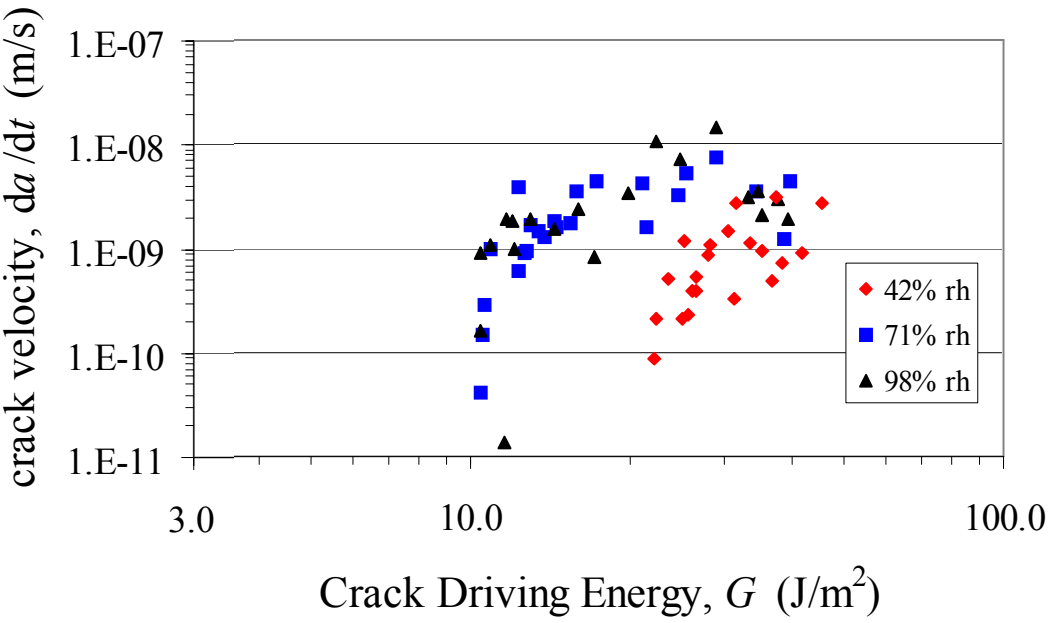

Figure 3-28 SLBT crack velocity (m/s) as a function of crack driving energy, G, (J/m^2) and relative humidity (25°C). The adhesive is the model epoxy.

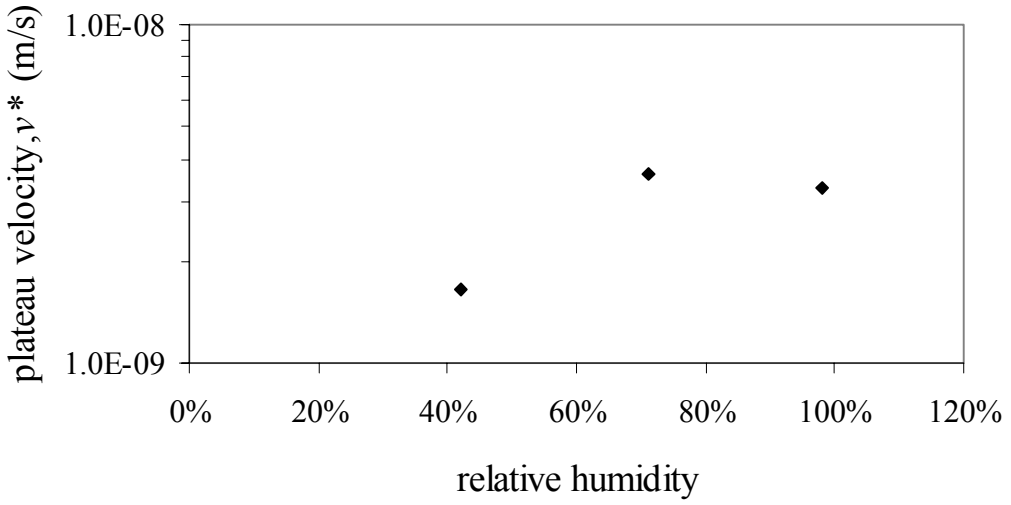

Figure 3-29 The crack velocity of Region II as a function of relative humidity (25°C). The adhesive is the model epoxy.

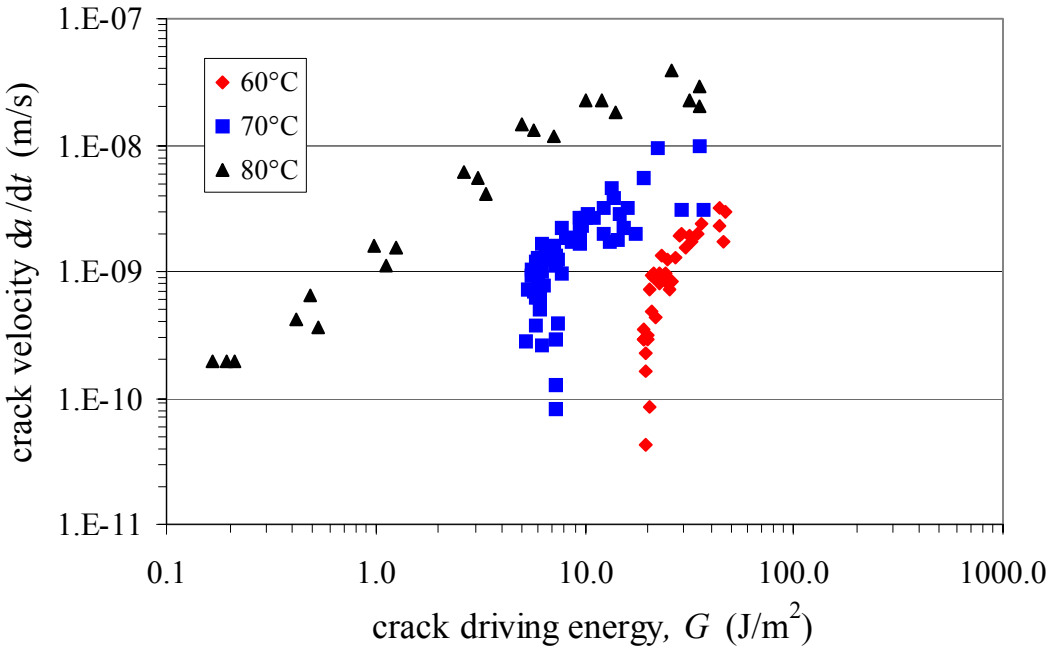

Figure 3-30 SLBT crack velocity (m/s) as a function of crack driving energy, G, (J/m^2) and temperature. The environment is water and the adhesive is the L4 epoxy.

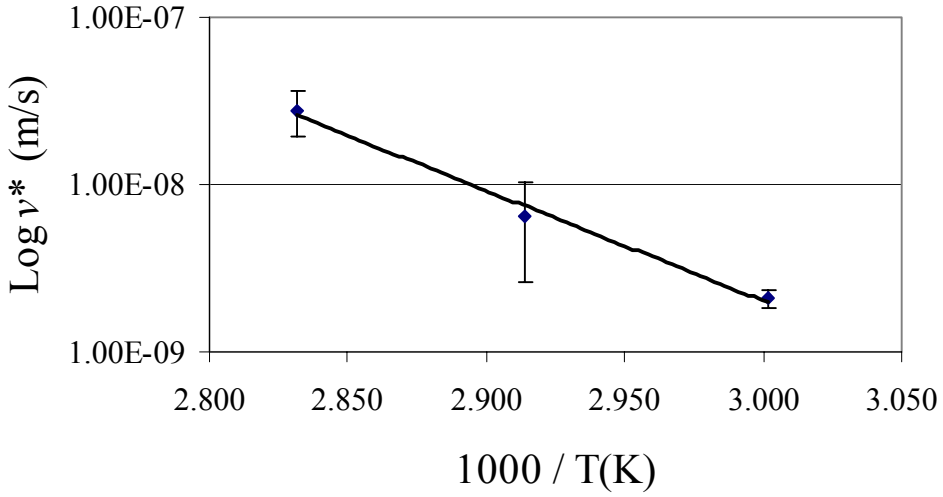

Figure 3-31 Arrhenius plot of the L4 adhesive plateau velocity exposed to water at 60, 70, and 80°C.

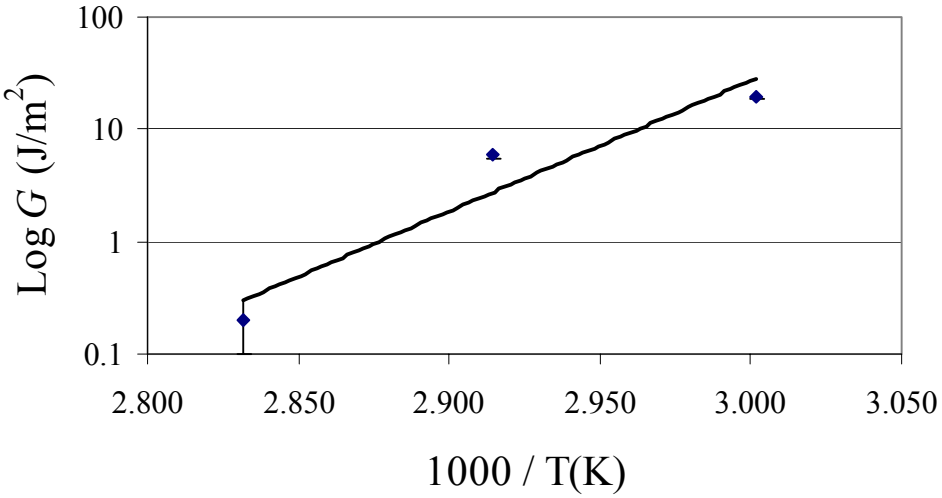

Figure 3-32 Arrhenius plot of the L4 adhesive threshold value of *G* exposed to water at 60, 70, and 80°C.

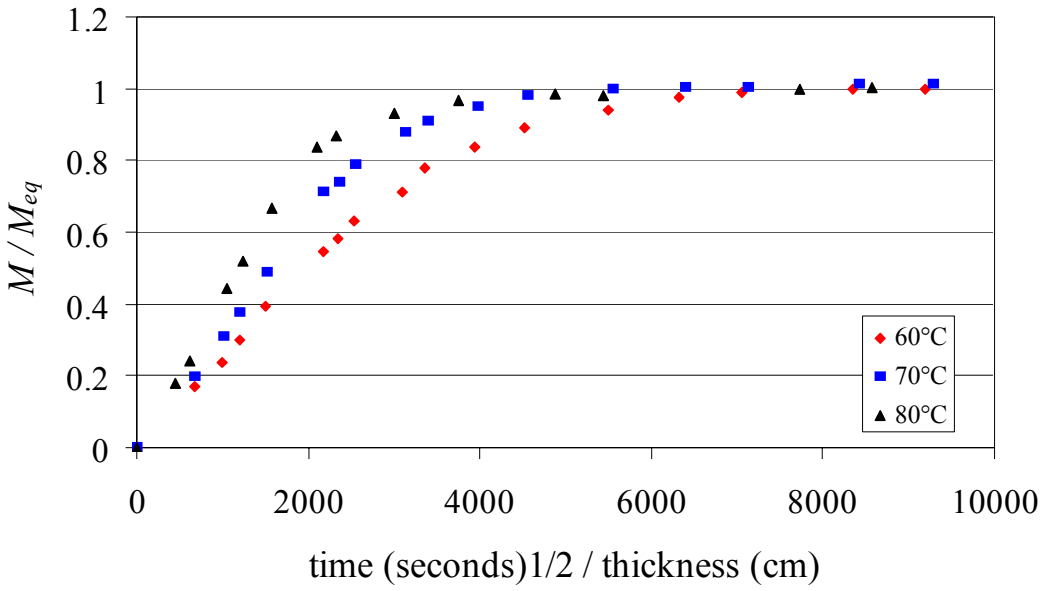

Figure 3-33 The normalized percent mass uptake as a function of the square root of time (seconds) normalized by the sample thickness for each temperature. The adhesive is the L4 epoxy.

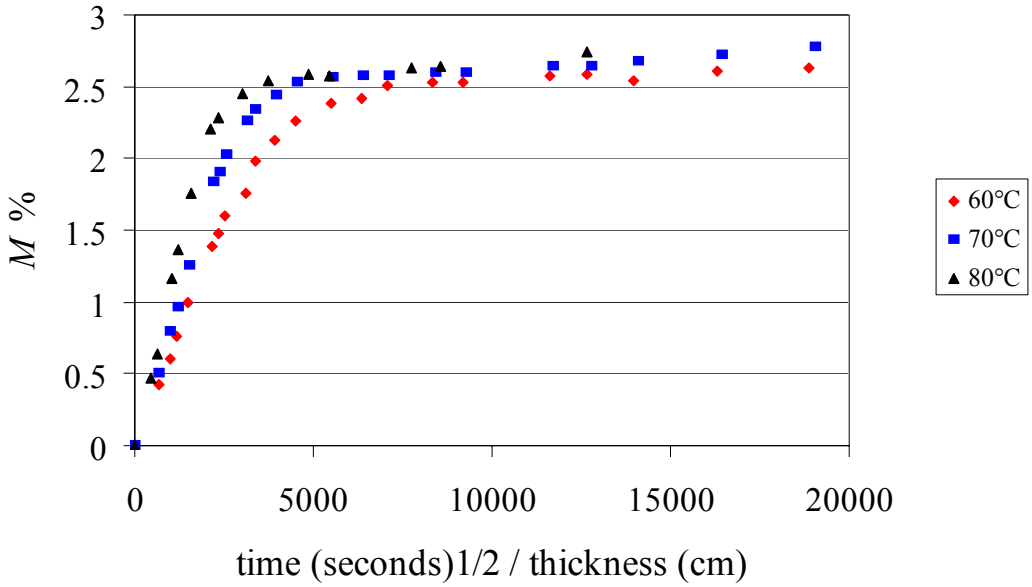

Figure 3-34 The percent mass uptake as a function of the square root of time (seconds) normalized by the sample thickness and for each temperature. The adhesive is the L4 epoxy.

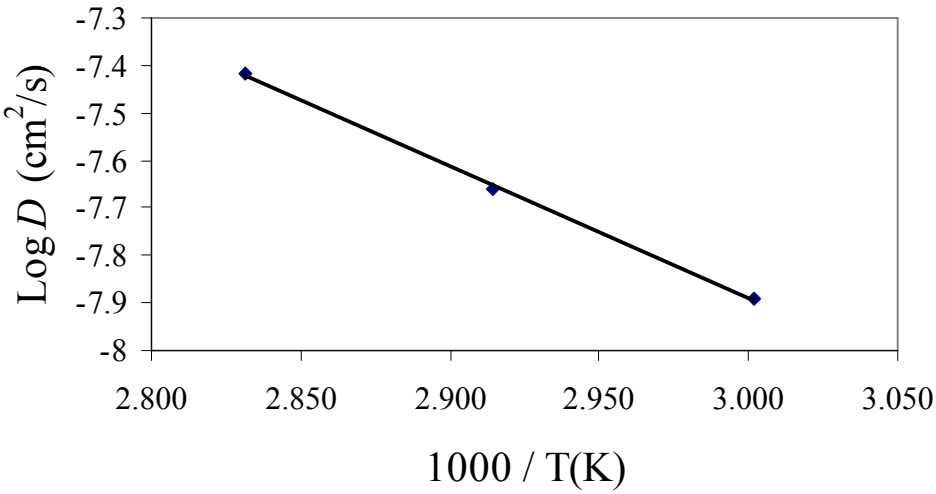

Figure 3-35 Arrhenius plot of the temperature dependence of the diffusion coefficient of water in the L4 epoxy.

3.4.7 Appendix: Measuring Diffusion Coefficients

3.4.7.1 Solutions to Fick's Law of Diffusion

Characteristic of ideal Fickian diffusion is that at short times the initial relative mass uptake is a linear function of $\sqrt{t}$ and that with time, an equilibrium or final value M_∞ is obtained. If indeed this is the case, there are several approximate solutions to Fick's law which can be written in terms of the capacitance of the film and used to solve for the diffusion coefficient and or concentration ($C_{p,t}$)as a function of time t and distance x. For a coating, where the polymer is insulated on one side, the coating thickness is L.

Utilizing the short time approximation ($M_t/M_\infty \leq 0.5$), the diffusion coefficient D can be calculated by equation 10 using the linear portion of the relative mass uptake vs. of $\sqrt{t}$ curve.

Equation 3-16
$$\frac{M}{M_\infty} = \frac{2}{L}\sqrt{\frac{tD}{\pi}}$$

If there is limiting data at short times ($M/M_\infty \leq 0.5$) then the long time solution may be utilized (equation 11).

Equation 3-17
$$\ln\left(1 - \frac{M}{M_\infty}\right) = \ln\left(\frac{8}{\pi^2}\right) - \frac{D\pi^2 t}{4L^2})$$

In addition, the diffusion coefficient may be calculated by measurement of the half time ($t_{0.5}$) where the relative mass fraction is equal to 0.5 then

Equation 3-18
$$D = \frac{0.04919 * 4L^2}{t_{0.5}}$$

Furthermore, the time for a material to attain 99.9% of its maximum possible fluid is:[130]

Equation 3-19 $$t_{sat} = \frac{0.67 \cdot 4L^2}{D}$$

.

4 INVESTIGATION OF THE DURABILITY OF ADHESIVE JOINTS AND COATINGS USING CONSTANT FREQUENCY IMPEDANCE SPECTROSCOPY

4.1 Introduction

Given the deleterious effects of fluids on adhesion, it is of great interest to know the transport rate and relative concentration of fluid at an adhesive interface. Utilizing constant frequency interfacial impedance spectroscopy (IIS) and a novel interdigitated electrode sensor design, changes in the concentration of absorbed fluid near the interface as a function of exposure time were correlated to the measured capacitance. These novel IIS sensors measure the impedance of mapped areas of the sensor defined with respect to the free edge of the coating. Consequently, these sensors can be used to measure the distribution and transport of fluids at the interface. This research is divided into the following sections:

1. The design and utility of the IIS sensor are demonstrated by studying the diffusion of acetone into a pressure sensitive adhesive tape bonded to the sensor.[131]

2. The capability to measure debonding of an adhesive is demonstrated using a pressure sensitive adhesive tape exposed to water.

3. The diffusion of an extremely aggressive fluid into a commercial filled epoxy was studied.

4. The diffusion of moisture into UV curable pressure sensitive adhesives was studied.

5. The effects of hygroscopic cycling on the commercial filled epoxy as a function of fluid environment, surface chemistry, and coating thickness was investigated

6. Sources of signal noise and recommended experimental set-up modifications are discussed.

4.2 Background on Impedance Spectroscopy

Impedance spectroscopy is one of several techniques that belong to a broad class of polymer characterization methods that are based on measuring a materials response to an electrical excitation. Impedance spectroscopy, dielectric spectroscopy, microdielectrometry, dielectric relaxation spectroscopy, and dielectric thermal analysis are all essentially the same technique and only differ by name and emphasis of observables. These techniques have been used to elucidate molecular relaxations [132,133], monitor in real time changes in the chemical and physical state in polymers brought about by crystallization [134] and cure [135], measure fluid diffusion into polymers [136], measure the moisture content of adhesive joints [137,138], and monitor the integrity of the adhesive joints and coatings [20,138,139].

The impedance Z^* or $Z(j\omega)$, is defined as the total opposition a component offers to the flow of an alternating current at a given frequency.[140] The impedance $Z(j\omega)$ can be expressed as:

Equation 4-1 $$Z(j\omega) = Z' + jZ''$$

where Z' and Z'' are the real and imaginary parts of the impedance, or in-phase and out-of phase components, respectively. The real part of impedance is equal to the resistance (R), and the capacitance (C) is related to the imaginary part of the impedance:

Equation 4-2 $$Z'' = \frac{1}{2\pi fC}$$

Therefore, the impedance is made up of both a capacitive and resistive component. The terms impedance and capacitance will be used interchangeably in this work.

4.2.1 Constant Frequency Impedance Measurements

For qualitative information about the evolution of coating properties as a function of exposure time to a fluid environment, single or constant frequency impedance measurements can be utilized.[141,142] Because the true coating resistance and capacitance are frequency dependent, more quantitative results may be obtained by exploring a wide range of frequencies (10^1 to 10^6 Hz) and by fitting the impedance to physically relevant equivalent circuits.[143] However, this current investigation utilizes a single frequency due to the limitations of the testing device. In a constant frequency experiment, the capacitance and resistance are measured as a function of time of exposure. The capacitance increases due to increase in the average permittivity of the medium as fluid is absorbed into the polymer. The resistance decreases due to the ionic or conductive nature of the absorbed fluid and dissolved ionic species. Alternatively, the impedance of the coating can be measured before and after exposure to test for the occurrence of irreversible damage.[143] This is the technique employed in the present research to measure the effects of hygroscopic cycling.

For many adhesive coatings, four regions of a graph of the coating capacitance as a function of exposure time can be distinguished (Figure 4-1).[139] Region I corresponds to an induction period where the fluid must ingress across the thickness of the coating until the fluid reaches the polymer/electrode interface. At the interface the change in capacitance resulting from the presence of the fluid can be detected.

In Region II, once the presence of the fluid is detected at the electrode interface, the concentration of absorbed fluid and capacitance continues to increase. If the adhesive coating exhibits Fickian diffusion, a linear relationship between the capacitance and $t^{1/2}$ is predicted.

In Region III the polymer is saturated with the fluid. If the adhesive coating exhibits Fickian diffusion, the values of capacitance and resistance will reach a plateau. If, however, the

adhesive coating exhibits non-Fickian diffusion, typical for glassy polymers, the adhesive coating will exhibit an indefinite uptake of fluid. Under such circumstances, a constant or equilibrium value of capacitance or resistance will not be observed. For the Fickian case, from Regions II and III the diffusion coefficient can be obtained using any of several solutions for Fick's second law.

Region IV is the final region; there, a rapid rise in capacitance and a rapid decrease in resistance are observed, corresponding to failure or debonding of the adhesive. The rapid rise or fall in measured values is attributable to an accumulation of fluid at the interface of the coating and displacement of the adhesive bonds immediately located next to the electrode interface.

Sekine proposed a method of evaluation based on the changes in the values of resistance of an adhesive coating.[144] The time when the resistance of the adhesive coating suddenly drops is defined as the breaking time t_b. The time when the resistance of the adhesive coating reaches the value of resistance of the substrate in contact with the fluid is defined as t_s. The values of t_b and t_s can be used as measures of the apparent lifetime t' of the adhesive (see Figure 4-2).

4.2.2 The Relationship between Capacitance and Fluid Concentration

Determining the diffusivity of a fluid utilizing capacitance data has been reviewed by Wind and Lenderink.[57] Capacitance data has been used extensively to measure the diffusivity of water in polymers largely due to the high sensitivity of the polymers dielectric constant to changes in the volume of absorbed water. The dielectric constant of the coating will change significantly as the polymer absorbs water because the dielectric constant of polymers is small ($\varepsilon \sim$ 3-8) compared to water ($\varepsilon \sim 80$). The dielectric constant of the wet polymer can be estimated if the water and polymer are treated as two separate individual phases having appropriate volume fractions. If we ignore the presence of incorporated air in the polymer and assume the value the dielectric

constant of absorbed water is roughly the same as free water, the dielectric constant of the wet polymer may be described by a rule of mixtures (an effective medium theory):

Equation 4-3 $$f(\varepsilon_{avg}) = (1 - \phi) f(\varepsilon_{coating}) + \phi f(\varepsilon_{water})$$

where f is the function characteristic of the mixing law, ε_{avg} is the dielectric constant of the wet polymer, ϕ is the volume fraction of absorbed water, $\varepsilon_{coating}$ is the dielectric constant of the coating and ε_{water} is the dielectric constant of water. For a stratified material the following functions may be appropriate:

parallel to the electric field: $f(\varepsilon_{avg}) = \varepsilon$

perpendicular to the electric field: $f(\varepsilon_{avg}) = 1 / \varepsilon$

For the case of a isotropic distribution of water in the polymer, Brasher and Kingsbury proposed the following empirical mixing laws for polymers absorbing water:[145]

Brasher and Kingsbury: $f(\varepsilon_{avg}) = \log(\varepsilon)$

More complex models include the Rayleigh function and the effective medium approximation (EMA).[57]

The capacitance and permittivity, for an ideal capacitor, are related by the following expression:

Equation 4-4 $$\varepsilon = C / Q$$

where Q is a geometric factor. For an ideal parallel plate capacitor, the constant, Q is:

Equation 4-5 $$Q = \varepsilon_0 A/d$$

where ε_0 is the permittivity of free space, A is the surface area of a single plate, and d is the plate spacing or dielectric thickness.

Note that the change in permittivity or capacitance is proportional to the change in volume fraction or concentration of fluid according to the above equations. For water polymer mixtures, the increase in permittivity and water concentration is proportional to the number of water dipoles present in the system.[146,147]

The most widely used empirical function that relates the capacitance to the volume fraction of water in coatings is that of Brasher and Kingsbury, which reduces to:

Equation 4-6
$$\phi(t) = \frac{\log(\frac{C(t)}{C_{coating}})}{\log(80)}$$

Where:

$\phi(t)$: the volume fraction of water at time t

$C(t)$: the measured capacitance of the mixture of the polymer coating and water at time t

$C_{coating}$: the measured capacitance of the dry polymer coating at $t = 0$

The assumptions of the Brasher-Kingsbury equation (Equation 4-6) are:[139]

1. The change in capacitance is entirely due to the permeation of water into the film.
2. The water uptake does not cause the coating to swell.
3. The water is distributed homogeneously in the coating.
4. The permittivity of water is constant and equal to 80.
5. No polar solvent is present in the coating.
6. The values of capacitance of the coating can be expressed by Equation 4-4 and Equation 4-5.
7. The volume fraction penetrated by water remains relatively small.

This list is a useful as a general guideline of the assumptions used in the application of any of the rule of mixtures or effective medium theories.

According to Fodor and Hill, for interdigitated structures the field decays at large distances ($z < L / \pi$), where z is the distance above the sensor surface and L is the line spacing.[148] For the IIS sensor electrode geometry (L = 72 microns) the field is expected to exponentially decay 23 microns above the surface. Despite this relatively large distance, interdigitated electrodes are regarded to be a local measurement of the capacitance at the surface and therefore of the concentration of fluid (C) near the surface of the sensor. Furthermore, the capacitance is not a measurement of the average mass of absorbed fluid (M) in the adhesive. Therefore, in an approach similar to that utilized by Day *et al* [136], Equation 2-2 can be expressed in terms of the capacitance.

Equation 4-7
$$\frac{C_t - C_{t=0}}{C_f - C_{t=0}} = 1 - \frac{4}{\pi}\sum_{n=0}^{\infty}\frac{(-1)^n}{2n+1}\exp\left[-\frac{D(2n+1)^2\pi^2 t}{4L^2}\right]\cos\left(\frac{(2n+1)\pi x}{2L}\right)$$

where C_t is the permittivity at any time t, $C_{t=0}$ is the initial permittivity of the polymer film and C_f is the permittivity at the surface after equilibrium or the final permittivity at any point after equilibrium.

4.2.3 Estimating the Area of Debonding

The double layer capacitance measured at the surface of coated specimens can be used to estimate the area of delamination.[145,149,150] This double layer capacitance is due to condensed water at the surface of the electrode and can be estimated from the frequency dependent impedance data. The delaminated area, A_d, can be calculated from the following expression (Equation 4-8):

Equation 4-8 $$A_d = C_d / C_d^0$$

Where C_d is the double layer capacitance and C_d^0 is the double layer capacitance of the uncoated metal. In this research we employ a similar technique to measure an apparent crack length in an epoxy coating as discussed in Section 4.7.

4.2.4 Figures

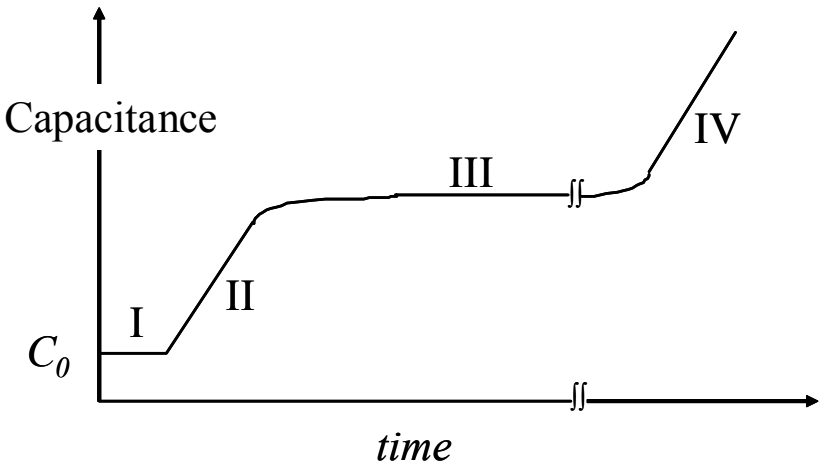

Figure 4-1. Schematic of the expected capacitance as a function of exposure time obtained from single-frequency impedance spectroscopy.

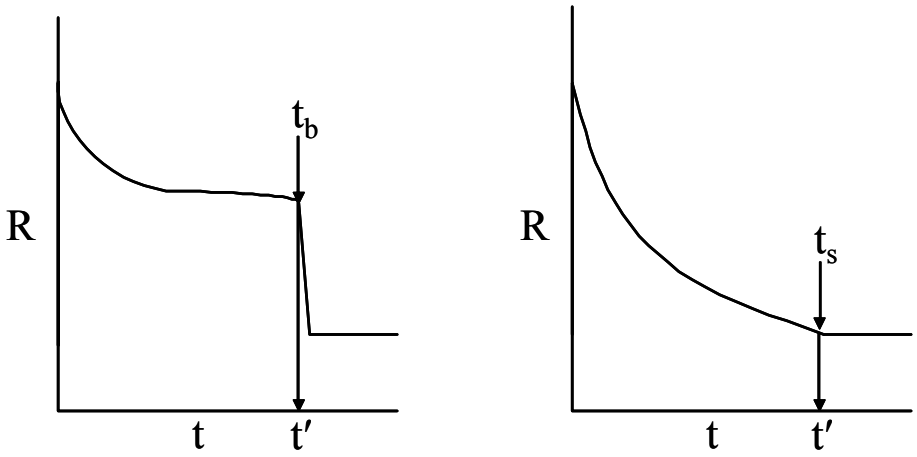

Figure 4-2. Schematic of the time to failure determined graphically from the resistance as a function of time obtained from single-frequency impedance spectroscopy.

4.3 A Novel Impedance Sensor Design for Measuring the Distribution and Transport of Fluids in Adhesive Joints

(*International Journal of Adhesion & Adhesives*, 23: 335-338, 2003)

4.3.1 Abstract

Given the deleterious effects of fluids on adhesion, it is of great interest to know the transport rate and concentration of fluid at an adhesive interface. Utilizing constant frequency interfacial impedance spectroscopy (IIS) and a novel interdigitated electrode sensor design, changes in the concentration of absorbed fluid near the interface as a function of exposure time were correlated to the measured capacitance. These novel IIS sensors measure the impedance of mapped areas of the sensor defined with respect to the free edge of the coating. Consequently, these sensors can be used to measure the distribution and transport of fluids at the interface. We report results obtained for the absorption of acetone into a pressure sensitive adhesive (PSA) tape with an aluminum foil backing bonded to the sensor. Because the backing is impermeable, diffusion was confined parallel to the bond plane. We demonstrate that the IIS technique is capable of detecting changes in the relative concentration of a fluid diffusing into an adhesive joint as a function of exposure time and with respect to the exposed free edge of the sensor.

4.3.2 Introduction

In this research the technique of interfacial impedance spectroscopy and a novel impedance sensor design has been used in order to obtain detailed measurements of the distribution and transport of fluids at an interface.

Bulk diffusion into adhesive joints has been studied considerably [151], however little work has focused on diffusion at adhesive interfaces, largely because of the limitations of experimental

techniques. Mass uptake experiments are a convenient method to study fluid absorption in adhesives. This method has been used to study interfacial diffusion by comparing the relative rates of diffusion from non-bonded or free-standing films with diffusion into the actual adhesive joint.[53,152] A disadvantage of mass uptake experiments is that the method does not provide any direct evidence of the concentration of fluid at the interface.

Additional techniques exist for measuring fluid absorption at adhesive interfaces. Fourier transform infrared spectroscopy in the multiple internal reflection mode (FTIR-MIR) is an available technique for studying diffusion at the interface. FTIR-MIR has provided direct evidence of water accumulation, and therefore adhesive debonding, at the interface.[22,153] The technique of neutron reflectivity has also shown that the concentration of absorbed fluid can be significantly greater at the interface than in the bulk adhesive.[25-28]

We utilize the technique of interfacial impedance spectroscopy to study fluid absorption at the interface of adhesive joints. The label, interfacial impedance spectroscopy was coined by Takahashi and Sullivan [23,24] to refer to impedance measurements made at the interface of a coated substrate. They detected changes in the impedance attributable to adhesive debonding and the accumulation of moisture at the interface, although, limited information about the distribution and transport of moisture at the interface was obtained.

Our research builds on this limited body of work concerning diffusion at the interface of adhesive joints. We have measured the interfacial diffusion process of acetone into a bonded pressure sensitive adhesive tape by employing the technique of interfacial impedance spectroscopy (IIS) and a novel interdigitated electrode sensor design.

4.3.3 Experimental

Interfacial impedance spectroscopy (IIS) detects changes in the capacitance (*C*) and resistance (*R*) at the IIS sensor surface resulting from fluid absorption. The change in concentration (or volume fraction) of absorbed fluid in the adhesive is proportional to the observed changes in capacitance.[139]

The IIS sensor was manufactured by Hewlett-Packard Co. and is shown schematically in Figure 4-3 and as a photograph in Figure 4-4. The size of the sensor is 10 mm x 30 mm x 0.068 mm. The IIS sensor is a series of 15 conductive gold traces supported on a silicon wafer having a 100 Å silicon oxide surface layer. These traces are patterned into a grid and arranged in parallel with respect to the free edge of a silicon wafer substrate. The interdigitated gold traces act as parallel plate capacitors on the surface of the wafer, where the dielectric medium (in this case, the adhesive) resides in the trenches formed by two or more adjacent traces. Individual gold traces are 75 microns wide and rise 1.26 microns off the silicon oxide surface. The traces are composed of a 60 nm bottom layer of tantalum and 1200 nm top layer of gold. The traces are separated by 72 microns. Because the traces lie on the surface, detected impedance changes reflect the concentration change and diffusion processes that occur near the surface or at the interfacial region.

Note that in experiments described in the next sections, the sensors just described were modified with additional surface layers of silicon nitride (SiN) and silicon carbide (SiC). Details of the SiC/SiN surface sensor are discussed later.

Individual traces or pairs of traces are connected to 10 individual gold pads that connect to a Hewlett-Packard HP4285A impedance analyzer. The impedance analyzer measures the capacitance and resistance as a function of frequency. As shown in Figure 4-3 (and Figure 4-4),

the gold pads are labeled 1 through 10. Two gold traces are connected to each gold pad, 1 through 5. A single gold trace is connected to each gold pad, 6 through 10. The capacitance can be measured between any two pads provided they are connected to any adjacent set of gold traces. For example, the capacitance can be measured from the pair of pads 1 and 10. In this case, the single gold trace from pad 10 lies between the two gold traces connected to pad 1, which forms the interdigitated electrode structure. From this arrangement, the sensors are unique in that they make it possible to map the impedance of specific areas of the sensor defined with respect to the free edge of the sensor. The impedance can be measured from the following pairs of pads, listed in order from the nearest to the most remote from the edge of the sensor: pairs 1-10, 1-2, 2-9, 2-3, 3-8, 3-4, 4-7, 4-5, and 5-6. From the aforementioned pair of pads, the impedance can be obtained as a function of x, the distance from the free edge of the sensor. The value of x ranges from $x = 0$ mm at the free edge of the specimen to $x = 5$ mm at the center of the specimen. The values of x measured by each pair of pads, based on the distance between the free edge of the sensor and the center of the working set of gold traces, are listed below in Table 4-1. The deviation associated with each value of x is 0.15 mm. The deviation is based on the width of the working set of traces.

Table 4-1 The value of x measured by each pair of pads. The deviation is +/- 0.15 mm.

Pair of pads	x (mm)
1-10	0.44
1-2	0.66
2-9	0.89
2-3	1.11
3-8	1.33
3-4	1.55
4-7	1.77
4-5	1.99
5-6	2.20

The frequency used in these experiments was 1 MHz. Measurements below a frequency of 1 MHz had significant scatter. The automated measurement for each pair of pads was obtained using an Agilent 34970A switchbox. Shielded coaxial cables were used between the switchbox and the impedance analyzer. The IIS sensor was placed into a 14 pin edge card connector mounted to a custom board which connects to 10 twisted parallel wires, one for each pad. The length of the wire between the switchbox and the die is approximately 0.6 meters in length.

A schematic of the environmental chamber is shown in Figure 4-5. A small glass bottle (approximately 40 mL) was utilized as the fluid reservoir. The sensor is partially submerged in the fluid reservoir and is fixed in place in by a plastic lid fabricated with a silicon rubber top. The silicon rubber top has a slit which acts as a soft holding clamp that the sensor passes partly through. The sensor contact pads sit above the silicon rubber top and the coated interdigitated

gold traces lie below in the sealed chamber formed by the lid and vial. Evaporation was slow and no appreciable reduction in the acetone level was noticeable after a week.

The PSA tape is manufactured by Compac Industries, Inc. (manufacturer part number 807). The backing is 51 microns thick aluminum foil with a 31 microns thick acrylic pressure sensitive adhesive. The surface of each sensor was washed with isopropyl alcohol and then blown dry with nitrogen prior to applying the pressure sensitive adhesive tape. Tests were conducted at room temperature using acetone as the liquid.

4.3.4 Results and Discussion

Shown in Figure 4-5 is the environmental chamber with the PSA tape adhered to the sensor. The path of diffusion of the acetone into the PSA tape is illustrated with several arrows. The path of diffusion is also illustrated in a schematic of the side-view of the edge of the specimen, shown in Figure 4-6. Because the backing is impermeable, the source and maximum concentration of acetone are at the sensor edge, and the confined path of diffusion is parallel to the bondline. Therefore, the acetone diffusion begins at the edge of the PSA tape and sensor. The acetone then proceeds toward the center of the bonded PSA tape and sensor, and across each gold trace. Changes in the capacitance, due to fluid absorption, are detected at the sensor surface.

The initial value of the capacitance and resistance obtained from each pair of pads is different because each trace has a slightly different geometry. In order to make comparisons among the different pairs of pads, the capacitance was normalized according to the following expression:

Equation 4-9 $$(C - C_0) / (C_f - C_0)$$

where C is the capacitance at a value of x and exposure time, and C_0 and C_f are the initial and final capacitance respectively at the particular value of x. Equation 4-9 is based on treating the

volume fractions of fluid and adhesive as two independent layers aligned parallel to the applied electric field. A perpendicular layer model and the Brasher-Kingsbury model [145] were also employed. The resulting normalized capacitance as a function of exposure time data were essentially identical for all three models.

Figure 4-7 shows the normalized capacitance as a function of exposure time, up to 2 hours. The final capacitance was obtained after 60 hours of exposure. For clarity, only data from the pair of contact pads 1-10, 2-9, 3-8, 4-7, and 5-6 are shown. Figure 4-7 illustrates that the rate of change in capacitance resulting from absorption of the acetone occurs faster in regions closer to the edge of the specimen. Figure 4-7 also shows the initial region of the normalized capacitance as a function of exposure time and illustrates a "lag" time necessary for the acetone to traverse across the sensor from the free edge to the respective pair of contact pads. If we assume the capacitance is a linear function of absorbed fluid, the normalized capacitance and normalized concentration are equivalent. From the data in Figure 4-7, the concentration profile of the acetone near the interface in the bonded PSA tape was determined. The concentration profile, shown in Figure 4-8, is the normalized concentration as a function of the distance from the edge of the specimen, x, for different values of exposure time. The absorption behavior of acetone into the PSA was clearly non-Fickian. This was not unexpected given that the PSA absorbs acetone readily and has poor cohesive strength, resulting in significant swelling and some loss of mass.

4.3.5 Summary

The absorption of acetone at room temperature into an adhered PSA tape was measured by applying the techniques of impedance spectroscopy and utilizing a unique interdigitated electrode sensor design. This study suggests these novel sensors are applicable for the study of

interfacial diffusion processes, and could be extended to other coatings or adhesives in a variety of environments.

4.3.6 Figures

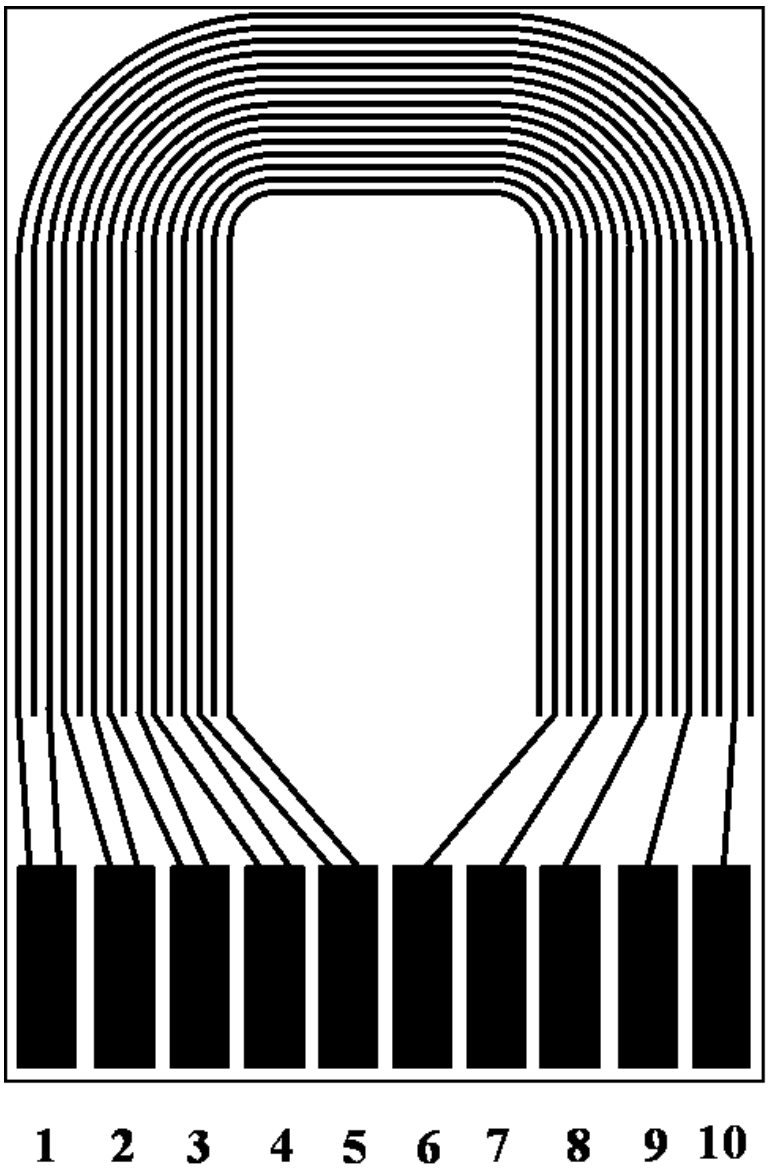

Figure 4-3 Schematic (not shown to scale) of the IIS sensor. The contact pads are labeled 1 through 10.

Figure 4-4 Photograph of the IIS sensor.

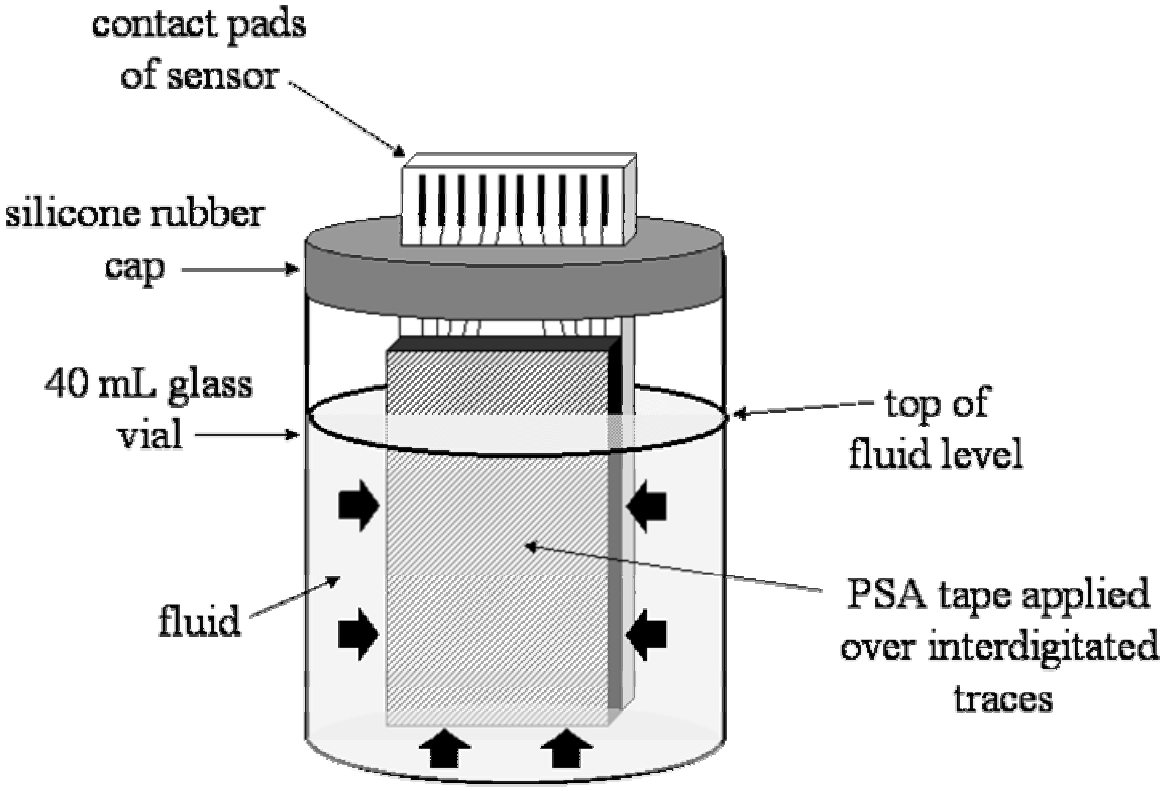

Figure 4-5 Schematic of the experimental set-up of the sensor and environmental chamber. The path of diffusion is shown with the arrows.

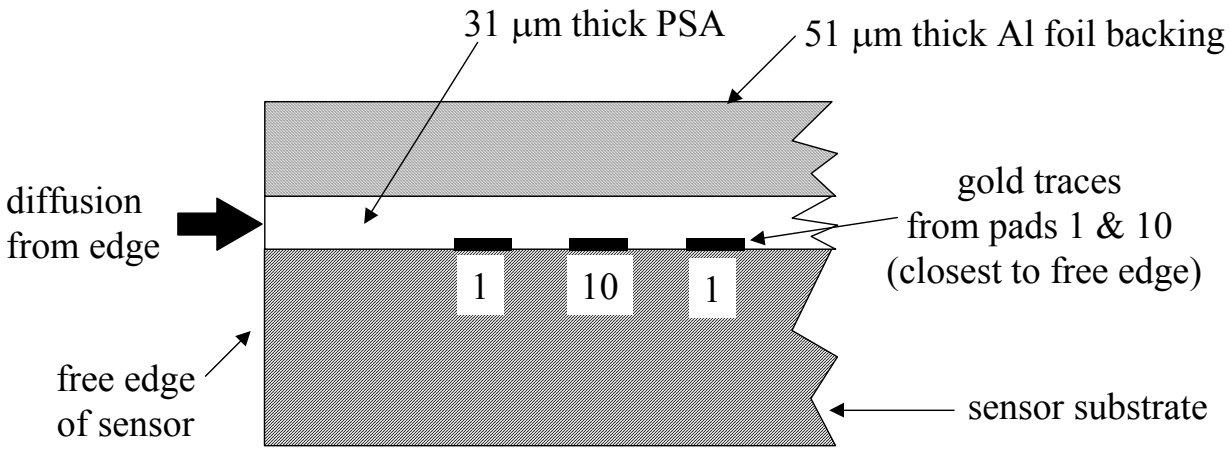

Figure 4-6 Schematic of the side-view of the bonded PSA tape illustrating the path of diffusion of acetone.

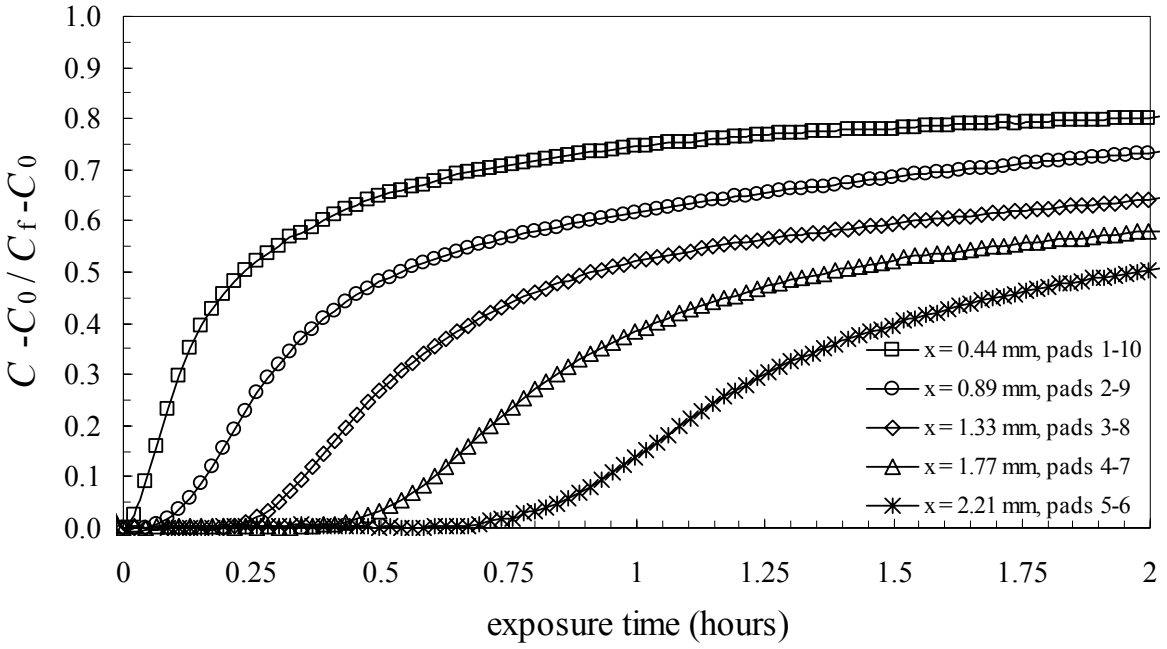

Figure 4-7 Initial region (up to two hours) of the normalized capacitance as a function of exposure time (hours) for different values of x.

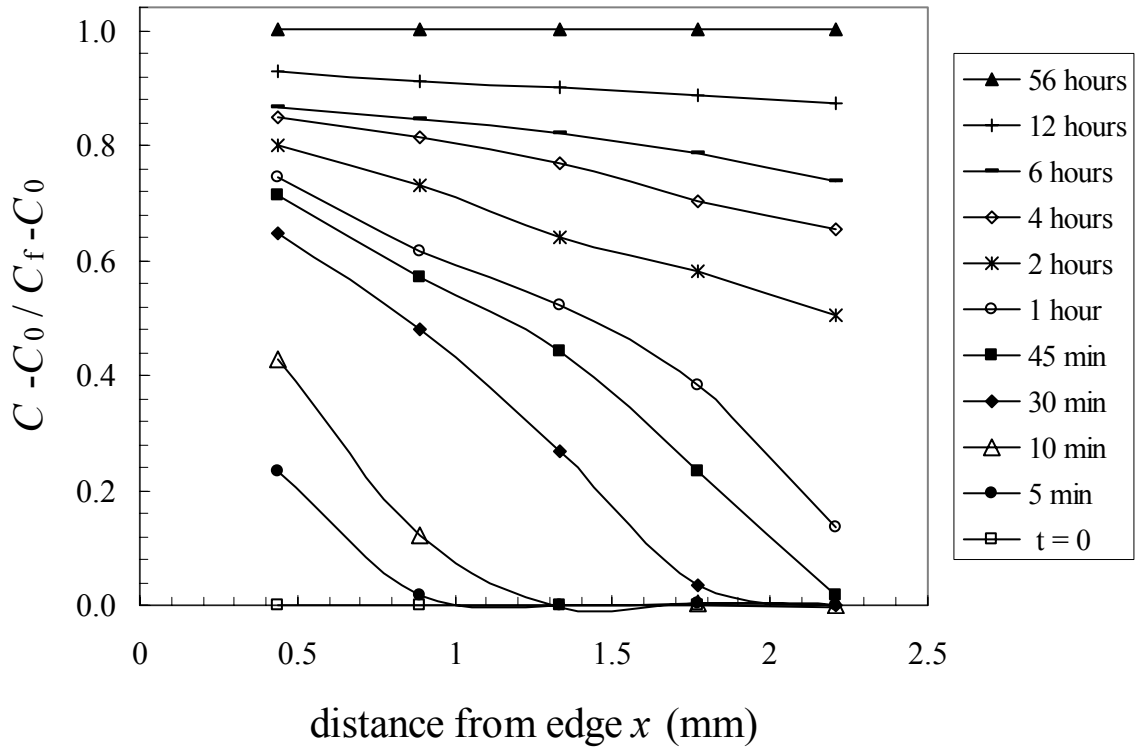

Figure 4-8 The concentration profile obtained from IIS sensor.

4.4 Diffusion of Water and Subsequent Debonding of a PSA Tape

4.4.1 Abstract

The effects of water absorption in a pressure sensitive adhesive tape were obtained using interfacial impedance spectroscopy and a novel senor design described in other sections. The results show characteristic behavior expected for adhesive debonding of coatings as a function of environmental exposure time.

4.4.2 Materials and Experimental

The pressure sensitive adhesive tape used in this study is the "Quill Invisible Mending Tape". The PSA tape was exposed to water at room temperature. According to the manufacturer, the pressure sensitive adhesive is acrylic based.

The novel IIS sensors used in this study can measure the impedance or capacitance of mapped areas of the sensor defined with respect to the free edge of the coated sensor. Details of the technique and experimental set-up can be found in Section 4.3 and in ref 125. The test frequency was 1000 kHz. The substrate was the homogeneous low surface energy substrate. The sensor was manufactured by taking the existing SiO_x/Au/Ta energy substrate and depositing a 250 nm layer of silicon nitride and then a 135 nm layer of silicon carbide. To prepare the surface of the substrate, they were first rinsed with HPLC grade isopropyl alcohol and then blown dry with ultra-high purity nitrogen gas.

4.4.3 Results

The capacitance as a function of time is shown in Figure 4-9. After an initial region characteristic of fluid diffusion into an adhesive coating, there is a significant increase in the capacitance at

approximately 15 hours. The dramatic increase in capacitance is attributable to a significant increase in the concentration of fluid at the sensor interface resulting from the PSA tape debonding. These results are similar to the expected results for an adhesive coating exhibiting debonding (Figure 4-1). However, the characteristic lag time necessary for the fluid to migrate across the surface to the respective pair of pads was not observed. This unexpected behavior is either an artifact of the experimental set-up or, if these results truly reflect diffusion at the interface, suggests that the fluid migrated instantly across the surface. Similar results were also obtained for the diffusion of acetone into the aluminum foil PSA tape bonded to the SiN/SiC surfaces. Nevertheless, these results illustrate that the sensor is capable of measuring adhesive debonding. Adhesive failure is believed to occur from degradation of the interface and also due to stress relaxation in the PSA tape backing. Stress relaxation caused the backing to shrink and curl at the edges resulting in the tape lifting off the substrate.

4.4.4 Conclusion

The results of exposure of a PSA tape to water prove that the sensor is capable of measuring adhesive debonding. Furthermore, the observed behavior follows similar trends that have been observed by other researchers using single-frequency impedance spectroscopy.

4.4.5 Figures

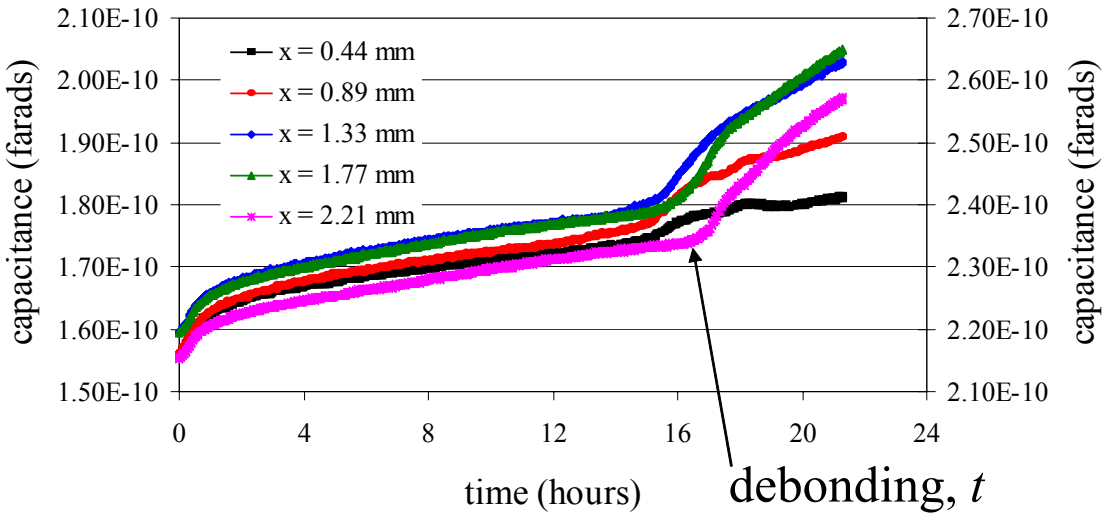

Figure 4-9. Capacitance as a function of exposure time for the Quill pressure sensitive adhesive tape in water.

4.5 Interfacial Diffusion of Aggressive Fluids into Epoxy Adhesive Joints and Coatings Measured by Constant Frequency Impedance Spectroscopy

4.5.1 Abstract

The diffusion of 0.1 M solution of NaOH into the commercial L4 epoxy adhesive joints and coatings at 60°C was measured by constant frequency interfacial impedance spectroscopy and a novel impedance sensor design described elsewhere. Several test specimens were investigated: 1) the L4 adhesive sandwiched between two sensor substrates, 2) the L4 adhesive sandwiched between two sensor substrates which have been coated with release agent, 3) the L4 adhesive sandwiched between two sensor substrates that have been fabricated with a shim, and 4) the L4 adhesive coated on the sensor substrate approximately 50 microns thick (no sandwich). This work suggest that the L4 adhesive interface is relatively durable and that differences in the diffusivity between the bulk, non-bonded adhesive and the bonded adhesive can not be distinguished using the current experimental set-up.

4.5.2 Research Objectives

The objective of this set of experiments was to address some fundamental questions regarding the degradation of glassy adhesive joints by environmental stress (exposure to temperature and fluid). Is fluid diffusion at the interface of an adhesive joint faster than fluid diffusion occurring in the bulk adhesive? Which fluid chemistries promote interfacial diffusion and/or bulk diffusion? Is the bulk diffusion coefficient a good indicator of the fluid's aggressiveness and mobility at an interface or adhesive joint? To attempt to answer these questions, the technique of

constant frequency interfacial impedance spectroscopy and a novel impedance sensor design were used to try to measure the diffusion of 0.1 M NaOH into bonded epoxy adhesive specimens. These novel IIS sensors measure the impedance of mapped areas of the sensor defined with respect to the free edge of the coating. Consequently, these sensors can be used to measure the distribution and transport of fluids at the interface. The adhesive was bonded between two impermeable substrates (the sensors) to form a sandwich specimen geometry. In such a geometry, because the backing is impermeable, fluid can enter the adhesive joint only from the edges. From the edges, the fluid can diffuse in either the bulk adhesive material, along the interface, or both. To determine the relative contribution to diffusion from the bulk and interface, the relative rate of diffusion of fluid at the interface of the adhesive joints measured by IIS could be compared to diffusion in bulk non-bonded adhesives. The study of the diffusion of 0.1 M NaOH is a worst case scenario. This fluid is water based, aggressive towards the interface, and has a stronger impedance signal than pure water.

4.5.3 Experimental

4.5.3.1 Materials

The adhesive that was used in these experiments was a commercial filled epoxy known as the L4 adhesive. Details about the adhesive can be found in Section 3.4.3.1. The adhesive coating was exposed to 0.1 M NaOH solution. The exposure temperature was 60° C. The high surface energy sensor, which is mostly SiO and Au, was used as the substrate. Details of the sensor can be found in Section 4.3 and also in the work of O'Brien et al.[131]

4.5.3.2 Sample Type 1: Sample Preparation of Sandwich Specimens (No Shim)

A schematic of the L4 adhesive sandwich specimen is shown in Figure 4-10. For each specimen, the L4 adhesive is sandwiched between two sensors. The change in capacitance as a function of x and exposure time was measured from the bottom sensor only. No signal is obtained from the top sensor. The sole purpose of the top sensor is to act as an impermeable barrier to fluid intrusion. The sensor surface chemistry of the top and bottom sensors is the same to eliminate any misleading effects due to asymmetric chemical potentials. The sensors were first rinsed with isopropyl alcohol and the blown dry with high-purity nitrogen. A Kapton® backing acrylic based pressure sensitive adhesive tape (PSAT) was used as a release liner to prevent any L4 adhesive from covering the contact pads. The bottom sensor contact pads (used to make the measurement) were covered with the Kapton® PSAT (later removed) before the adhesive was applied. A generous amount of L4 adhesive was coated on the bottom sensor. The top sensor was carefully placed on top of the coated bottom sensor to ensure that the contact pads were not covered. The top sensor and bottom sensor were then pressed together and the adhesive was squeezed out between the two sensors to reduce the formation of air bubbles. The sandwich was held together using a pair of binder clips. Before curing, excess adhesive flashing from the sides was wiped away to form a clean edge. Any excess adhesive detected after cure was removed with a razor blade. The resulting coating thickness was approximately 50 +/- 5 microns.

4.5.3.3 Sample Type 2: Sample Preparation of Sandwich Specimens with Release Agent

Sample Type 2 specimens were prepared identically to Sample Type 1, with the exception that the bottom sensor was coated with Teflon release agent prior to application of the epoxy adhesive. The release agent was applied to determine if surface contamination and a reduction in

the fracture resistance of the interface had any effect on the interfacial diffusion behavior in the sandwich specimens.

4.5.3.4 Sample Type 3: Sample Preparation of Sandwich Specimens with Shim

Specimens fabricated with a glass shim in the center were also tested. A schematic of the side view of a sandwich specimen with the glass shim is shown in Figure 4-11. A glass shim was added to the center of the sandwich specimen to reduce the path of diffusion by half, from 5 mm to 2.5 mm. The shim is approximately 4.75 mm wide, 20 mm long and 0.15 mm thick. The glass shim occupies volume that would normally be filled with adhesive and any absorbed fluid. Note that in the center of the sensor, from x = 2.5 - 5.0 mm, there are no conductive gold traces. The glass shim is fastened to the bottom substrate in the correct center position by a small amount of L4 adhesive which was pre-cured at 60°C for 30 minutes. The sample was then prepared identically to Specimen Type 1.

4.5.3.5 Sample Type 4: Preparation of Adhesive Coatings

L4 adhesive applied to the sensor using a pneumatically driven doctor blade fabricated by Hewlett-Packard. The resulting coating thickness was approximately 50 microns. The surface was prepared identically to Specimen Type 1.

4.5.3.6 Constant Frequency Interfacial Impedance Spectroscopy

Details of the technique and experimental set-up can be found in Section 4.3 and also in the International Journal of Adhesion and Adhesives[131]. The test frequency was 400 kHz. The number of tested specimens for each condition was two and the exposure time was 30 days.

4.5.3.7 Concentration Profile

The normalized concentration (C^*) of fluid as a function of exposure time in the adhesive joint can be modeled using any of the several equations arising from Fick's second law. For the bonded L4 epoxy system, solutions to Fick's Law do not account for the residual stress in the joint, the change in stress state due to moisture absorption in the adhesive, or the non-Fickian diffusion. For a semi-infinite planar interface, where $x \geq 0$ at the interface, the concentration as a function of distance from the specimen edge, x, and time, t, is expressed in Equation 4-10:[52]

Equation 4-10
$$\frac{C(x,t) - C_0}{C_f - C_0} = 1 - erf\left(\frac{x}{2\sqrt{Dt}}\right)$$

where *erf* is the error function, D is the diffusion coefficient, $C(x, t)$ is the concentration as a function of distance from the edge, x , and exposure time, t, C_0 is uniform initial concentration, and C_f is the equilibrium concentration. Equation 4-10 may be applied to the measured capacitance as a function of x and t because the concentration of fluid and capacitance are expected to be proportional to one another. In this case the normalized concentration can be replaced by the normalized capacitance.

Alternatively, the concentration profile in a polymer or adhesive joint of thickness, $2L$, or a coating of thickness L can be modeled using a solution to Fick's law shown in Equation 4-11.[45]

Equation 4-11
$$\frac{C(x,t) - C_0}{C_f - C_0} = 1 - \frac{4}{\pi}\sum_{n=0}^{\infty}\frac{(-1)^n}{2n+1}\exp\left[-\frac{D(2n+1)^2\pi^2 t}{4L^2}\right]\cos\left(\frac{(2n+1)\pi x}{2L}\right)$$

From either Equation 4-10 or Equation 4-11 the concentration profile as function of exposure time and x can be calculated. The calculated concentration profile obtained from Fick's law can be compared to the concentration profile obtained from the capacitance data. To determine the concentration profile from the capacitance date, the time to saturation and initial

and final capacitance values must be measured. By comparing the two concentration profiles, the diffusivity, D, can be estimated.

4.5.4 Results and Discussion

4.5.4.1 Sample Type 1: Sandwich Specimens (No Shim)

The measured capacitance as a function of x and exposure time for samples 1 and 2 are shown in Figure 4-12 and Figure 4-13 respectively. Recall that a value of $x = 0$ corresponds to the free edge of the sensor. Qualitatively, the capacitance signal from the graphs show that the capacitance increases with exposure time as expected. The change in the capacitance and the rate of change of capacitance appear greater for smaller values of x. In addition, identical peaks and valleys in the capacitance appear for all values of x. Theses peaks and valleys are suspected to be noise and are not due to a change in concentration of fluid. To effectively model the diffusion into the sandwich specimen, the change in capacitance and time to saturation must be known. Unfortunately, these parameters are nearly impossible to quantify because of the substantial noise in the data. As a result, no qualitative diffusion measurements were made. However, some qualitative conclusions were made from these experiments.

The data obtained after 30 days of exposure suggests that the fluid concentration at the surface is relatively low - lower than in any of the pressure sensitive adhesives tested (Section 4.3 and 4.6), and lower than L4 adhesive coatings damaged by hygroscopic cycling (Section 4.7). Under these test parameters, the concentration was low enough that the surface was not significantly damaged to cause debonding (and the subsequent large change in capacitance). Furthermore, the concentration is low enough that the change in capacitance due to fluid absorption at the surface is not enough to overwhelm the signal-to-noise ratio.

The signal-to-noise ratio of the experiment is poor because the change in the capacitance due to fluid absorption is small, on the order of 1 pF. This value was obtained from experiments of thin L4 coatings where saturation was reached after only several hours (see Section 4.7). At short experimental times, the effects of the poor signal-to-noise ratio are reduced because there is less time for the baseline to change. The path of diffusion in the sandwich specimens is long (5 mm) and the time to 99% saturation of the adhesive in the sandwich specimen is approximately 440 days. Therefore, the 1 pF change in capacitance is spread out over a long period of time. As shown in Figure 4-12 and Figure 4-13 the capacitance signal is susceptible to small but misleading changes in the signal and baseline.

The expected concentration profile for diffusion of 0.1 M NaOH in the L4 adhesive at 60°C for the sandwich specimen (no shim, L = 5 mm) was calculated using Equation 4-11 based on the diffusivity, D, of distilled water. The resulting concentration profile is shown in Figure 4-14. The concentration measured at x = 0.44, 0.89, 1.33, 1.77, and 2.21 are marked with dashed vertical lines. The time for 80% of saturation (in concentration) at the outermost pair of pads (pads 1-10, x = 0.44 mm) is approximately 25 days. After reaching 80% concentration, additional increases in concentration were slow. Therefore, after 30 days of exposure, the signal from the pad pair 1-10 is expected to reach roughly the maximum capacitance value. An exposure time of 30 days therefore represents the expected minimum time necessary to obtain the maximum capacitance change at x = 0.44 mm.

The signal-to-noise ratio can be improved by either increasing the mass of fluid absorbed in the bulk and the surface or by decreasing the time-to-saturation. For most polymers, the equilibrium mass of fluid absorbed can be increased by raising the exposure temperature. However, the operating temperature of the instrument is already at a maximum. To decrease the

time-to-saturation, either the temperature can be increased or the path of diffusion can be reduced. The path of diffusion was reduced by occupying a significant volume of the sandwich specimen with a shim. Results from sandwich specimens that incorporate a shim are discussed in a later section. Alternatively, the concentration of fluid at the surface could be increased by reducing the toughness of the interface and making the adhesive susceptible to debonding.

4.5.4.2 Sample Type 2: Sandwich Specimens with Release Agent

The measured capacitance as a function of x and exposure time for samples 1 and 2 are shown in Figure 4-15 and Figure 4-16 respectively. The results are similar to the samples without release agent (Sample Type 1). The change in capacitance and time-to-saturation as a function of x can not be quantified. In fact, the results from the release agent treated samples are more difficult to quantify than the non-treated samples. The result from sample 1, shown in Figure 4-15, suggests that despite degradation of the interface by the release agent, the epoxy still appears to remain bonded to the surface. However, the result from sample 2, shown in Figure 4-16, shows that after 24 days the capacitance increases dramatically, suggesting that the adhesive has debonded up to 0.44 mm from the edge of the sensor.

4.5.4.3 Sample Type 3: Sandwich Specimens with Shim

The time to 99.9% saturation has been reduced from approximately 7 months to approximately 2 months by incorporating a spacer or shim in the sandwich specimen. The estimated concentration profile for this specimen is shown in Figure 4-17. Examination of Figure 4-17 reveals that after 30 days of exposure the relative concentration is 80% or greater for x = 0.44 and 0.89 mm. In contrast, in the Sample Type 3 specimens, after 30 days the relative concentration is 80% or

greater only for $x = 0.44$. Therefore, by using the spacer, the time to saturation has been reduced and the instrument sensitivity has been increased.

The results from these experiments are shown in Figure 4-18 and Figure 4-19, where the measured capacitance as a function of x and exposure time for sample 1 and 2, respectively, have been graphed. Similar to the Sample Type 1 and 2, the results are difficult to quantify, despite the significant reduction in the diffusion path length.

4.5.4.4 Sample Type 4: Adhesive Coating

Graphs of capacitance as a function of exposure time for the L4 coatings for samples 1 and 2 are shown in Figure 4-20 and Figure 4-21, respectively. Examination of Figure 4-20 and Figure 4-21 reveals a dramatic change in capacitance after several days of exposure. This dramatic change in capacitance is due to adhesive debonding an accumulation of fluid at the sensor surface. For the adhesive coating, saturation was reached after only 1.4 hours. This experiment suggests that after only several days of exposure to 0.1 M NaOH, the interface is significantly degraded in order to result in coating delamination.

4.5.4.5 Discussion of Durability of Sandwich Specimens

In light of the results from the exposed adhesive coating (Section 4.5.4.4), the durability of the sandwich specimens may be discussed. The durability of the L4 sandwich specimens is likely attributable to the stress state of the adhesive sandwiched between the two impermeable substrates. Abdel Wahab and coworkers studied the change in stress due to moisture diffusion in epoxy adhesives bonded between aluminum.[154] Using finite element analysis they report the stress state in the adhesive at different exposure times. Of interest is their result after 6 weeks of exposure where the normalized concentration in the adhesive they studied is similar to our

system after 30 days of exposure. Abdel Wahab and coworkers report that the peak peel stress is reduced at the edge due to swelling and a reduction in modulus. In addition, changes in the direction of shear stress and a reduction in the peak plastic strain were predicted. As a result, they expected no reduction in joint strength, which agreed with their experimental adhesion measurements of single lap joints. In contrast, the tested coatings exhibited debonding once the crack driving energy due to residual stress exceeded the interfacial toughness. This published work provides an additional example that coatings are typically less durable than adhesives sandwiched between two substrates. These experimental results suggests that an interesting future experiment would be to measure the diffusion of an aggressive fluid into an adhesive layer sandwiched between the sensor and a flexible, yet impermeable backing, with good chemical resistance (e.g tantalum film).

4.5.5 Conclusions

Constant frequency interfacial impedance spectroscopy was utilized to investigate the diffusion of 0.1 M NaOH into bonded L4 epoxy adhesive sandwich joints and coatings. A number of conclusions have been made that are unique to this adhesive system, but have wider implications. For the sandwich specimens, the sensitivity of the instrument and sensors was not sufficient to determine the change in capacitance or time to saturation, two important diffusion parameters, within a reasonable error. The sandwich adhesive bond appears durable and, within the sensitivity of the instrument, does not appear to have any fluid accumulation or debonding. In contrast, the adhesive coating exhibited delamination after only several days of exposure. This work provides an additional example that coatings are typically less durable than adhesives sandwiched between two substrates. These results suggest that the experimental set-up must be modified in order to obtain enough sensitivity to detect the migration of fluids into durable

structural adhesive joints. Recommendations for improving the resolution of the instrument are discussed in Section 0.

4.5.6 Figures

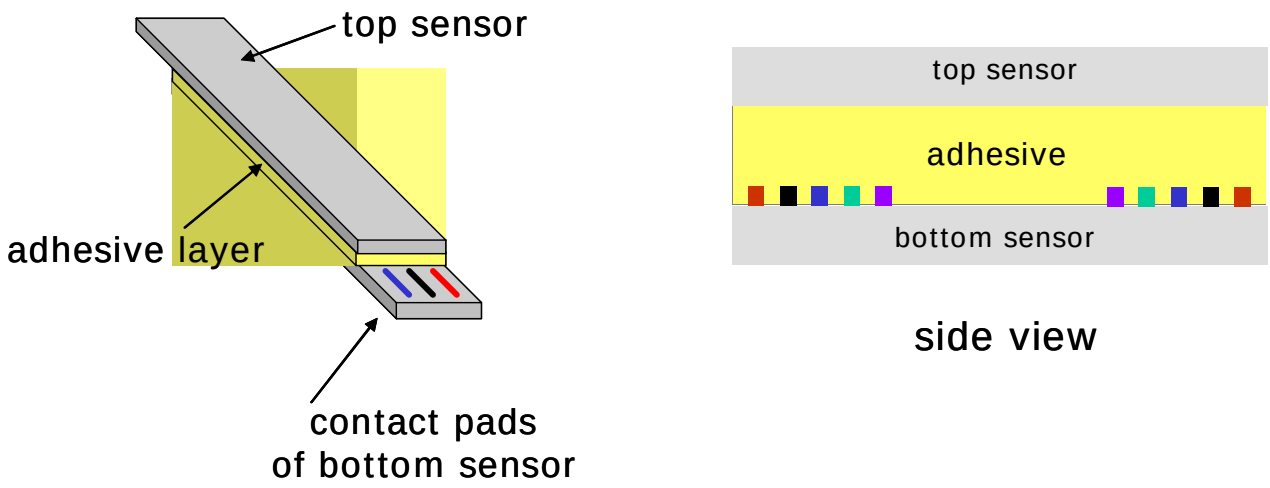

Figure 4-10 Schematic of adhesive sandwich specimen.

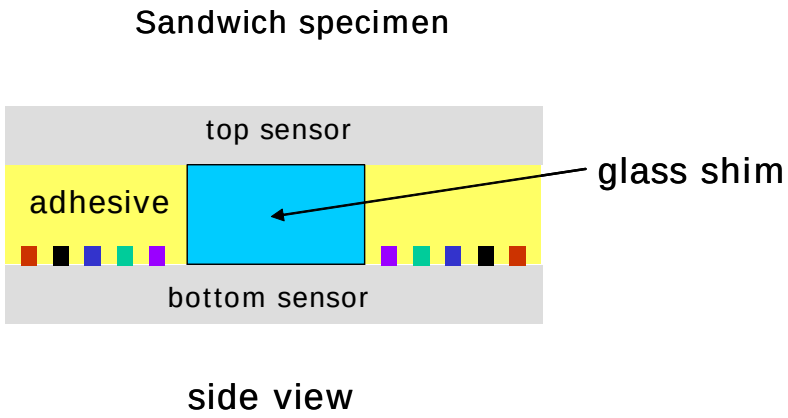

Figure 4-11 Schematic of the adhesive sandwich specimen with glass shim.

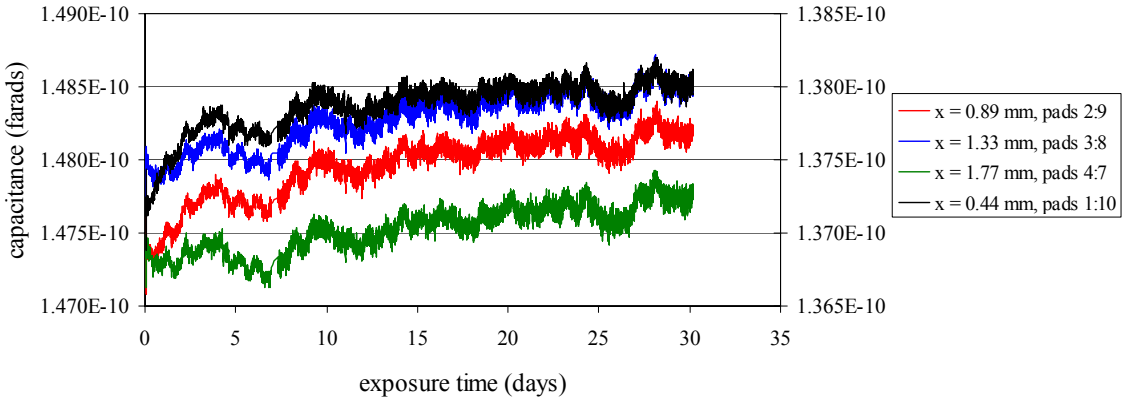

Figure 4-12 The capacitance as a function of exposure time (days) for the L4 adhesive sandwich specimens Type 1 Sample 1 exposed to 0.1 M NaOH.

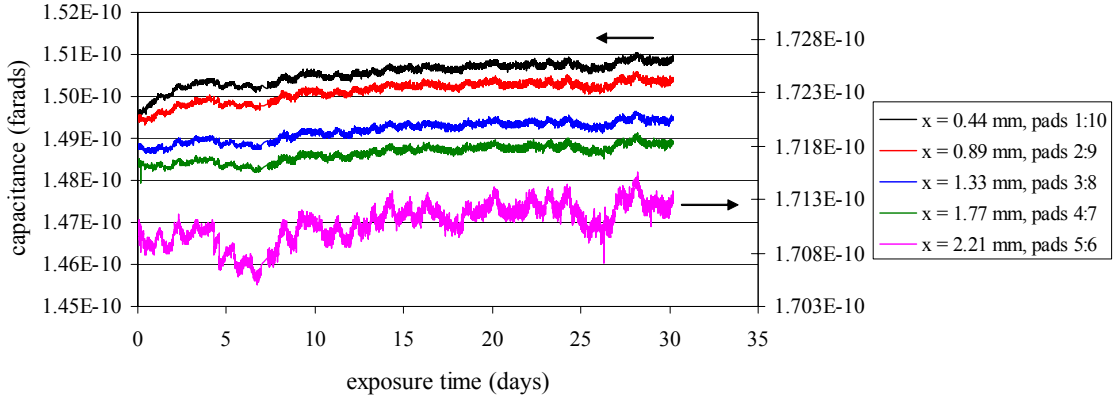

Figure 4-13 The capacitance as a function of exposure time (days) for the L4 adhesive sandwich specimens Type 1 Sample 2 exposed to 0.1 M NaOH.

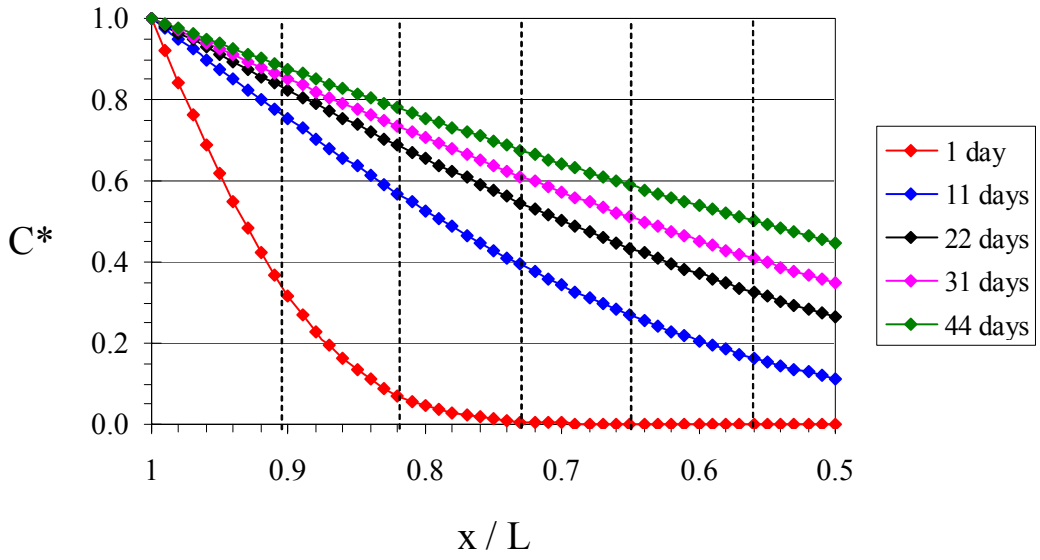

Figure 4-14 Normalized concentration (C^*) as a function of normalized distance from the edge (x / L). $x / L = 1$ is the edge and $x / L = 0$ is the center of the sensor. This is for the sample without a shim, where L = 5.0 mm. The vertical dashed lines represent the value of x that each pair of pads measures for pads 1-10 ($x / L = 0.91$), 2-9, 3-8, 4-7, and 5-6 ($x / L = .56$).

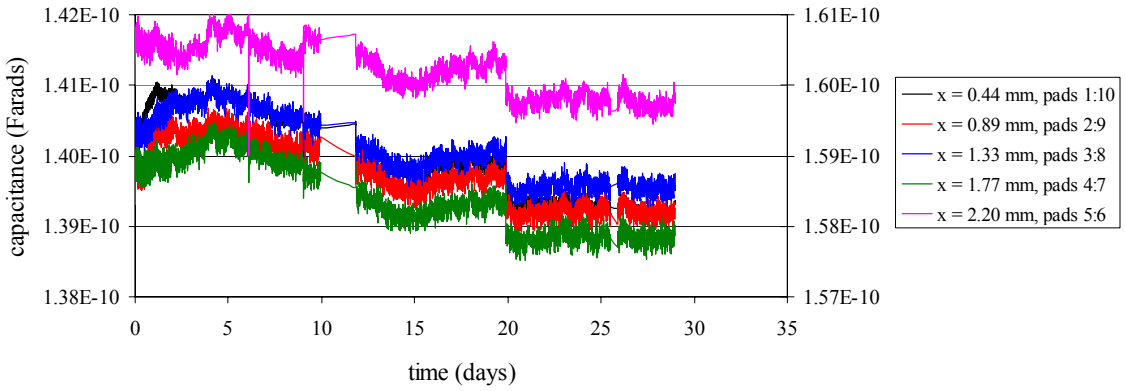

Figure 4-15 The capacitance as a function of exposure time (days) for the L4 adhesive sandwich specimens Type 2 Sample 1 exposed to 0.1 M NaOH. The surface was treated with release agent.

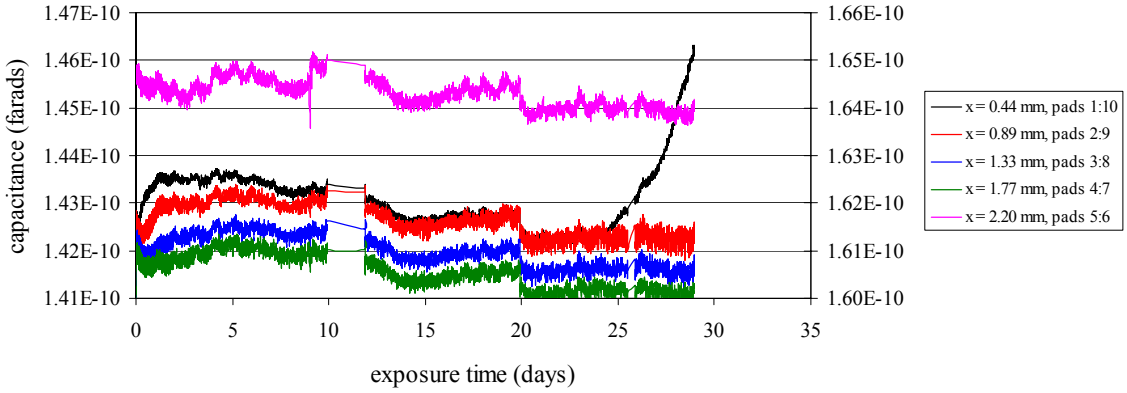

Figure 4-16 The capacitance as a function of exposure time (days) for the L4 adhesive sandwich specimens Type 2 Sample 2 exposed to 0.1 M NaOH. The surface was treated with release agent.

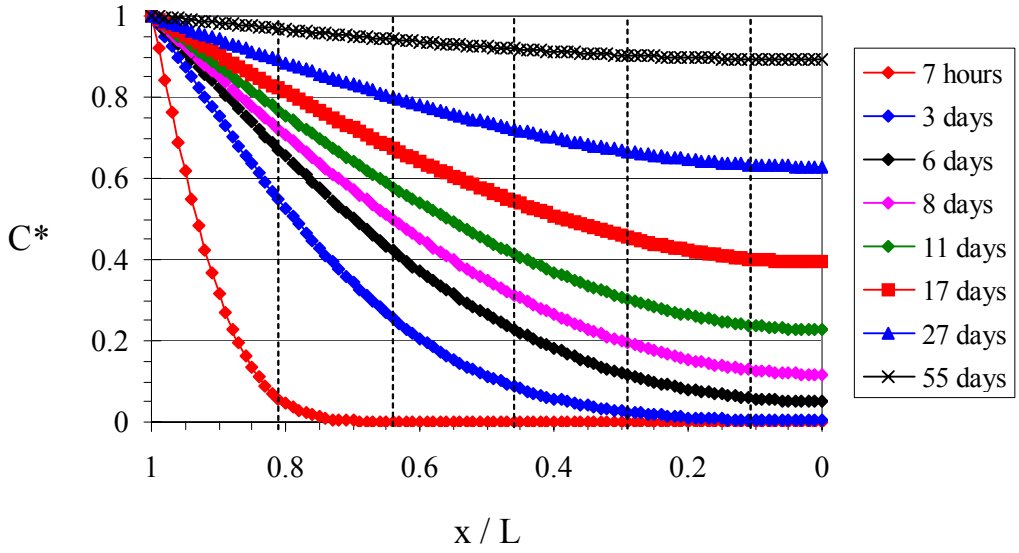

Figure 4-17 Normalized concentration (C^*) as a function of normalized distance from the edge (x / L). $x / L = 1$ is the edge and $x / L = 0$ is the center of the sensor. This is for the sample with a shim, where L = 2.5 mm. The vertical dashed lines represent the value of x that each pair of pads measures for pads 1-10 ($x / L = 0.91$), 2-9, 3-8, 4-7, and 5-6 ($x / L = .56$).

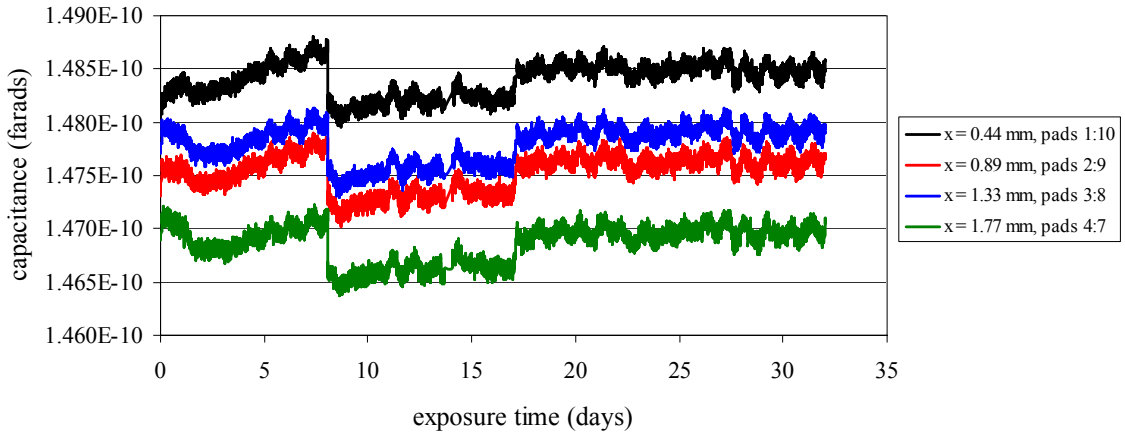

Figure 4-18 The capacitance as a function of exposure time (days) for the L4 adhesive sandwich specimens Type 3 Sample 1 exposed to 0.1 M NaOH. The sample was equipped with a shim.

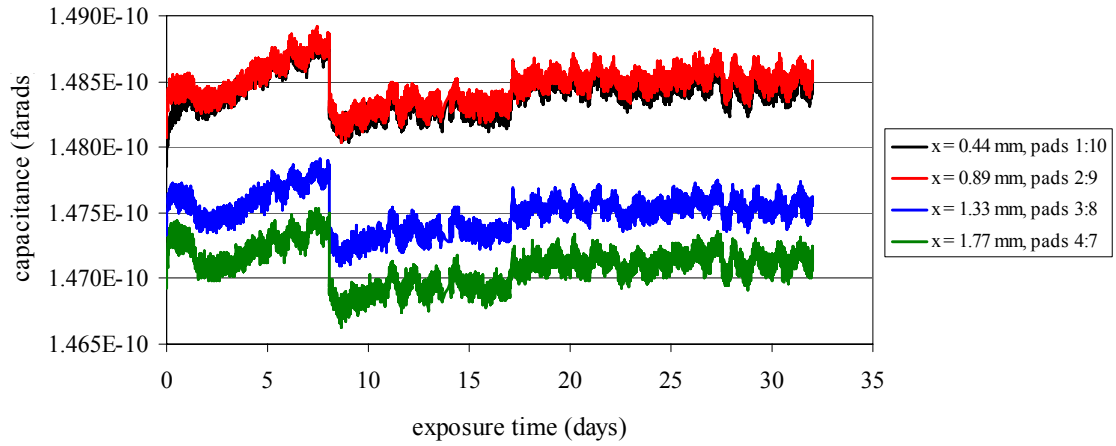

Figure 4-19 The capacitance as a function of exposure time (days) for the L4 adhesive sandwich specimens Type 3 Sample 2 exposed to 0.1 M NaOH. The sample was equipped with a shim.

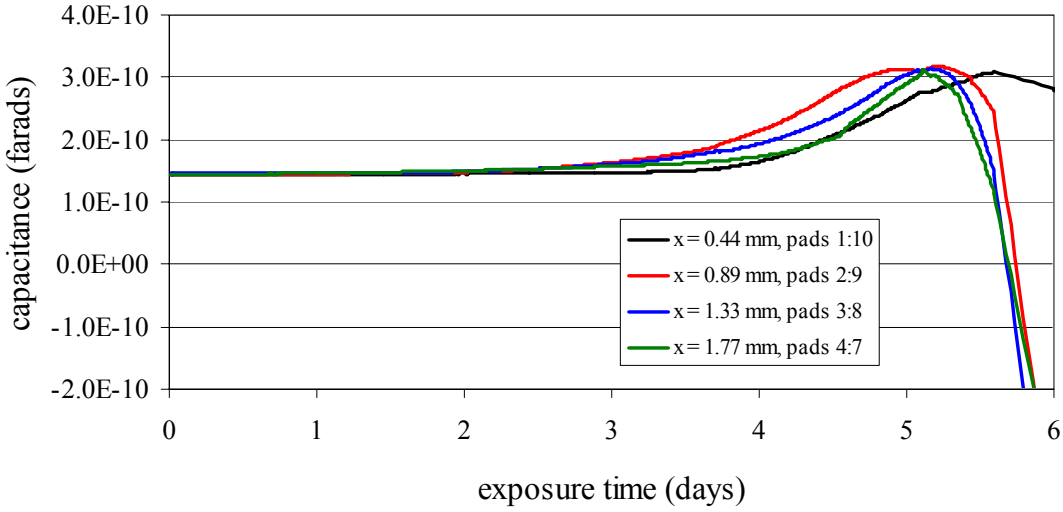

Figure 4-20 The capacitance as a function of exposure time (days) for the L4 adhesive coatings Type 4 Sample 1 exposed to 0.1 M NaOH.

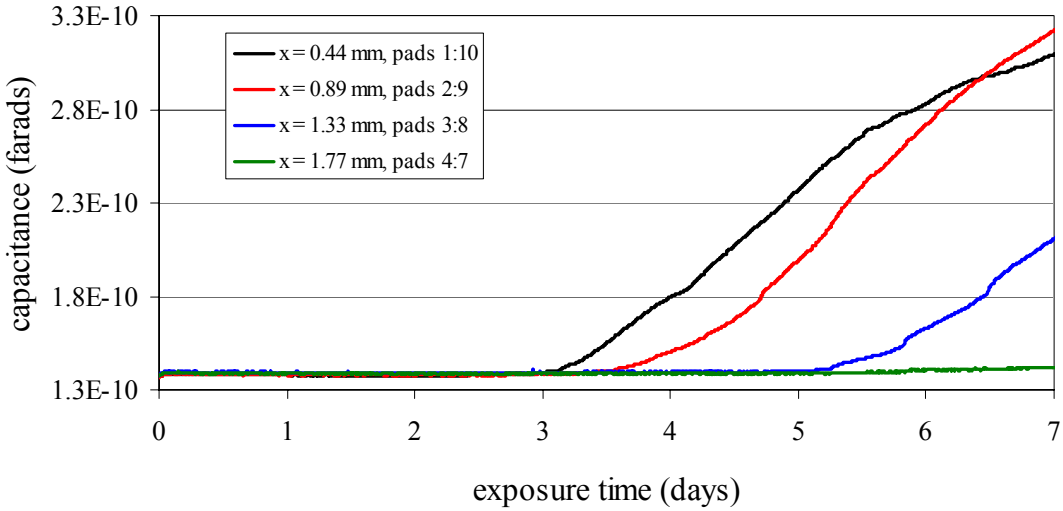

Figure 4-21 The capacitance as a function of exposure time (days) for the L4 adhesive coatings Type 4 Sample 2 exposed to 0.1 M NaOH.

4.6 Moisture Diffusion from the Edge in Bonded UV Curable Pressure Sensitive Adhesives Measured by Constant Frequency Impedance Spectroscopy

4.6.1 Abstract

Moisture diffusion into a series of UV curable pressure sensitive adhesives was measured using constant frequency interfacial impedance spectroscopy and a novel impedance sensor design. Adhesives Research Incorporated of Glen Rock, Pennsylvania supplied and fabricated the samples. Either a permeable poly(ethylene terephthalate) backing or an impermeable glass backing was used to control the path of diffusion into the bonded adhesive. Several different types of adhesives were tested. Samples were conditioned in either 60° water or in 60°C 100% relative humidity environments. This work illustrates the wide variety of diffusion behaviors of bonded adhesives and demonstrates the utility of the IIS technique as an effective tool for screening adhesive formulations.

4.6.2 Experimental

4.6.2.1 General Adhesive Description and Sample Preparation

The adhesives used in this study were manufactured by Adhesives Research Incorporated. The details of the structure are proprietary. However, the adhesives are UV curable and are epoxy based. Acrylate groups provide the necessary groups to make the adhesive UV curable. The uncured adhesive is tacky and will fibrillate readily when stretched.

Samples were prepared at Adhesive Research Incorporated. The high surface energy sensor substrates (SiO/Au) were utilized in this research. The sensor surfaces were prepared by

first rinsing with isopropyl alcohol and then blow-drying the sensor with high-purity nitrogen. The PSA adhesive film initially has two transfer liner layers on either side of the film to facilitate handling. A single liner was removed and the adhesive was carefully applied to the sensor so that no bubbles are formed. The second transfer layer was removed and either the glass or poly(ethylene terephthalate) (PET) backing was applied. The adhesives were 63.5 microns (2.5 mils) thick and the PET liner was 50.8 microns (2.0 mils thick).The glass backing was carefully applied to ensure no air bubbles were formed. The specimen was then placed in an oven at 65 °C for 1-2 minutes to soften the adhesive and promote wetting. Some specimens were not subjected to the 65 °C oven step. The specimen is then hand pressed and exposed to UV dose to cure. Note some samples were uncured. Bonded specimens were then immediately stored in dessicant.

4.6.2.2 Experimental

The adhesive formulation is denoted as ARiA (ARi id# 480-52-A). ARiA was tested under several conditions where the effects of the backing properties, the state of water, sample preparation (and consequently the interfacial toughness) and cure were investigated. The samples are desiganted:

1. ARiA (no 65 °C step) PET backing in 60 °C liquid water
2. ARiA (no 65 °C step) PET backing in 60 °C water vapor
3. ARiA (no 65 °C step) Glass backing in 60 °C liquid water
4. ARiA (no 65 °C step) Glass backing in 60 °C water vapor
5. ARiA (with 65 °C step) no cure, Glass backing in 60 °C water vapor
6. ARiA (with 65 °C step) cured, Glass backing in 60 °C water vapor

For these samples, “no 65” denotes that the during the sample fabrication process, specimens were not exposed to the 65°C oven for 1-2 minutes. Exposure of the sample to the 65 °C step improved adhesion.

To control the path of diffusion into the bonded adhesive, either a permeable PET backing (Figure 4-22) or an impermeable glass backing were utilized (Figure 4-23). As shown in Figure 4-22, the PET backing allows for moisture transport through the top of the PET backing and adhesive in the direction of the interface and also from the edge of the sensor. Note that the path of diffusion is much shorter, and therefore faster, through the top of the bonded adhesive than from the edge of the sensor. The impermeable glass backing controls the path of diffusion so that fluid enters the adhesive from the edge of the sensor only and results in the highest concentration of fluid at the sensor edge. Unfortunately, the bulk diffusion behavior of the adhesive could not be accurately measured. Therefore, the moisture diffusion behavior determined from IIS could not be correlated to bulk diffusion in the adhesive.

4.6.3 Results and Discussion

4.6.3.1 ARiA (no 65 °C) PET Backing in 60 °C Liquid Water

A graph of the capacitance as a function of x and exposure time is shown in Figure 4-24 for ARiA (no 65 °C) PET backing in 60°C liquid water. The capacitance changes for each value of x are essentially the same value. This suggests that the diffusion of water to the electrode interface is predominantly though the top of the backing and that diffusion from the edge is not significant. Additional evidence suggesting diffusion from the edge is not significant comes from the graph of the capacitance as a function of x and exposure time for the first few hours, shown in Figure 4-25. The necessary lag time for the water to diffuse through the film to the surface and

begin to accumulate is apparent in Figure 4-25. This lag time is independent on the distance from the edge of the sensor, *x*. Also of interest is the change in capacitance is positive up to approximately 3.5 hours and negative following that time. The dramatic change in slope after approximately 3.5 days does not necessarily mean the adhesive has been saturated. The change in slope is likely due to a change in the phase angle brought about by a large fluid concentration.

4.6.3.2 ARiA (no 65 °C) PET Backing in 60 °C Water Vapor

The graph of the capacitance as a function of *x* and exposure time is shown in Figure 4-26 for ARiA (no 65 °C) PET backing in 60 °C water vapor. For this adhesive (ARiA no 65 °C PET backing), the shape of the capacitance curve was essentially the same as for the 60°C liquid water and water vapor condition. The time when the capacitance dramatically changes slope was approximately 4.5 days. In addition, the magnitude of the change in capacitance observed for samples exposed to 60°C relative humidity was much less than in the 60°C water. The difference in the change in capacitance is probably not due to a different concentrations of water at the sensor surface because the time to saturation were similar and because there was no theoretical difference between the water transport mechanism for liquid water and water vapor.[155] Additional samples are needed to determine the reproducibility and error of these experiments. Note that it would be advantageous to use water vapor when studying the absorption of water into adhesives, since this would eliminate any misleading effects caused by liquid water evaporation.

4.6.3.3 ARiA (no 65 °C) Glass Backing in 60°C Liquid Water

The graph of the capacitance as a function of *x* and exposure time is shown in Figure 4-27 for ARiA (no 65 °C) Glass backing in 60 °C liquid water. As expected, the change in capacitance

was greater closer to the edge of the sensor and there was also a lag time necessary for the fluid to diffuse from the edge and across the sensor surface. These trends are more easily observed in the graph of the resistance as a function of *x* and exposure time is shown in Figure 4-28. After roughly 20 to 25 days the adhesive was saturated up to a value of x = 1.77 mm.

4.6.3.4 ARiA (no 65 °C) Glass Backing in 60 °C Water Vapor

A graph of the capacitance as a function of *x* and exposure time is shown in Figure 4-29 for ARiA (no 65 °C) Glass backing in 60 °C water vapor. Also a plot of the resistance as a function of *x* and exposure time is shown in Figure 4-30. Again, the expected trends in capacitance and resistance were observed. After roughly 20 to 25 days the adhesive was saturated up to a value of x = 1.77 mm. The large change in capacitance, visible lag time and saturation time from the ARiA (no 65 °C) adhesive with a glass backing (liquid and vapor water) indicate that moisture diffuses into the ARiA at larger concentrations relative to the epoxy adhesives studied in Section 4.5. As discussed previously, moisture diffusion into the bonded PSA could occur from the either the interface, the bulk, or from both sources.

4.6.3.5 ARiA (With 65 °C) no Cure Glass Backing in 60 °C Water Vapor

The uncured (no UV exposure) ARiA adhesive formulation with a glass backing was exposed to 60°C water vapor. Here, the sample underwent the 65 °C step for 1-2 minutes. The sample was exposed for approximately 10 days. Two samples were tested to demonstrate the repeatability of the experiment. The measured capacitance as a function of *x* and exposure time for samples 1 and 2 are shown in Figure 4-33 and Figure 4-32, respectively. In sample 1, the uncured adhesive exhibited a peak in the capacitance after only 6 hours for all values of *x*. In sample 2, the uncured adhesive exhibited a peak in the capacitance after only 8 hours for all values of *x*. In both

samples, a small lag time (up to 2 hours) necessary for the moisture to migrate from the edge of the specimen was observed. The similar behavior between sample 1 and 2 illustrates the repeatability of the experiments. No significant difference in the lag time or peak in capacitance was observed for different values of x. This suggests that the fluid rapidly migrates across the sensor surface and that moisture transport from the interface must be significant. If diffusion occurred predominantly in the bulk and from the edge of the specimen, then a lag time would have been observed. The data suggest that the uncured adhesive is not durable and that moisture diffused into the adhesive rapidly (less than several days). Comparing the cured and uncured systems strongly suggest that curing the adhesive is essential to increasing the durability.

4.6.3.6 ARiA (With 65°C) Cured with Glass Backing in 60 °C Water Vapor

The measured capacitance as a function of x and exposure time is shown in Figure 4-33 and Figure 4-34, respectively. The UV cured samples exhibited a minimal change in capacitance of approximately 1 – 2 pico-farads. Both samples exhibited a greater change in capacitance and a peak in the capacitance values of x = 0.44 and 0.89 mm. This result and others indicate that these experiments have good repeatability. Furthermore, these results suggest that the change in capacitance at these values of x is likely to have a physical meaning and is not just a result of noise in the data. We can speculate that the increase in capacitance at the edge of the specimen is due to greater swelling and a greater concentration of moisture at the edge than in the center of the specimen. A large jump in the capacitance is observed in sample 1 and 2 after 8 days of exposure; however, it is unclear if the increase is due to noise or a real physical event in this case. This relatively small change in capacitance at the center of the specimen is similar in magnitude to the tested L4 epoxy adhesives exposed to the aggressive fluid (Section 4.5). The similar behavior with the L4 epoxy adhesives suggests the UV cured PSA may be as effective as

the epoxy. Comparing the results from the ARiA adhesive with and without the 65 °C step, indicates that significant more durability is imparted on the sample when the 65 °C step was employed, presumable due to better wetting and a corresponding increase in the interfacial toughness. Both conditions (with and without the 65 °C step) utilize the same adhesive and therefore have similar bulk (non-bonded) adhesive diffusion rates. Differences in the diffusion behavior detected by IIS are therefore a result of differences in the interface. These experiments show that the sensor can distinguish differences in the interface durability. The two extremes of moisture absorption behavior have been measured. In the case of poor durability (AriA UV no cure and AriA cured no 65 °C step), changes in capacitance indicate a significant contribution to diffusion from the interface. In the case of good durability (L4 adhesive and AriA cured with the 65 °C step), changes in capacitance due to fluid absorption are small and the capacitance signal is subject to noise.

4.6.4 Conclusions

A wide variety of diffusion behavior has been illustrated by studying several different types of UV curable pressures sensitive adhesives. Utilizing constant frequency IIS, differences were observed among samples with different paths of diffusion into the bonded adhesive, state of cure, and interfacial toughness. Most importantly is the dramatic difference in diffusion behavior between relatively non-durable adhesives and durable adhesives. For non-durable adhesives, changes in capacitance indicate a significant contribution to diffusion from the interface. For durable adhesives, changes in capacitance due to fluid absorption are relatively small and the capacitance signal is subject to noise.

4.6.5 Figures

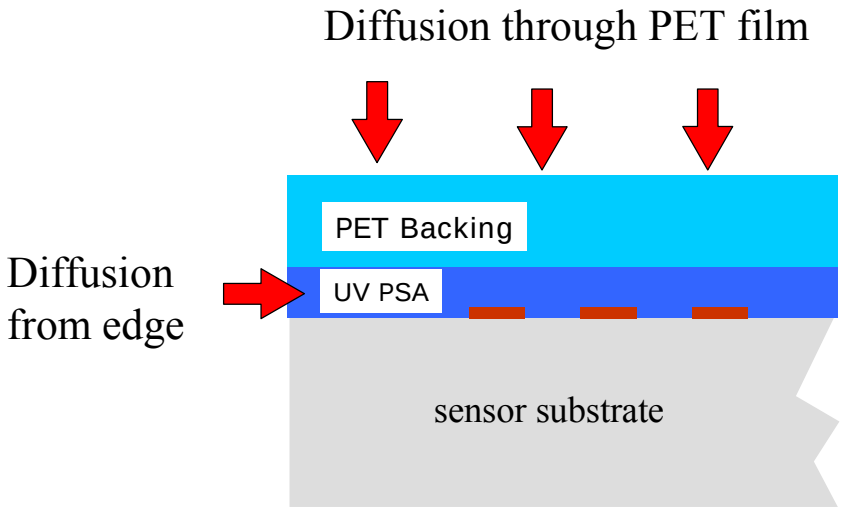

Figure 4-22 Schematic of the profile view of the adhesive with the PET backing bonded to the sensor. The paths of diffusion are illustrated with the red arrows.

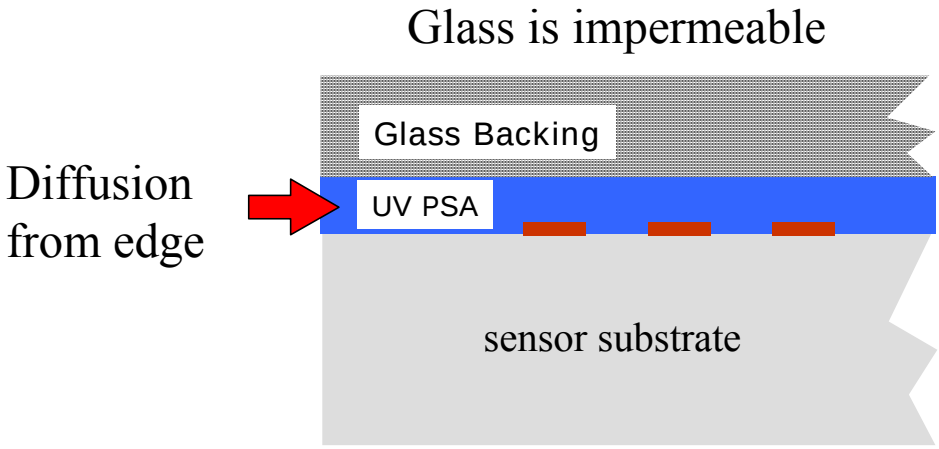

Figure 4-23 Schematic of the profile view of the adhesive with the glass backing bonded to the sensor. The path of diffusion is illustrated with the red arrows.

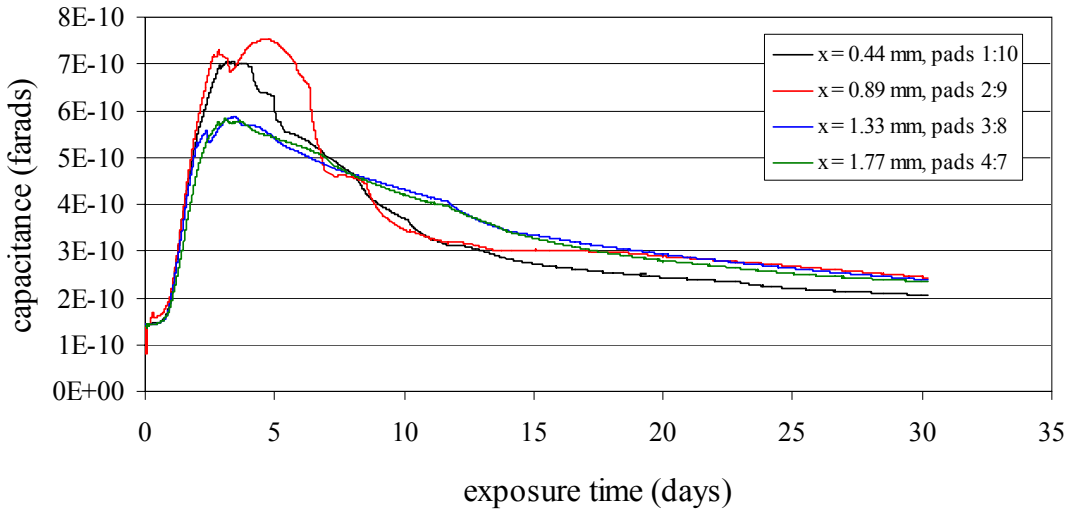

Figure 4-24 The measured capcitance (pF) as function of exposure time (days) for the AriA adhesive with the PET backing in 60°C water.

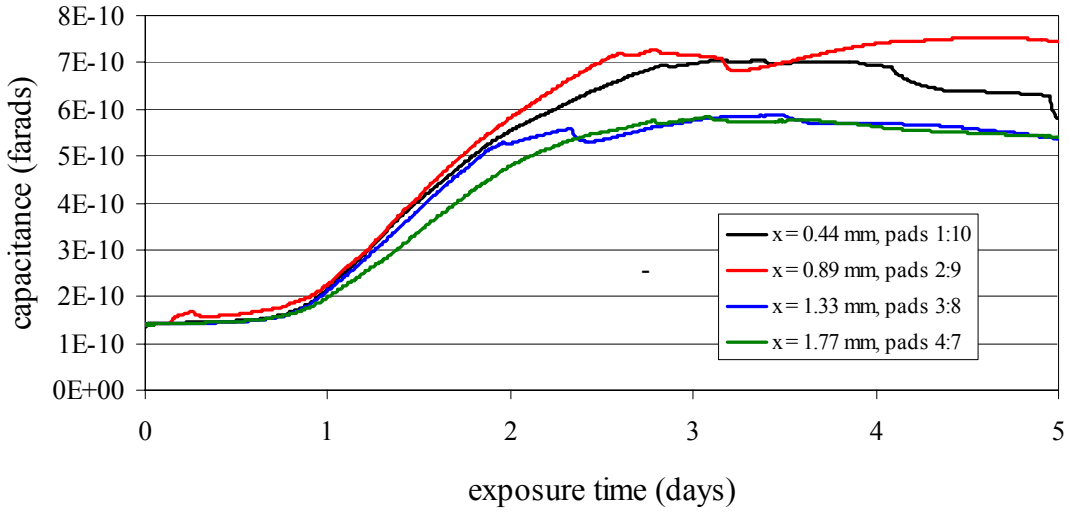

Figure 4-25 The measured capcitance (pF) as function of exposure time (days) for the AriA adhesive with the PET backing in 60°C water. The first few hours are shown to illustrate the lag time necessary for the fluid to diffuse to the sensor surface.

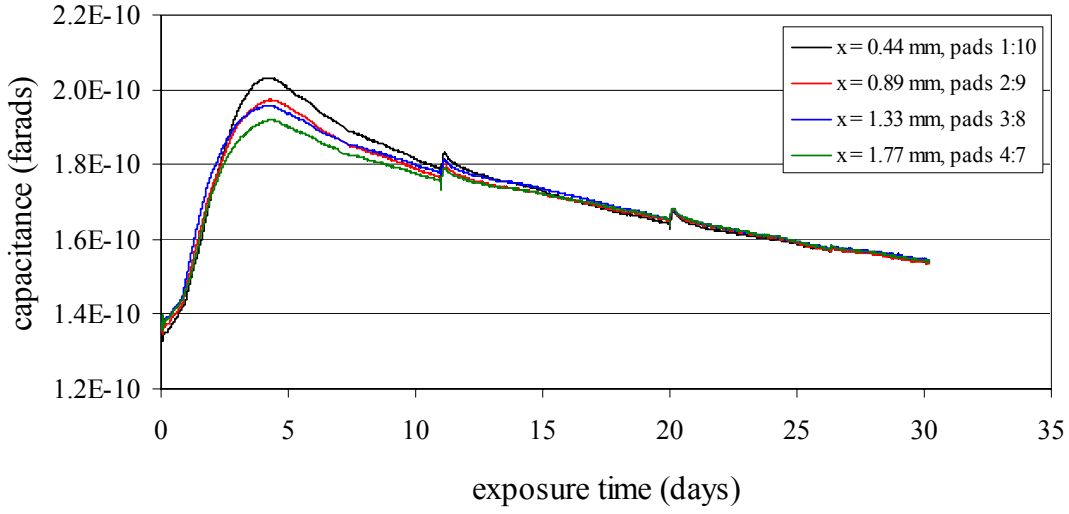

Figure 4-26 The measured capacitance (pF) as function of exposure time (days) for the AriA adhesive with the PET backing in 60°C 100% relative humidity.

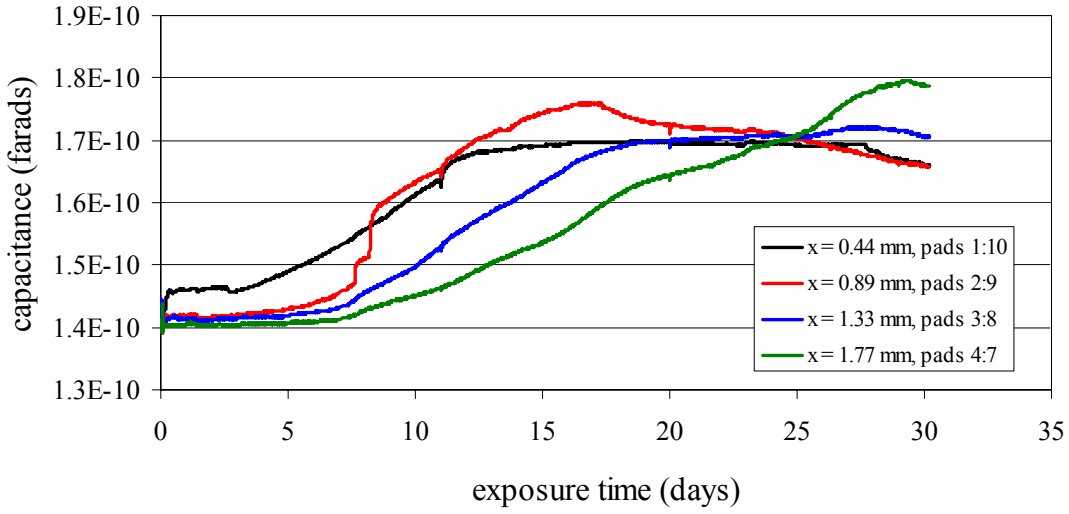

Figure 4-27 The measured capacitance (pF) as function of exposure time (days) for the AriA adhesive with the glass backing in 60°C water.

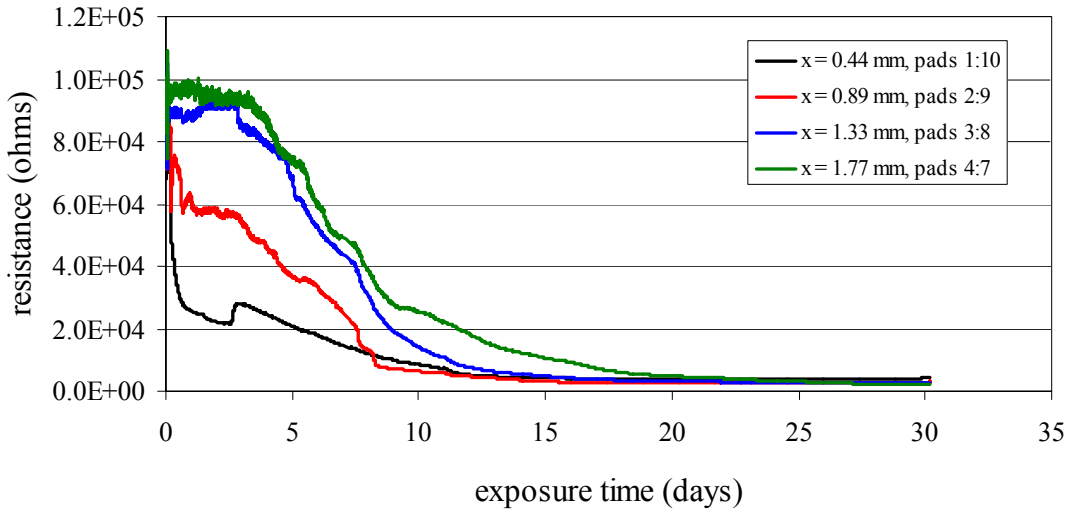

Figure 4-28 The measured resistance (ohms) as function of exposure time (days) for the AriA adhesive with the glass backing in 60°C water.

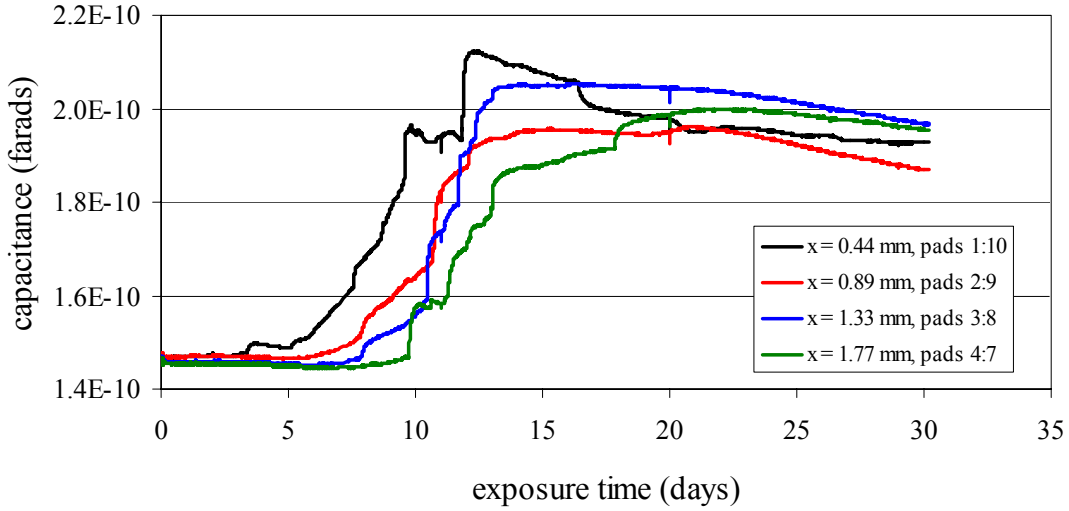

Figure 4-29 The measured capacitance (pF) as function of exposure time (days) for the AriA adhesive with the glass backing in 60°C 100% relative humidity.

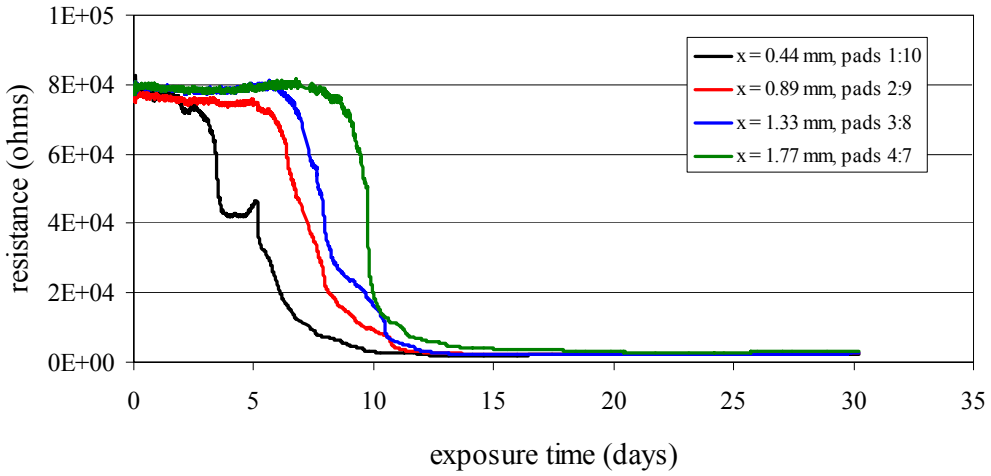

Figure 4-30 The measured resistance (ohms) as function of exposure time (days) for the AriA adhesive with the glass backing in 60°C 100% relative humidity.

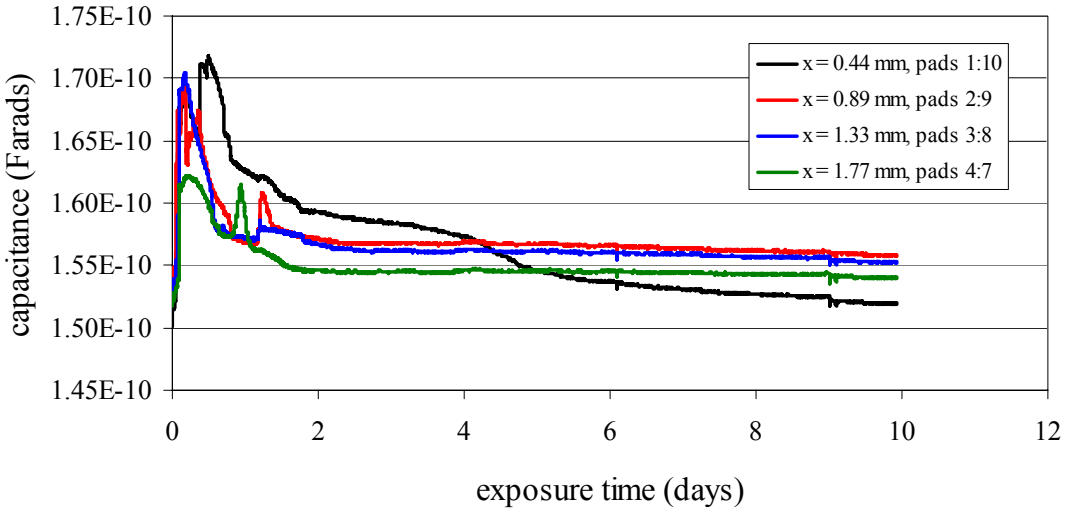

Figure 4-31 The measured capacitance (pF) as function of exposure time (days) for the ARi 480-52-A No UV cure (Sample 1)

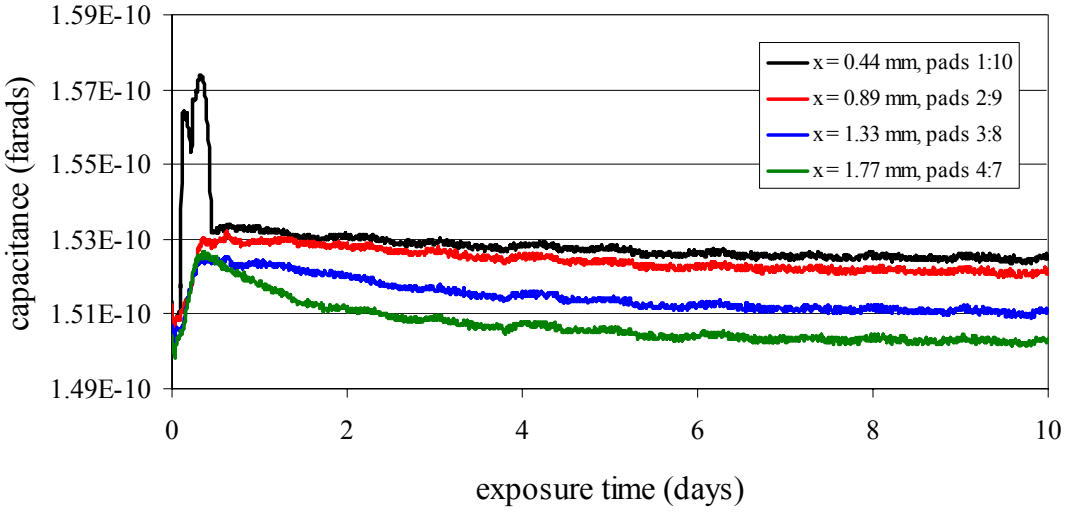

Figure 4-32 The measured capacitance (pF) as function of exposure time (days) for the ARi 480-52-A No UV cure (Sample 2)

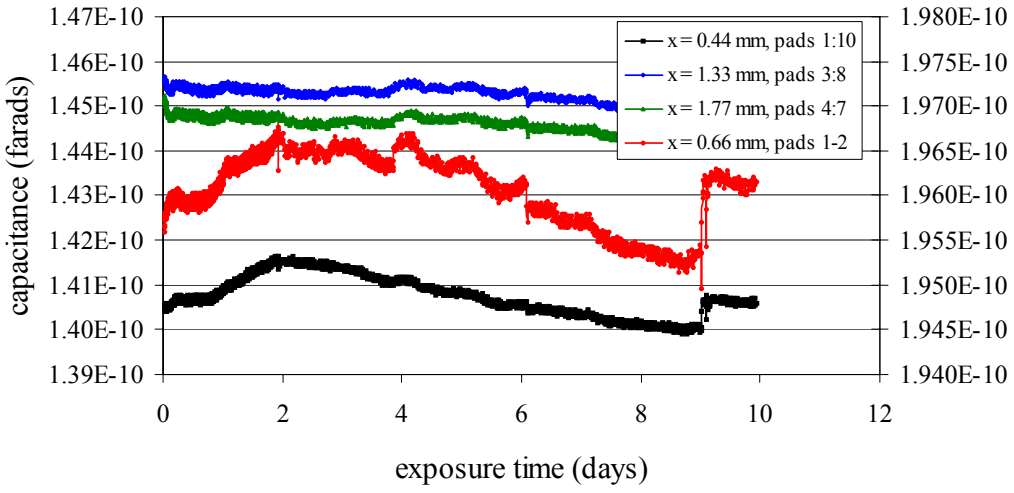

Figure 4-33 The measured capacitance (pF) as function of exposure time (days) for the ARi 480-52-A High UV cure (Sample 1).

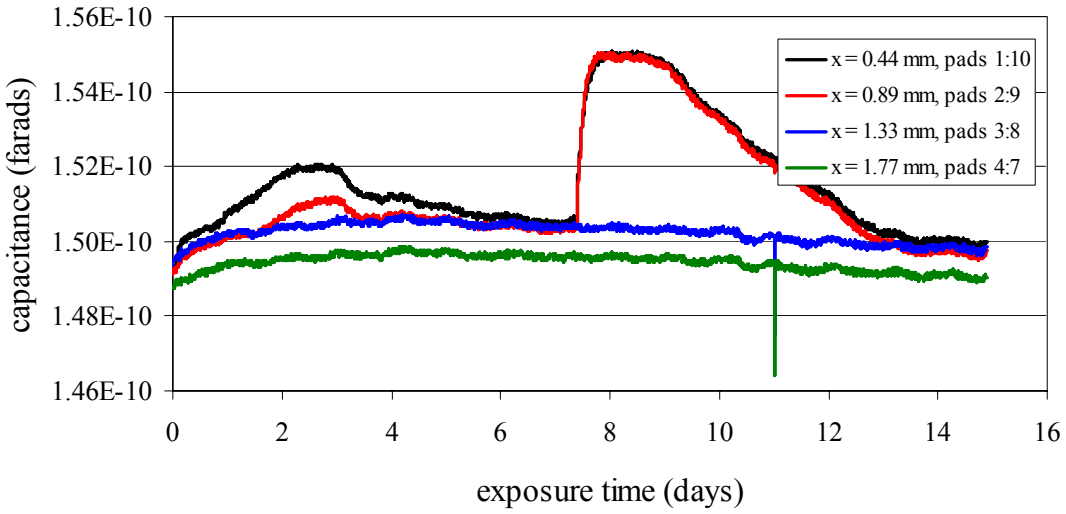

Figure 4-34 The measured capacitance (pF) as function of exposure time (days) for the ARi 480-52-A High UV cure (Sample 2).

4.7 Durability of Adhesive Coatings Subjected to Hygroscopic Cycling Measured by Constant Frequency Impedance Spectroscopy

4.7.1 Abstract

The technique of constant frequency interfacial impedance spectroscopy (IIS) coupled with a novel interdigitated electrode sensor design were used to investigate the effects of hygroscopic cycling on the durability of epoxy adhesive coatings. Using IIS enabled measurement of the change in capacitance resulting from fluid absorption as a function of the distance from the edge of the sensor, x, and the number of exposure cycles. This information was utilized to determine the number of cycles required to initiate adhesive failure and also the "apparent crack length" growth rates of the failure as a function of the number of exposure cycles. During a single cycle the coated specimens were first exposed to fluid at 60°C for 24 hours, then cooled to room temperature in the fluid environment for 30 minutes, and then dried in a dessicator (~ 5 % relative humidity) for an additional 24 hours. It is in the last stage of the cycle, during the drying step, that the adhesive coatings debonded. Evidence for adhesive debonding was evident from large changes in the capacitance resulting from interfacial displacement of the adhesive and the large concentration of fluid at the substrate sensor surface. The number of cycles until failure was determined as a function of coating thickness, fluid environment, and sensor surface chemistry.

4.7.2 Introduction

4.7.2.1 Residual Stresses in Adhesive Joints

Internal residual stresses can significantly affect the durability of adhesives and composites [8-11]. These stresses can cause adhesive failure by leading to the formation of cracks [11] which tend to initiate at bimaterial interface corners or edges.[156,157] Residual stress in adhesives joints and coatings can originate from processing or solidification of the adhesive. Heating or cooling where there is a difference in the coefficient of thermal expansion (CTE) between the adhesive and substrate lead to such stresses, as do the absorption of moisture and other fluids.[11,158,159] Internal residual stresses in adhesive coatings can either be contractive or expansive in nature.[160] Contractive internal stresses impart a tensile stress on the coating and develop from volume shrinkage typical of coating formation and/or thermal contractive stresses. Volume shrinkage during coating formation can result from either cure shrinkage or from solvent loss, or a combination of the two. Contractive stresses in adhesives arise from the CTE mismatch between the substrate and adhesive coating described above. The usual case is where the CTE of the substrate (O ~ 1-10 for glasses) is less than the CTE of the polymer (O ~ 60 - 100). Under such conditions, if the stresses are (equal) biaxial, the residual stress σ_r in the coating (or sandwich specimen) can be estimated from the following expression:[126,161,162]

Equation 4-12
$$\sigma_r = -\frac{E}{(1-\nu)}\Delta\alpha\Delta T$$

where E is the modulus of the coating, $\Delta\alpha = \alpha_a - \alpha_s$ is the difference between the linear coefficient of thermal expansion of the adhesive coating α_a and substrate α_s, $\Delta T = T - T_{SFT}$ is the difference between the temperature of the adhesive T and the stress free temperature T_{SFT}, and ν is the Poisson ratio of the adhesive coating (typically ca. 0.4 for an epoxy). The stress free

temperature is near the glass transition of the adhesive; however, the stress free temperature can vary by as much as 40°C because of differences in cooling the adhesive (quench vs. slow cool).[163] Based on a stress singularity approach, Lefebvre and co-workers predicted that with high glass transition materials, where (T_{cure} - T_{SFT}) ~ 200, under unfavorable conditions (high modulus, high CTE, poor adhesion) residual stresses can initiate debonding at interface corners, where cracks tend to initiate.[156,157]

Crack initiation at the edge of an adhesive bond is exacerbated at interface corners where the coating shear stresses due to CTE mismatch are at a maximum. These shear stresses decrease away from the edge and are zero in the center of the coating.[162] The tensile residual stresses, on the other hand is zero at the edges and at a maximum in the center of the adhesive joint. In the work of Humfield and Dillard[12], crack initiation at the edge of adhesive joints was attributed to shear and peeling stresses at the interface edge resulting from residual stresses. These residual stresses were generated by adhesive shrinkage during cure and the discussed difference in CTE between the adhesive and substrate. They suggested that crack growth will tend to occur at lower temperatures when the residual stresses and strain energy release rate are highest.[12]

Although the residual stress is independent (as Equation 4-12 reveals) of the coating thickness, the strain energy release rate G or crack driving energy is proportional to the film thickness h and is expressed in Equation 4-13.[126,162]

Equation 4-13
$$G = Z\frac{h\sigma_r^{\,2}(1-\upsilon)}{E}$$

where Z is equal to 1.028 during crack initiation and 0.5 for steady state crack growth. Furthermore, a critical thickness h_c is predicted above which debonding is predicted to occur [162]:

Equation 4-14
$$h_c = \frac{1}{Z}\frac{\Gamma_c E}{\sigma_r^{\,2}(1-\upsilon)}$$

where Γ_c is the debonding energy or toughness of the interface.

Volume expansion of the coating by swelling with water and/or other fluids, or an increase in temperature can cause the internal stresses to be compressive.[160] Similar to residual stresses cased by CTE mismatch, the residual stress due to swelling can be expressed as:

Equation 4-15
$$\sigma_r = -\frac{E}{(1-\nu)}\varepsilon_{swelling}$$

where $\varepsilon_{swelling}$ is the strain induced by swelling or absorption of the penetrant. The value of $\varepsilon_{swelling}$ can be expressed in terms of a linear hygroscopic expansion coefficient that is a function of temperature [161]:

Equation 4-16
$$\sigma_r = -\frac{E}{(1-\nu)}\Delta\beta\Delta T$$

where $\Delta\beta = \beta_a - \beta_s$ is the difference between the linear hygroscopic expansion coefficient of the adhesive coating, β_a, and of the substrate, β_s, and $\Delta T = T - T$ is the temperature difference. Alternatively, the value of $\varepsilon_{swelling}$ can be expressed in terms of a linear hygroscopic expansion coefficient that is a function of absorbed mass:[162]

Equation 4-17
$$\sigma_r = -\frac{E}{(1-\nu)}\Delta\beta\Delta M$$

where ΔM is the change in absorbed mass. Vanlandingham *et al*. found that for epoxy resins cured with amines that the value of β was 0.22 mm per mm per wt% and also found reductions in Tg ranging from 5 – 20 °C.[56]

It should also be noted that stresses influence the absorption of moisture. Yaniv and Ishai showed that for epoxies the maximum amount of absorbed moisture is not stress dependent;

however, in tension the diffusion rate increased and in compression the diffusion rate was reduced.[164]

It is relevant to note Weitsman's results for an adhesive constrained between two rigid adherends, which apply to an adhesive undergoing expansion due to either elevated temperature or moisture absorption.[165] Weitsman showed that during the initial stage of the swelling process: 1) the resulting normal stresses are compressive at the edge of the joint, 2) there is a peak tensile stress at a place slightly inside the interface, and 3) the stress is zero far away from the edge. For the fully saturated (equilibrium) condition, the normal tensile stresses are at a maximum at the edge of the joint. For thin films the stresses were found to be slightly compressive away from edge, similar to the stress state in a peel test geometry. Furthermore, during the drying process of an initially swollen adhesive similar peel stresses can be generated at the edge.

4.7.2.2 Thermal and Hygroscopic Cycling of Adhesive Joints and Coatings

Thermal cycling can also dramatically reduce the lifetime of an adhesive bond. Humfeld and Dillard describe the mechanism for adhesive failure due to thermal cycling.[12] They propose that residual stresses are built up with each cycle until the available strain energy release rate is large enough to initiate debonding. Residual stress build up is caused by three factors: structural changes occurring at elevated temperature due to expansion of the adhesive, the accompanying increase in molecular mobility, and the relaxation of the resulting compressive stresses. The resulting structural changes in the adhesive are then frozen into the adhesive upon cooling. With each cycle, hey found structural changes cause the adhesive to shrink, leading to a build up of residual stresses.

Hygroscopic cycling or changing the content of absorbed moisture or other fluids can produce the same effect as temperature cycling.[12] This is because both increasing the temperature

and the fluid content of the adhesive are processes that cause an increase the volume of the adhesive and also increase frequency and amplitude of molecular motions in the polymer chains. Fluid desorption produces a similar effect as decreasing the temperature by reducing the adhesive volume and slowing down molecular motions. The effects of cycling and subsequent adhesive failure may be more dramatic if the temperature and fluid content are reduced simultaneously. Fluid absorption can also make the adhesive more susceptible to the deleterious effects of residual stress by changing the chemistry of the interface, by reducing the toughness of the interface, or by migration to the interface to form a weak boundary layer.

In addition to the changes in structure by temperature and hygroscopic cycling, physical aging can also induce harmful structural changes in adhesives. Physical aging is the phenomenon associated with conformational changes of the polymer chain backbone leading to a reduction in free volume and a change in structure that occurs below the glass transition temperature.[166] Physical aging can lead to adverse effects such as an increase in density and elastic modulus and a reduction in the impact strength, fracture toughness, and rate of creep and stress relaxation.

4.7.3 Experimental

4.7.3.1 Constant Frequency Interfacial Impedance Spectroscopy

The novel IIS sensors used in this study can measure the impedance or capacitance of mapped areas of the sensor defined with respect to the free edge of the coated sensor. Details of the technique and experimental set-up can be found in Section 4.3 and also in the International Journal of Adhesion and Adhesives.[131] The test frequency was 400 kHz in the work described in this section. Using the technique of constant frequency IIS and the novel sensor design we have measured the change in capacitance as a function of the distance from the edge of the sensor, x,

and number of exposure cycles and used this information to determine the number of cycles until adhesive failure. Using the same capacitance data, an apparent crack growth rate as a function of the number of exposure cycles was measured. Previously, this type of information has been traditionally obtained using more conventional fracture mechanics techniques.

4.7.3.2 Adhesive System and Fluid Environments

The adhesive that was used in these experiments was a proprietary commercial filled epoxy known as "L4" adhesive. The adhesive was supplied by Hewlett-Packard Co. Detail about the adhesive can be found in Section 3.4.3.1. The range of coating thickness was between 25 and 400 microns with a standard deviation ranging between 2 - 5 microns. Coatings were applied to the substrate using a pneumatically driven doctor blade. The fluids studied were distilled water, a basic solution of 0.1 M NaOH, an acidic solution of 1.0 M H_2SO_4, and two ink vehicles. The ink vehicles, supplied by Hewlett-Packard Co., are designated "Magenta" and "Cyan". Ink vehicles do not contain dye molecules and are therefore optically clear. A clear ink is advantageous for adhesive testing because the immersed test specimen can be visually inspected for any crack formation. In addition to water, ink and ink vehicles contain aggressive components such as surfactants, salts, alcohols, and other proprietary chemicals. These components may interact strongly to plasticize the adhesive[36] and to promote structural changes during hygroscopic cycling. Therefore, we can expect that the inks act more aggressively toward the adhesive than water.

Two different types of surfaces were used in this study. The first type of substrate was a high surface energy substrate (described previously in Section 4.3 and ref 131) consisting of a silicon oxide surface with gold electrode traces. The surface energy of silica is 287 mJ/m^2 and the surface energy of gold is 120 - 160 J/m^2.[167] The other substrate had a low surface energy

consisting mostly of silicon carbide and some silicon nitride. The surface free energy of silicon carbide is 35 – 60 J/m^2 [168]. The sensor was manufactured by taking the existing high surface energy substrate and depositing a 250 nm layer of silicon nitride followed by a 135 nm layer of silicon carbide. A schematic of the high and low surface energy substrate sensors are shown in Figure 4-35. To prepare the surface of the substrate, they were first rinsed with HPLC grade isopropyl alcohol and then blown dry with ultra-high purity nitrogen gas. The L4 adhesive was applied immediately thereafter, cured at 140°C for 30 minutes and cooled slowly (approximately 30 minutes) to room temperature. Coated sensors were stored in a dessicator (5% relative humidity) prior to testing.

4.7.3.3 Description of Environmental Cycles

The cycle used in this study can be divided into three stages:

Stage 1. 15 minute preheat in 60°C air followed by immersion in 60°C fluid environment for 24 hours.

Stage 2. Cooling from 60°C to room temperature in fluid environment (approximately 30 minutes).

Stage 3. Drying of the adhesive coating at 5% relative humidity for 24 hours.

In the initial stage the dry epoxy coated sensor is placed in the convection oven to equilibrate at 60°C for approximately 15 minutes. The adhesive coating is then immersed in the fluid environment at 60°C. During this initial stage, the capacitance is recorded as a function of exposure time. Exposure to the fluid environment is approximately 24 hours. It should be *emphasized* that the change in capacitance is measured only during the fluid exposure step (stage

1). In the second stage, the adhesive (still immersed in the fluid environment) is removed from the oven and allowed to cool off to room temperature (approximately 20°C). This step takes approximately 30 minutes, and eliminates any thermal shock to the adhesive coating which would accelerate the failure process. As pointed out by Humfield and Dillard, faster changes in temperature increase the rate of stress development and the magnitude of stress, and therefore reduce adhesive bond life.[12] In the third stage, the adhesive coating is dried in a dessicator (~ 5% relative humidity) for 24 hours. In this last stage, significant debonding is believed to take place.

4.7.3.4 Common Features of the Adhesive Debonding Measurements: Failure Criteria and Apparent Crack Length

4.7.3.4.1 Capacitance Changes Due to Fluid Absorption in an Undamaged Coating

Using the technique of constant frequency IIS and the novel impedance sensor design, data was obtained on the change in capacitance as a function of the distance from the edge of the sensor, x, and the number of exposure cycles. The absorbed volume of fluid at the sensor surface is proportional to the measured change in capacitance. In undamaged coatings the change in capacitance due to fluid absorption is roughly 1 pF (pico-Farad) for both the low and high surface energy sensors. The change in capacitance is the difference between the capacitance measured after 24 hours of fluid exposure and the initial dry capacitance (t = 0 hours). Figure 4-36 illustrates the change in capacitance as a function of exposure time typically observed during the initial cycle.

4.7.3.4.2 Capacitance Changes Due to Fluid Absorption in an Damaged Coating

In the event of adhesive debonding, a dramatic increase in capacitance is detected due to displacement of the adhesive from the substrate surface and an accumulation of fluid at the

sensor surface. For the epoxy adhesive and fluids studied, debonding occurs during the final stage of the cycle in the dessicator. Evidence for adhesive debonding during this drying process is obtained from the change in capacitance measured in the subsequent cycle as the coated sensor is immersed in the fluid environment. As an example, Figure 4-37 illustrates the dramatic change in capacitance for adhesive coatings that have debonded in the drying stage of the previous cycle.

Figure 4-37 shows that the capacitance continues to rise dramatically for up to several hours. This observation suggests that either further crack growth occurs in the fluid exposure step, or that this is simply a result of additional fluid diffusion. Nonetheless, the most significant damage is believed to have has occurred in the previous cycle.

For each cycle, the change in capacitance due to fluid absorption and/or debonding as a function of x can be determined from graphs similar to Figure 4-36 and Figure 4-37. The data from each cycle can then be plotted collectively as shown in Figure 4-38. The change in capacitance as a function of x and number of cycles for the Magenta ink vehicle is displayed in Figure 4-38. For clarity, the capacitance is plotted on a log scale Figure 4-38.

4.7.3.4.3 Values of the Change in Capacitance

The change in capacitance observed in a damaged coating is depends on several factors such as the concentration of fluid at the surface, the total area of debonding, the fluid chemistry, surface of the sensor (SiO_2/Au vs. SiC/SiN) and the specific pair of connection pads (or value of x) from which the measurement was made. These many factors, and others not discussed, significantly affect the capacitance measurements and make it difficult to obtain qualitative information about the actual concentration of fluid at the sensor surface. The change in capacitance due to the presence of fluid at a debonded region of the sensor surface can be as large as 1000 pF for the low surface energy (SiC/SiN) sensor. For the high surface energy (SiO/Au) sensor, with the

exception of a distilled water environment, the change in capacitance due to adhesive debonding is positive at low concentrations while at high concentration the change in capacitance is negative. Therefore adhesive coatings bonded to the high surface energy sensor exhibited a negative capacitance if complete coating debonding has occurred. This effect is due to the highly ionic nature of the non-water fluids which can cause a large change in the detected phase angle of the complex impedance.

4.7.3.4.4 The Minimum Change in Capacitance Suggesting Adhesive Failure; Apparent Crack Length

Using the novel impedance sensor design, the capacitance can be measured as a function of location from the edge of the bond, x. Because the change in capacitance is roughly proportional to the change in concentration of fluid at the surface, damaged regions of the adhesive also can be detected as a function of x. As expected, crack initiation always started at the free edge of the coated sensor (x = 0 mm) and crack growth was always in the direction toward the center of the sensor. If such a crack has advanced in the coated sensor from the edge, then it is expected that the change in capacitance will be large in the debonded regions and low in the bonded regions. For several reasons explained below, a change in capacitance exceeding a value of 10 pF is indicative of adhesive failure. Conversely, a change of less than 10 pF suggests that the adhesive coating is undamaged. Therefore, if the crack has advanced 1.33 mm, then for values of x less than or equal to 1.33 we expect a change in capacitance greater than 10 pF. For the inner section of the senor where x > 1.33 mm, we would observe a change in capacitance less than 10 pF.

4.7.3.4.5 Justification for the Failure Criteria

As suggested previously, a measured change in capacitance of 10 pF or greater is believed to indicate that significant debonding has occurred at that particular value of x. Also mentioned previously, the change in capacitance due to fluid absorption in an undamaged coating is roughly 1 pF. A value of 1 pF agrees well with rough estimates based on the rules of mixtures (Section 4.2.2) for an epoxy adhesive absorbing 1 - 2 wt% of fluid in the bulk. Based on the same calculation, a change of 10 pF corresponds to an epoxy adhesive absorbing 15 wt% of fluid. Assuming a typical number such that the adhesive absorbs roughly 2.5 wt% in fluid at equilibrium in the bulk, any amount exceeding this indicates a surplus of fluid most likely due to debonding and displacement of the adhesive by the fluid. Therefore, 10 pF and an absorption of 15 wt% of fluid is a conservative estimate of the change in capacitance indicating damage to the coating.

Utilizing a value greater than 10 pF also ensures that the change in capacitance is due to the presence of the fluid and not to other outside or uncontrollable sources of capacitance changes. The most prevalent source of noise is the unavoidable change in capacitance due to changing the contact pressure and position of the sensor within the fixture. The change due to this effect is roughly 2 – 4 pF.

Changes in capacitance less than 10 pF also appear to be reversible in some cases. Several examples were found where the capacitance changed by as much as 8 pF during a cycle, whereas on the subsequent cycle exhibited a change in capacitance of only 1 – 2 pF. In addition, samples that have exhibited a change in capacitance greater than 10 pF were visually inspected - it was confirmed that these adhesive coatings had areas of debonding.

4.7.3.4.6 Defining an Apparent Crack

The measured crack length is "apparent" because the capacitance measurements are a global average of the damage to the sensor. Crack formation may not be entirely symmetric around the edge of the sensor and debonding may have occurred at capacitance changes less than (or greater than) 10 pF. In many cases the crack growth was observed visually to be non-uniform. In addition, the change in capacitance can vary due to variation in the concentration of fluid at the surface and the total area of debonding, as well as differences in fluid chemistry and the specific pair of pads from which the measurement was taken. Hence an apparent crack is detected while its location has some uncertainty.

4.7.3.4.7 Cycles Until Failure

Assessment of the degree of damage to the adhesive incurred from the drying process is made during the subsequent cycle. Therefore when referring to the number of cycles until failure, the specific reference is to the number of cycles until failure is *observed* or detected by the change in capacitance.

4.7.4 Results and Discussion

4.7.4.1 Effect of Water

The graph of the number of cycles until failure as a function of coating thickness for both the low and high surface energy sensors is shown in Figure 4-39. For the purpose of discussion, specimens have been categorized based on the thickness of the coating: 1) less than 50 microns, 2) between 50 – 150 microns and 3) greater than 150 microns. The number of samples tested is listed in Table 4-2. The number of cycles until failure in Figure 4-37 has been categorized

according to the coating thickness and shown in Table 4-3. Coatings adhered to both substrate chemical types and less than 50 microns and did not exhibit any crack initiation or growth for as many as 20 cycles. For samples with a thickness in the range of 50 – 150 microns, the number of cycles until failure was 11.3 +/- 2.1, identical for both substrate surface chemistries. For samples with a thickness greater than 150 microns, the number of cycles until failure was 4.0 +/- 1.0 and 4.7 +/- 1.5 for the high and low surface energy substrates, respectively. These results support the idea that decreasing the thickness of the coating improves adhesive durability by reducing the crack driving energy attributable to residual stresses.

Table 4-2 The number of samples tested as a function of coating thickness and sensor surface chemistry. The fluid environment is water.

Coating Thickness (microns)	*SiO/Au Surface*	*SiC/SiN Surface*
< 50	2	2
50 - 150	3	3
> 150	3	3

Table 4-3 The number of cycles until failure as a function of coating thickness and substrate surface chemistry. The fluid environment is water. The average and a single standard deviation are listed.

Coating Thickness (microns)	*SiO/Au Surface*	*SiC/SiN Surface*
< 50	Greater than 20	Greater than 20
50 - 150	11.3 +/- 2.1	11.3 +/- 2.1
> 150	4.0 +/- 1.0	4.7 +/- 1.5

The numbers of cycles until failure of both the low and high surface energy sensors were similar. This is not surprising, given that adhesion for both surfaces can be attributed to forces resulting from secondary bonds (hydrogen-bonds, van der Waal's, etc.). Therefore, both substrates may be subject to similar adhesive failure mechanisms. For samples less than 50 microns, the build up of residual stresses was not enough to increase the available strain energy to cause debonding despite the degradation of the interface that may have occurred. This behavior is in sharp contrast to samples with a coating thickness greater than 50 microns which failed catastrophically. To be clear, catastrophic failure is defined by the initiation and formation of a crack 2.2 mm in length, the maximum detectable value of x (obtained from the innermost pair of contact pads). Failure is presumably attributable to residual stress build up increasing the available strain energy such that it exceeds the interfacial toughness. The catastrophic adhesive failure is also different than what is observed for other environmental fluids where crack initiated occurred at the sensor edge and crack growth occurred over a period of many cycles in the direction of the center of the sample.

For water at 60°C, the respective time to saturation as a function of coating thickness is shown in Table 4-4. The time to saturation (99.9%) was calculated from Equation 4-18[130,169] and a diffusion coefficient of 1.3 x 10^{-8} cm^2/s.[36]

Equation 4-18

$$t_{sat} = \frac{0.67 \cdot 4L^2}{D}$$

Where L is the coating thickness and D is the diffusion coefficient. The results listed in Table 4-4 show that the 50 micron coatings are saturated within a few hours. Coatings approximately 250 microns in thickness are not saturated on the first cycle. Saturation may or may not occur on a subsequent cycle(s) if the fluid begins to accumulate in the adhesive. The time to saturation for the other fluids has not been measured. However, similar diffusion coefficients are expected because the major component of each fluid is water.

Table 4-4 The time to saturation as a function of coating thickness for the L4 adhesive at 60°C water.

Coating Thickness (microns)	*Time To Saturation (hours)*
50	1.5
100	5.5
150	12
200	22
250	34
300	49

4.7.4.2 Effect of 0.1 M Sulfuric Acid

The number of cycles until failure as a function of coating thickness and sensor surface chemistry for the 60°C 0.1 M sulfuric acid environment is shown in Figure 4-40. The number of samples tested is listed in Table 4-5. The average number of cycles until failure as function of coating thickness and surface chemistry are listed in Table 4-6. As expected, the acidic environment is more aggressive than the distilled water environment. Again, no difference in the number of cycles until failure between the low and high surface energy sensors was observable. The dependence of the durability on coating thickness was also less pronounced than for the specimens exposed to water.

In contrast to samples exposed to the water environment, adhesive failure for the acidic samples was not catastrophic. For samples with a range of coating thickness less than 50 microns, the graphs of the apparent crack length as a function of the number of exposure cycles are shown in Figure 4-41 and Figure 4-42, for the low and high energy surfaces, respectively. In each case, 2 cycles are required to initiate crack growth that begins from the free edge of the sensor. Once the crack growth has been initiated, the crack grows at a rate of 1.1 mm/cycle and 0.8 +/- 0.4 mm/cycle for the low and high surface energy sensors, respectively.

Table 4-5 The number of samples tested as a function of coating thickness and sensor surface chemistry. The fluid environment is 0.1 M sulfuric acid.

Coating Thickness (microns)	*SiO/Au Surface*	*SiC/SiN Surface*
< 50	2	2
50 - 150	2	3
> 150	2	2

Table 4-6 The number of cycles until failure as a function of coating thickness and substrate surface chemistry for the 0.1 M sulfuric acid environment. The average and a single standard deviation are shown.

Coating Thickness (microns)	*SiO/Au Surface*	*SiC/SiN Surface*
< 50	5.0 +/- 1.4	4.0 +/- 0.0
50 - 150	2.5 +/- 0.7	2.3 +/- 0.6
> 150	2.5 +/- 0.7	2.0 +/- 0.0

4.7.4.3 Effect of 1.0 M NaOH

The number of cycles until failure as a function of coating thickness and surface chemistry for the 60°C 1.0 M NaOH environment is shown in Figure 4-43. The number of samples tested for each coating thickness range and surface was two. These results show that for the entire range of

coating thicknesses, the adhesive coating fails catastrophically after only 2 cycles. This is clearly the most aggressive of the five tested fluids. No difference between the low and high surface energy sensors was observable. The aggressiveness of the fluid may be attributable to hydrolysis of the epoxy-substrate bond near the interface, or to an actual etching of the substrate.

All adhesive coatings, independent of the thickness, failed catastrophically after the drying stage of the first cycle. In contrast to the other fluid environments, reducing the thickness below 50 microns does not reduce the energy available for crack growth to extend the life of the adhesive coating in the NaOH environment. The adhesive coatings greater than 250 microns which are predicted to not saturate (see Table 4-4) also fail catastrophically after the drying stage of the first cycle. This suggests that the adhesive does not need to be saturated for the interface to be degraded substantially. This is consistent with the idea that concentration in the adhesive only needs to exceed a critical concentration to degrade the interface. An additional mechanism for adhesive failure that would not require the adhesive to be saturated could be due to degradation of the adhesive at the edge of the specimen. At the edge of the specimen, the diffusion path is short and the concentration of fluid is high. At the edge, the bulk adhesive and interface can be degraded enough to cause crack initiation. Once the crack is initiated, the adhesive can fail catastrophically if the residual stress and the coating thickness are large enough. An alternative and less substantiated is that the fluid diffuses rapidly at the interface into the adhesive joint and degrades the adhesive joint much faster than expected.

4.7.4.4 Effect of Cyan Ink Vehicle

The number of cycles until failure as a function of coating thickness and surface chemistry for the 60°C Cyan ink vehicle environment is shown in Figure 4-44. The number of samples tested is shown in Table 4-7. The average number of cycles until failure as function of coating

thickness and surface chemistry are listed in Table 4-8. For adhesive coatings greater than 50 microns, catastrophic failure occurs after only 2 cycles. No difference between the low and high surface energy sensors was observable. These results show that by reducing the coating thickness below 50 microns, the lifetime of the adhesive joint may be extended beyond two cycles. Furthermore, these results also suggest that Cyan is more aggressive than either water or acid, but not as aggressive as the basic solution. For the Cyan ink vehicle, adhesive failure was not catastrophic. The graphs of the apparent crack length as a function of the number of exposure cycles are shown in Figure 4-45 and Figure 4-46 for both the low and high energy surface substrates respectively. The crack growth rate determined from IIS is 0.9 +/- 0.3 mm/cycle and 1.0 +/- 0.2 mm/cycle for the low and high surface energy substrates, respectively.

Table 4-7 The number of samples tested for the range of coating thickness for each surface chemistry.

Coating Thickness (microns)	*SiO/Au Surface*	*SiC/SiN Surface*
< 50	4	4
50 - 150	4	3
> 150	2	2

Table 4-8 The number of cycles until failure as a function of coating thickness and substrate surface chemistry for the Cyan ink vehicle environment. The average and a single standard deviation are shown.

Coating Thickness (microns)	*SiO/Au Surface*	*SiC/SiN Surface*
< 50	3.5 +/- 0.6	3.5 +/- 0.6
50 - 150	2.0 +/- 0.0	2.0 +/- 0.0
> 150	2.0 +/- 0.7	2.0 +/- 0.0

4.7.4.5 Effect of Magenta Ink Vehicle

The number of cycles until failure as a function of coating thickness and surface chemistry for the 60°C Magenta ink vehicle environment is shown in Figure 4-47. The number of samples tested as function of coating thickness and surface chemistry is shown in Table 4-9. The average number of cycles until failure as function of coating thickness and surface chemistry are listed in Table 4-10. Coatings of 50 microns or less tend to be more durable than coatings with a greater thickness. Thin coatings (< 50 microns) bonded to the low energy SiC/SiN surface had a greater durability than the high energy SiO/Au surface. The Magenta ink vehicle is the only fluid where differences between the two surface chemistries were observed; however, these differences are observed only for coatings less than 50 micron. The low surface energy sensor appears more durable than the high surface energy sensor. This phenomenon may be fundamentally similar to the increase in adhesion energy for two low energy surfaces (like the epoxy and substrate) in the presence of high surface energy fluid like water. The graphs of the apparent crack length as a

function of the number of exposure cycles are shown in Figure 4-48 and Figure 4-49 for the low and high energy surface chemistries, respectively. The rate of apparent crack growth determined by IIS was 0.4 +/- 0.1 and 1.0 +/- 0.2 mm/cycle for the low and high surface energy surface substrate respectively.

Table 4-9 The number of samples tested as a function of coating thickness and surface chemistry. The fluid environment is Magenta ink vehicle.

Coating Thickness (microns)	*SiO/Au Surface*	*SiC/SiN Surface*
< 50	3	3
50 - 150	3	2
> 150	2	3

Table 4-10 The number of cycles until failure as a function of coating thickness and substrate surface chemistry for the Magenta ink vehicle environment. The average and a single standard deviation are shown.

Coating Thickness (microns)	*SiO/Au Surface*	*SiC/SiN Surface*
< 50	3.3 +/- 0.6	6.33 +/- 0.6
50 - 150	2.0 +/- 0.0	2.0 +/- 0.0
> 150	2.0 +/- 0.0	2.0 +/- 0.0

These results suggest that the Cyan ink vehicle is more aggressive than the Magenta ink vehicle. This result is in contrast to what was observed by H. Singh and D. A. Dillard (personal communication). They found that chinook magenta was more aggressive than cyan 1 using sub-critical fracture test methods. The discrepancy between the two findings may be attributable to the different failure mechanisms in the two cases. In our IIS experiments, adhesive failure is a function of the degradation of the interfacial toughness by exposure to the fluid and also the rate of residual stress development and magnitude of residual stress, processes which are tied closely to the nature of the fluid absorption and desorption. Specifically, the extent of swelling and shrinkage due to the diffusion of the fluid and plasticization can effect residual stress development. Furthermore, the diffusivity, solubility, vapor pressure of the ink vehicle and each ink vehicle component effect residual stress development and also the degradation of the interface. Clearly, the adhesive failure mechanism by hygroscopic cycling is not simple. In contrast, adhesive fracture testing does not typically subject the adhesive specimen to cyclic exposure to fluids. In this case, as with Singh and Dillard's work, the adhesive failure mechanism is not complicated by the desorption behavior of the fluid. In addition, the wedge test used by Singh and Dillard is not sensitive to residual stresses. Therefore it is safe to expect that each test is exploring a different failure mechanism and that the results may not agree. We observed that the Cyan has a higher vapor pressure than the Magenta. The higher vapor pressure may lead to faster and more fluid desorption than the lower vapor pressure counterpart. This may lead to larger residual stresses and faster adhesive failure.

4.7.5 Summary

The technique of interfacial impedance spectroscopy has been used to investigate the effects of hygroscopic cycling on a commercial filled epoxy adhesive. The change in capacitance as a

function of x was measured to study adhesive durability as a function of coating thickness, fluid environment, and surface chemistry.

Several observations are put forth as a result of the experiments.

1. The durability of the adhesive coatings is improved by reducing the adhesive coating thickness, presumably due to a reduction in the available energy for crack growth from residual stress.

2. Experimental evidence supports the general observation that adhesive cracks tend to initiate at free edges. Furthermore, crack initiation occurred in the drying stage of cyclic environmental swelling and drying.

3. Constant frequency impedance spectroscopy and a novel senor design were successfully used to determine the number of cycles until failure and the rate of apparent crack length growth as a function of the number of exposure cycles.

4.7.6 Figures

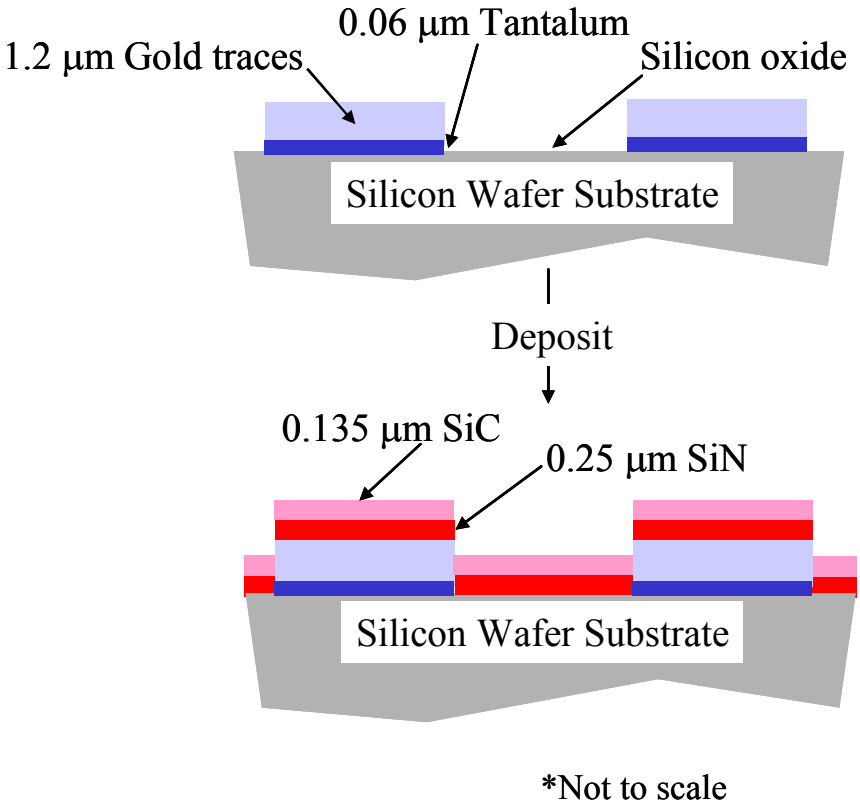

Figure 4-35 Schematic (not to scale) of the high surface energy substrate (shown in top) and the low surface energy substrate (shown in bottom)

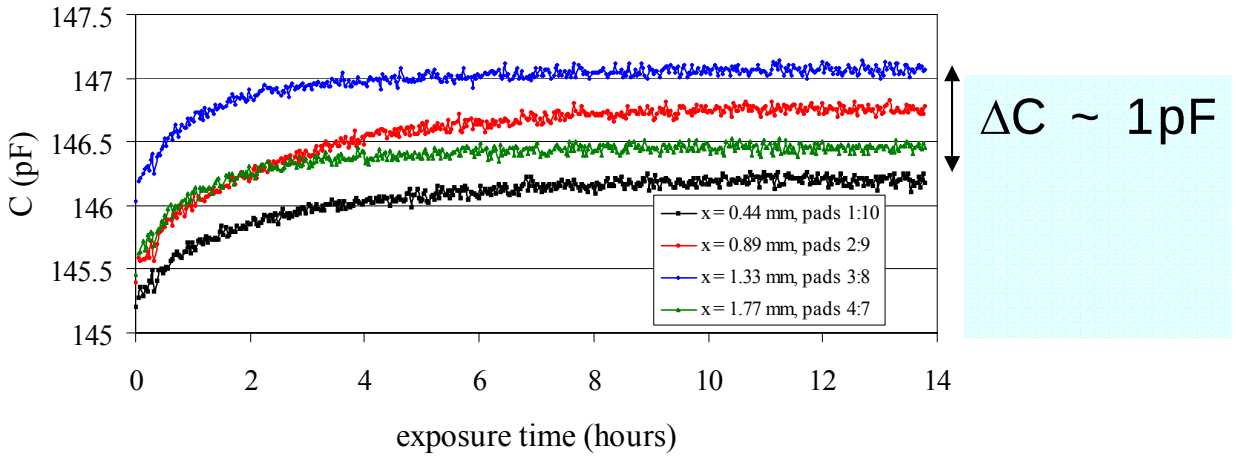

Figure 4-36 Change in capacitance as a function of exposure time for different values of *x*. This data was obtained from the first cycle and illustrates a change in capacitance of approximately 1 pF, attributable to fluid absorption.

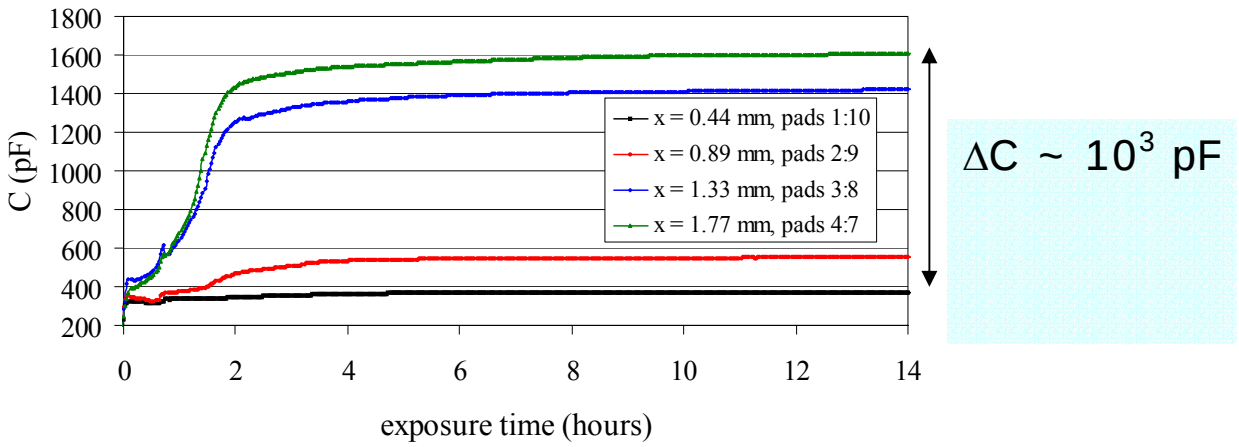

Figure 4-37 Change in capacitance as a function of exposure time for different values of *x*. This data was obtained from the second cycle and illustrates a change in capacitance of approximately 1000 pF, attributable to fluid absorption at debonded areas of the sensor.

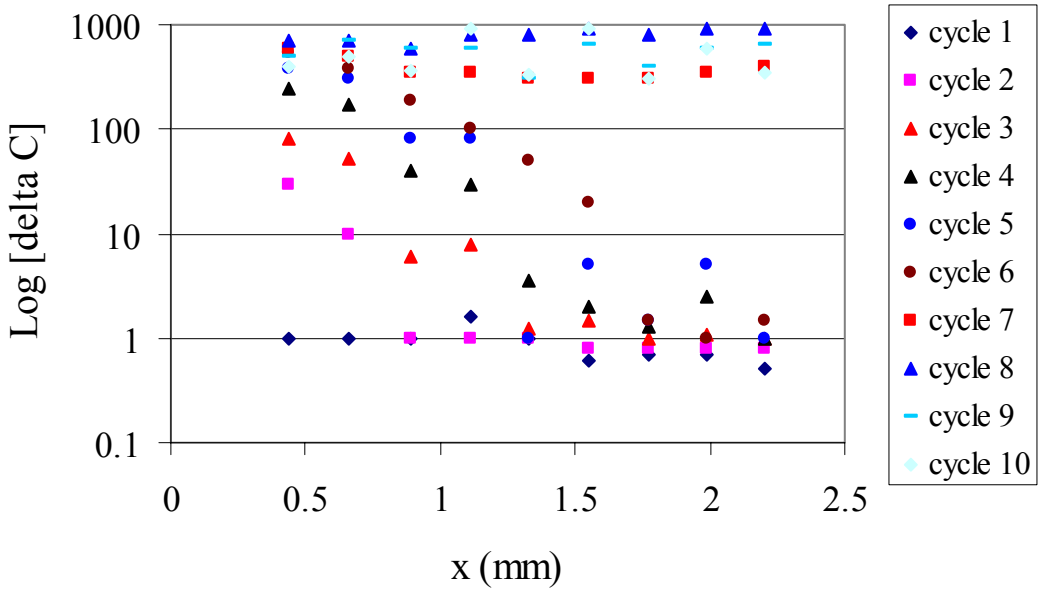

Figure 4-38 The change in capacitance due to fluid absorption plotted on a log scale as a function of the distance from the edge of the sensor, *x*, for different exposure cycles. This for a 30 micron coating exposed to the Magenta ink vehicle.

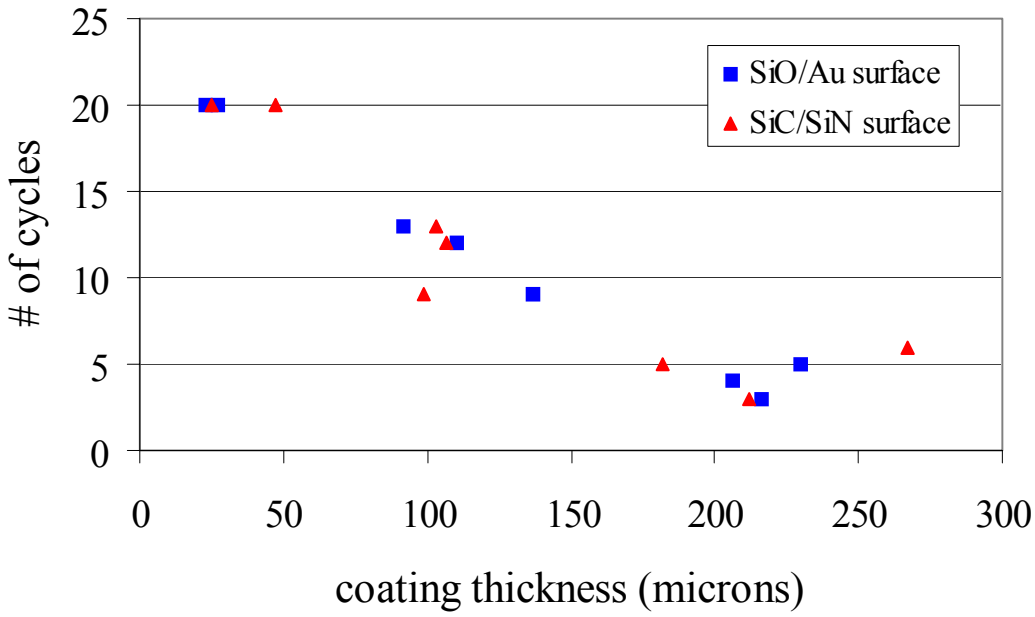

Figure 4-39 The number of cycles until failure as a function of coating thickness for the 60°C distilled water environment.

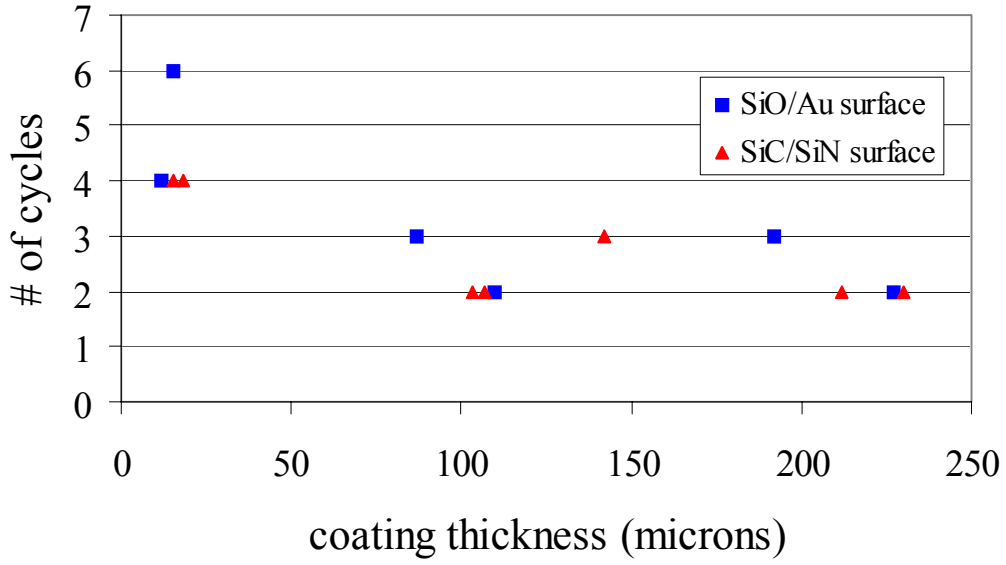

Figure 4-40 The number of cycle until failure as a function of coating thickness for the 60°C 1 M sulfuric acid environment.

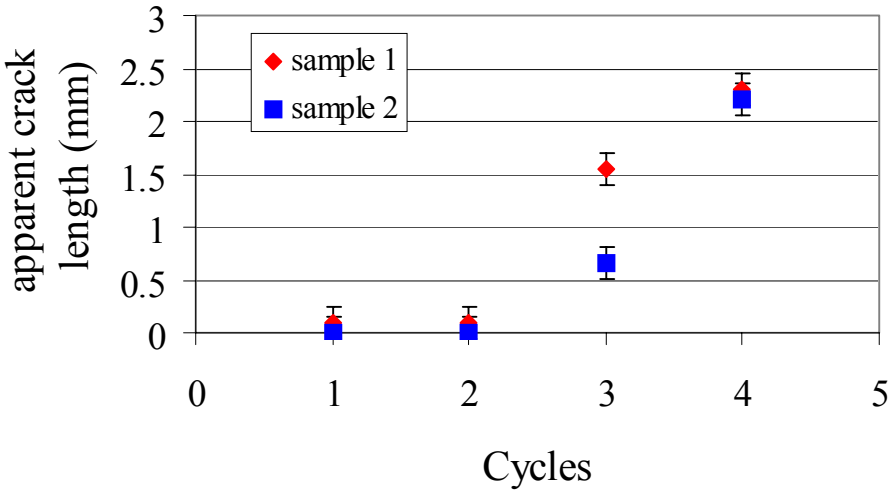

Figure 4-41 The apparent crack length (mm) as a function of exposure cycles. This for coatings less than 50 microns bonded to the silcon carbide surface and exposed to the sulfuric acid solution.

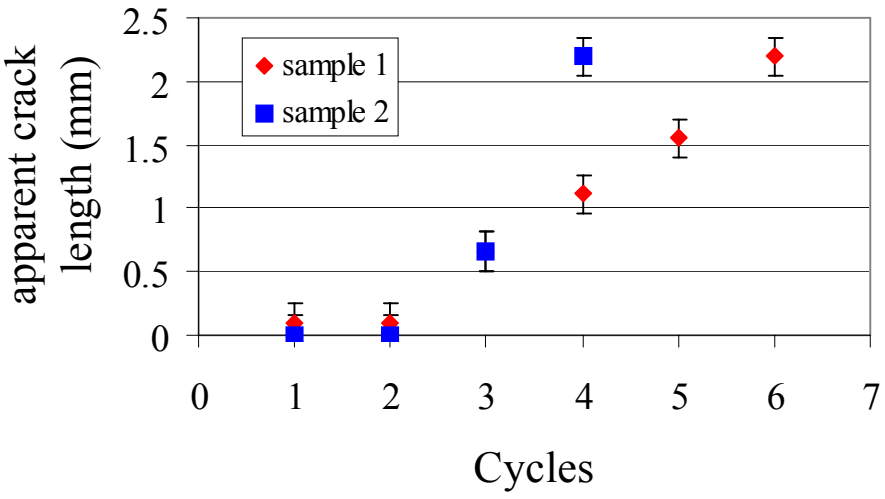

Figure 4-42 The apparent crack length (mm) as a function of exposure cycles. This for coatings less than 50 microns bonded to the silcon oxide and gold surface and exposed to the sulfuric acid solution.

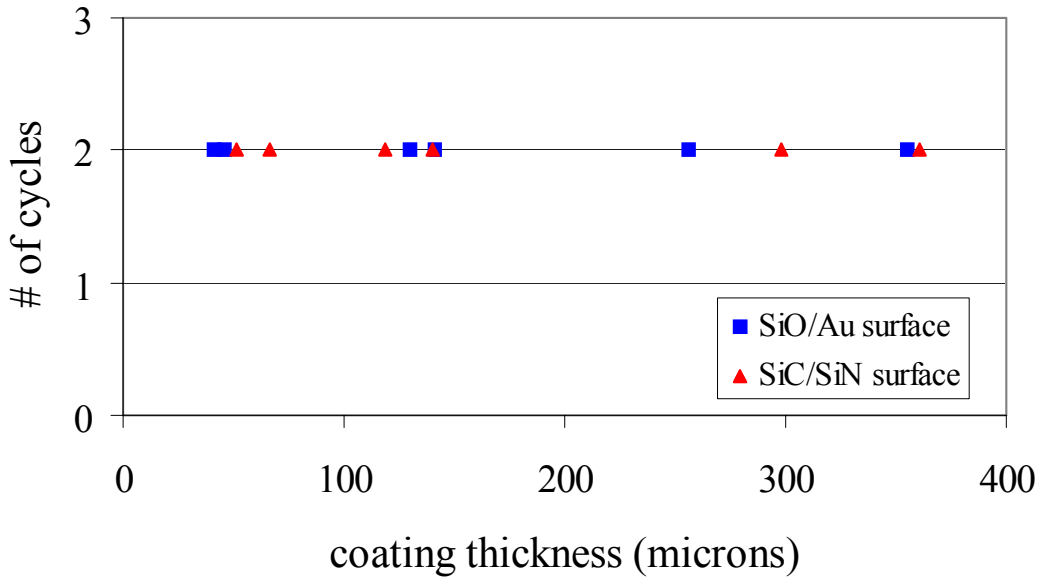

Figure 4-43 The number of cycle until failure as a function of coating thickness for the 60°C 0.1 M NaOH environment.

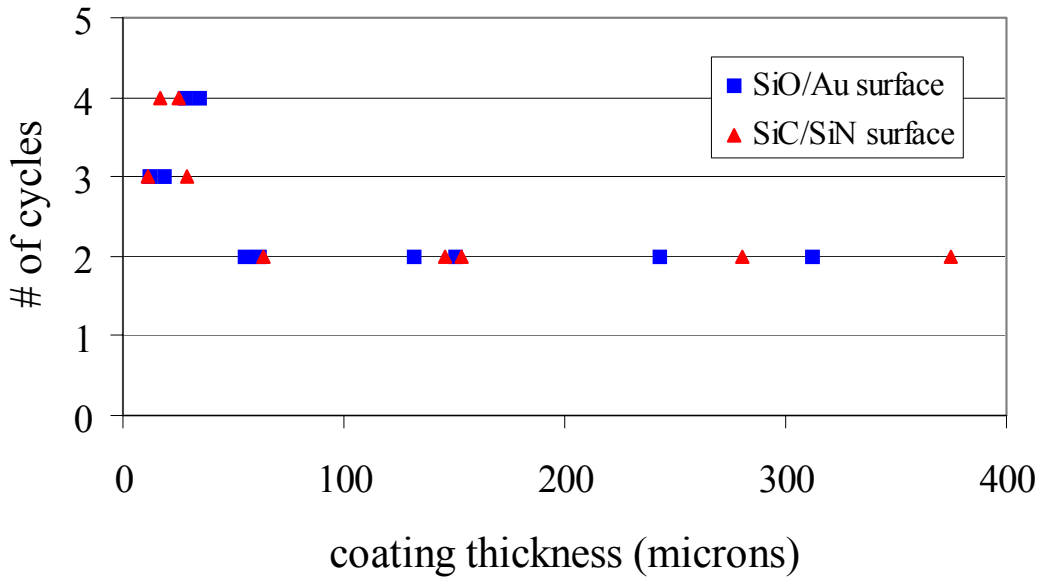

Figure 4-44 The number of cycle until failure as a function of coating thickness for the 60°C Cyan ink vehicle environment.

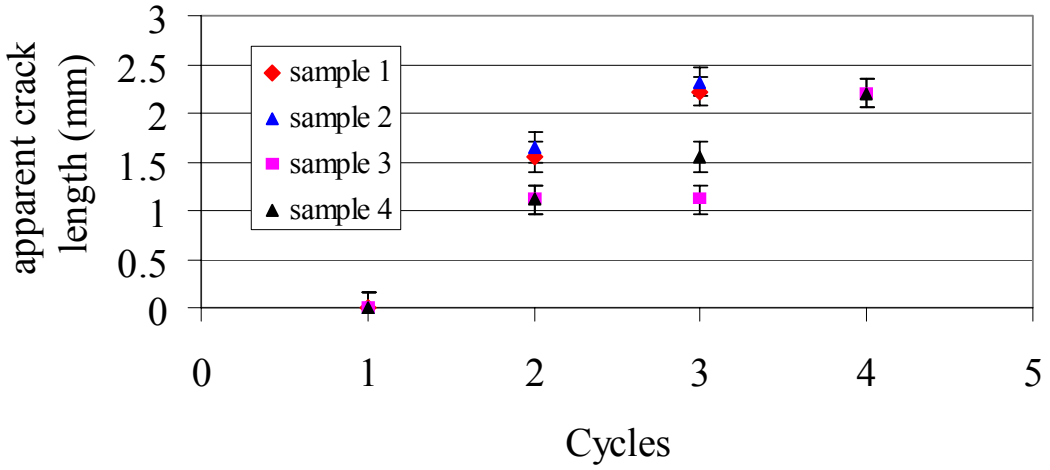

Figure 4-45 The apparent crack length (mm) as a function of exposure cycles. This for coatings less than 50 microns bonded to the silcon carbide surface and exposed to the Cyan ink vehicle.

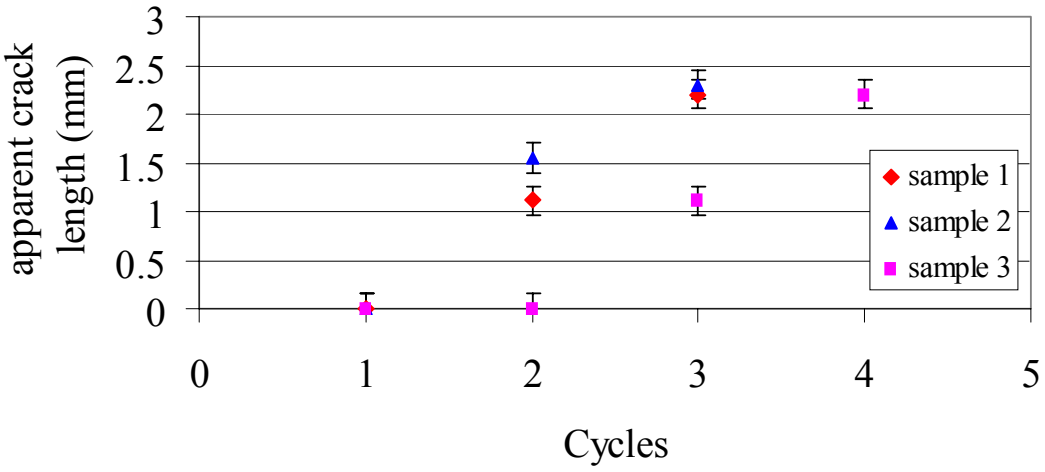

Figure 4-46 The apparent crack length (mm) as a function of exposure cycles. This for coatings less than 50 microns bonded to the silcon oxide and gold surface and exposed to the Cyan ink vehicle.

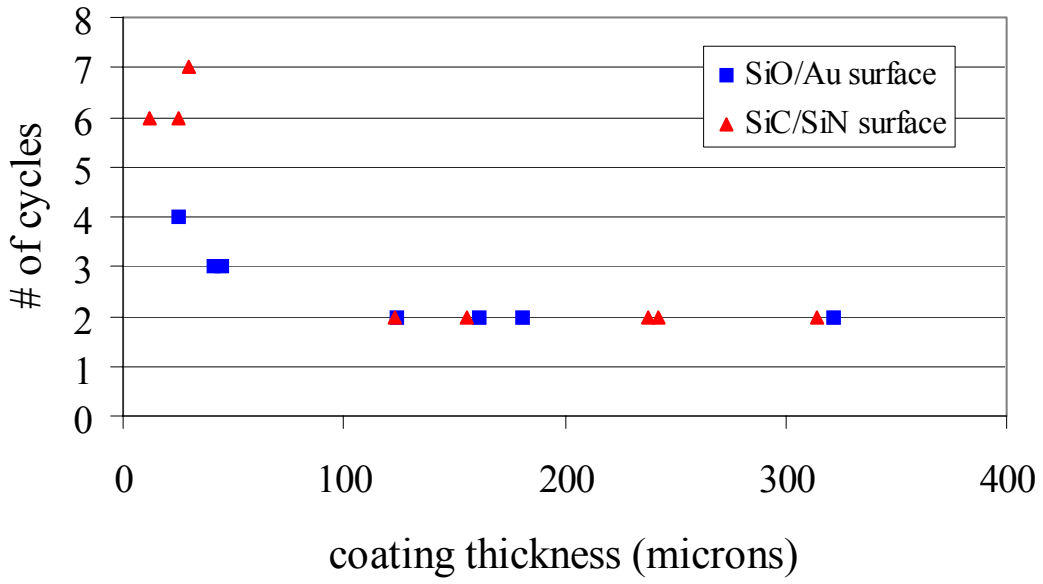

Figure 4-47 The number of cycle until failure as a function of coating thickness for the 60°C Magenta ink vehicle environment.

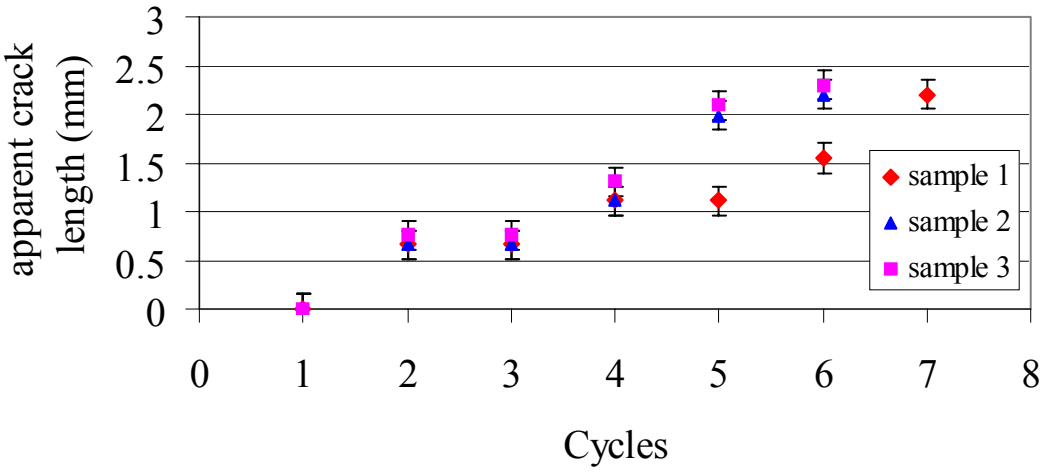

Figure 4-48 The apparent crack length (mm) as a function of exposure cycles. This for coatings less than 50 microns bonded to the silcon carbide surface and exposed to the Magenta ink vehicle.

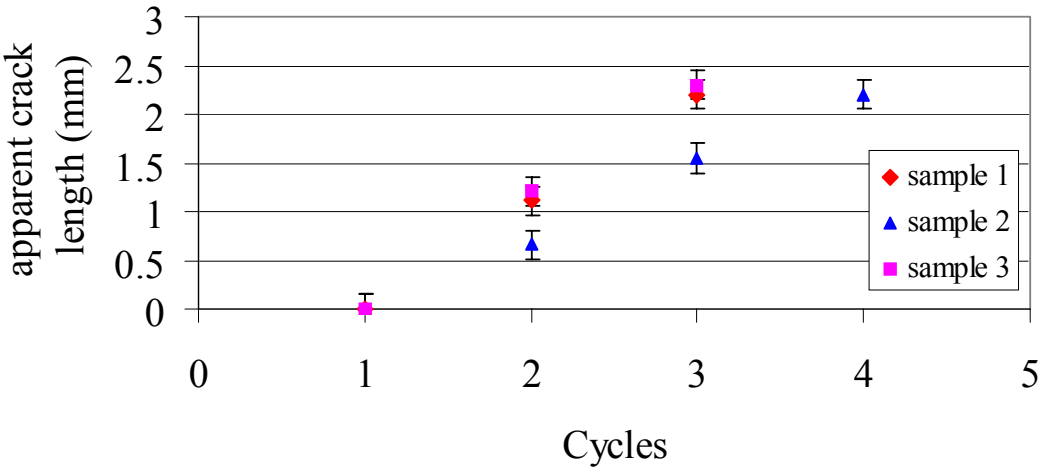

Figure 4-49 The apparent crack length (mm) as a function of exposure cycles. This for coatings less than 50 microns bonded to the silcon oxide and gold surface and exposed to the Magenta ink vehicle.

4.8 Recommendations and Modifications for Constant Frequency Interfacial Impedance Spectroscopy

4.8.1 Abstract

Modifications are recommended to achieve the full potential of the novel sensor design for interfacial impedance spectroscopy and in the experimental set-up for the study of diffusion in adhesive joints. In addition, some experimental details are discussed for any future investigators.

4.8.2 Sources of Signal Noise

There are many sources of noise in the experiment. The most prevalent and serious is the constant change in temperature of the experimental equipment outside the oven. To a lesser extent, the activity of persons and other instruments in the room is also a source. The noise in the capacitance signal was found to closely follow changes in the temperature. The activity of the room also followed the temperature fluctuations and therefore can not be ruled out as a possible source of error. Most importantly, opening and closing the oven door should be avoided. The first recommendation would be to reduce temperature changes by containing the switch box, impedance analyzer, and oven in a controlled temperature environment.

4.8.3 Recommended Modifications

The twisted cables of the connectors should be replaced with shielded coaxial cables. This should significantly reduce any noise in the data as well as reduce the difference in the initial capacitance among the different pairs of contact pads.

Several modifications to the sensor design are recommended to improve the sensitivity of the instrument. The modifications are based on the work of Senturia and Garverick who designed

an interdigitated impedance sensor with built-in amplification that is sensitive at frequencies as low as 1 Hz. In addition, they utilize a second or reference transistor so that the response of the sensor to background effects that are not of interest can be cancelled out. In the literature, they refer to the technique as "microdielectrometry". A detailed description of the sensor which includes the circuit diagrams can be found in ref 170, 171, and 172.[170,171,172] This microdielectrometry device was utilized to study the cure of two epoxy systems[173] and as a humidity sensor.[174]

The ability to test a large number of specimens without monopolizing the instrument for one would be an ideal situation. This could be accomplished by conditioning the samples in a separate environment and then periodically removing the samples for testing. A reproducible signal would be a prerequisite. One obstacle to creating a reproducible signal is creating a virtual identical low resistance, reproducible contact between the fixture and sensor contact pads. A new contact device could be fabricated which would likely involve a clamp or pressure contact and would move away from the spring set-up in the current fixtures.

The basic sensor geometry could be modified in several ways. To increase the capacitance, the conductive traces could be made longer and the space between the traces could be reduced. An example in the literature has the conductive traces as small as 8 microns wide with an 8 micron spacing.[174] In addition, the region in the center of the sensor where no traces are present should be eliminated. This region effectively increases the diffusion path length by a factor of two and substantially increases the time to saturation by a factor of four.

The available frequency range of the instrument is limited and spans only over 3 decades, ranging from a minimum of 75 kHz to a maximum of 10 MHz. The choice of the test frequency is based on two factors. As the frequency is decreased, the impedance signal becomes more

sensitive to water and the baseline quality is reduced. Equation 4-19 illustrates how the frequency is related to the capacitance and resistance:

Equation 4-19

$$C = \frac{\Delta I}{\Delta E f 2\pi}$$

where ΔI is the complex sinusoidal current measurement, ΔE is the complex sinusoidal voltage (usually the input signal),and f is the applied frequency. This relation suggests as the frequency is decreased the instrument sensitivity (the ratio of the output signal to input signal) must increase proportionally.[142]

A wide range of frequencies would provide quantitative information into the underlying mechanism of diffusion and fluids at the interface of adhesive joints. Unlike the qualitative information yielded by constant frequency testing, multi-frequency impedance spectroscopy can be used to distinguish absorbed water and condensed water, as well as other phenomena. To obtain this information, an equivalent circuit model is used to fit the impedance data as a function of frequency data.[139]

5 CONCLUDING REMARKS

The durability of adhesive joints was characterized using the shaft-loaded blister test and a novel impedance sensor design. The SLBT was demonstrated to be a simple and convenient method for characterizing the environmental degradation of adhesive bonds. The traditional SLBT was adapted to constant-load sub-critical fracture testing. The plateau velocity and threshold value of G were shown to be not solely controlled by bulk diffusion of fluids into the adhesive. The capability of the sensor was demonstrated by measuring the diffusion the diffusion of acetone parallel to the bondline into a PSA tape.

Diffusion of moisture into durable adhesives can not be quantified due to the limited sensitivity of the current experimental set-up. The technique of IIS was demonstrated to be sensitive to the interfacial toughness of UV curable pressure sensitive adhesives. Moreover, this sensor was shown to be an invaluable tool in quantifying the effects of hygroscopic cycling and was used to measure the rate of apparent crack growth in adhesive coatings.

This research has provided additional evidence of the harmful effects of moisture, temperature, hydroscopic cycling and has provided the adhesives industry two new and useful test methods for adhesive evaluation.

6 REFERENCES:

(1) Kinloch, A. J. *Adhesion and Adhesives: Science and Technology*; Chapman and Hall: New York, 1987.
(2) Dickstein, P. A.; Spelt, J. K.; Sinclair, A. N.; Bushlin, Y. *Materials Evaluation* **1991**, 1498-1515.
(3) Nguyen, T.; Byrd, E.; Bentz, D. *Journal of Adhesion* **1995**, *48*, 169-194.
(4) Bowden, F. P.; Throssell, W. R. *Nature* **1957**, *167*, 601.
(5) Kinloch, A. J. *Journal of Adhesion* **1979**, *10*, 193-219.
(6) Weitsman, Y. J. *Mechanics of Time Dependent Materials* **2000**, *4*, 107-126.
(7) Reboa, P. F., Personal Communication
(8) Kook, S. Y.; Dauskardt, R. H. *Journal of Applied Physics* **2002**, *91*, 1293-1303.
(9) Piens, M.; DeDeurwaerder, H. *Progress in Organic Coatings* **2001**, *43*, 18-24.
(10) Clyne, T. W. *Key Engineering Materials* **1996**, *116-117*, 307-330.
(11) Sato, K. *Progress in Organic Coatings* **1980**, *8*, 143-160.
(12) Humfeld Jr, G. R.; Dillard, D. A. *Journal of Adhesion* **1998**, *65*, 277-306.
(13) Sung, N. H.
(14) McBreirty, V. J.; Keely, C. M.; Coyle, F. M.; H., X.; K., V. J. *Faraday Discussions* **1996**, *103*, 255-268.
(15) Antoon, M. K.; Koenig, J. L. *Journal of Polymer Science: Polymer Physics Ed* **1981**, *19*, 197-212.
(16) Apicella, A.; Nicolais, L.; Astarita, G.; Orioli, E. *Polymer* **1979**, *20*, 1143-1148.
(17) Diamant, Y.; Marom, G.; Broutman, L. J. *Journal of Applied Polymer Science* **1981**, *26*, 3015-3025.
(18) Leidheiser, H.; Funke, W. *Journal of Oil Colour Chemists' Association* **1987**, *5*.
(19) Gao, J.; Weitsman, Y. J. *University of Tennesse Report MAES 98-4.0-CM* **1998**.
(20) Davis, G. D.; Krebs, L. A.; Drzal, L. T.; Rich, M. J.; Askeland, P. *Journal of Adhesion* **2000**, *72*, 335-358.
(21) Funke, W.; Haagen, H. *Ind. Eng. Chem.Prod. Res. Dev.* **1978**, *17*, 50.
(22) Linnossier, I.; Gaillard, F.; Romand, M.; Nguyen, T. *Journal of Adhesion* **1999**, *70*, 221-239.
(23) Takahashi, K. M.; Sullivan, T. M. *J. Appl. Phys.* **1989**, *66*, 3192.
(24) Takahashi, K. M. *J. Appl. Phys.* **1990**, *67*, 3419.
(25) Wu, W. L.; Orts, W. J.; Majkrzak, J.; Hunston, D. L. *Polymer Science and Engineering* **1995**, *35*, 1000-1004.
(26) Kent, M. S.; Smith, G. S.; Baker, S. M.; Nyitray, A.; Browning, J.; Moore, G.; Hua, D., W. *Journal of Materials Science* **1996**, *31*, 927-937.
(27) Kent, M. S.; McNamara, W. F.; Fein, D. B.; Domier, L. A.; Wong, A. P. Y. *Journal of Adhesion* **1999**, *69*, 121-138.
(28) Kent, M. S.; McNamara, W. F.; Baca, P. M.; Wright, W.; Domier, L. A.; Wong, A. P. Y.; Wu, W. L. *Journal of Adhesion* **1999**, *69*, 139-163.
(29) Kinsella, E. M.; Mayne, J. E. O. *Br. Polym.* **1969**, *1*, 173.
(30) Mayne, J. E. O.; Scantlebury, J. D. *Br. Polym.* **1970**, *2*, 240.
(31) Lekatou, A.; Qian, Y.; Faidi, S. E.; Lyon, S. B.; Islam, N.; Newman, R. C. *Proc. Materials Research Soc. Symp.* **1993**, *12*, 1263.

(32) Cuthrell, R. E. *Journal of Applied Polymer Science* **1968**, *12*, 1263.
(33) Maxwell, I. D.; Pethrick, R. A. *Journal of Applied Polymer Science* **1983**, *28*, 2363.
(34) Kong, E. S. W. *Proc. Org. Coat. Appl. Polym. Sci.* **1983**, *48*, 727.
(35) Funke, W.; Zorll, U.; Murphy, B. G. K. *J. Paint Technol.* **1969**, *41*, 210.
(36) Case, S. L.; Ward, T. C. In *Department of Chemistry*; Virginia Polytechnic and State University: Blacksburg, VA, 2003.
(37) Tu, Y.; Spelt, J. K. *Journal of Adhesion* **2000**, *72*, 359-372.
(38) Funke, W. *Progress in Organic Coatings* **1981**, *9*, 29.
(39) Kittelberger, W. W.; Elm, A. C. *Ind. Eng. Chem.Prod. Res. Dev.* **1946**, *38*, 695.
(40) Perera, D. Y.; Heertjes, P. M. *Journal of Oil Colour Chemists' Association* **1971**, *54*, 546.
(41) vanderMeer-Lerk, L. A.; Heertjes, P. M. *Journal of Oil Colour Chemists' Association* **1975**, *58*, 79.
(42) Pleudemann, E. P. *Silanes*; Plenum Press, 1982.
(43) Whittle, B. R.; Whittle, J. D.; Ellis, B.; Hand, R. J.; Short, R. D. *Journal of Adhesion* **2001**, *77*, 1-24.
(44) Shreiber, H. P., 2001, Chemical Engineering Department, Ecole Polytechnique, Montreal, Canada
(45) Crank, J. J. *The Mathematics of Diffusion*; Clarendon Press: Oxford, 1956.
(46) Shen, C. H.; Springer, G. S. *J. Composite Materials* **1976**, *10*, 2-20.
(47) McKnight, S. H.; Gillespie, J. W. J. *Journal of Applied Polymer Science* **1997**, *64*, 1971-1985.
(48) Berens, A. R.; Hopfenberg, H. B. *Polymer* **1978**, *19*, 489.
(49) McBrierty, V. J.; Martin, S. J.; Karasz, F. E. *Journal of molecular liquids* **1999**, *80*, 179-205.
(50) Long, F. A.; Richman, D. *Journal of the American Chemical Society* **1960**, *82*, 513.
(51) Tsotsis, T. K.; Weitsman, Y. *Journal of Materials Science Letters* **1994**, *13*, 1635-1636.
(52) Crank, J. *The Mathematics of Diffusion*; Oxford University Press: Oxford, 1975.
(53) Zanni-Deffarges, M. P.; Shanahan, M. E. R. *International Journal of Adhesion and Adhesives* **1995**, *15*, 137-142.
(54) Nyugen, T.; Byrd, E.; Bentz, D.; Lin, C. *Progress in Organic Coatings* **1996**, *27*, 181.
(55) Vine, K.; Cawley, P.; Kinloch, A. J. *Journal of Adhesion* **2001**, *77*, 125-161.
(56) Vanlandingham, M. R.; Eduljee, R. F.; Gillespie, J. W. J. *Journal of Applied Polymer Science* **1999**, *71*, 787-798.
(57) Wind, M. M.; Lenderink, H. J. W. *Prog. Org. Coat.* **1996**, *28*, 239-250.
(58) Lefebvre, D. R.; Dillard, D. A.; Ward, T. C. *Journal of Adhesion* **1989**, *27*, 1-18.
(59) Soles, C. L.; Yee, A. F. *Journal of Polymer Science, Part B: Polymer Physics* **2000**, *38*, 792-802.
(60) McBrierty, V. J.; Martin, S. J.; Karasz, F. E. *Journal of Molecular Liquids* **1999**, *80*, 179-205.
(61) Banks, L.; Ellis, B. *Polymer Bulletin* **1979**, *1*, 377-382.
(62) Jelinski, L. W.; Dumais, J. J.; Cholli, A. L.; Ellis, T. S.; Karasz, F. E. *Macromolecules* **1985**, *18*, 1091-1095.
(63) Luo, S.; Leisen, J.; Wong, C. P. *Journal of Applied Polymer Science* **2002**, *85*, 1-8.
(64) O'Brien, E. P.; Ward, T. C.; Guo, S.; Dillard, D. A. *Journal of Adhesion* **2003**, *79*, 69-97.
(65) Lai, Y. H.; Dillard, D. A. *Journal of Adhesion Science and Technology* **1994**, *8*, 663-678.
(66) Kim, J.; Kim, K. S.; Kim, Y. H. *J. Adhesion Sci. Technol.* **1989**, *3*, 175-187.

(67) Kendall, K. *J. of Physics D* **1971**, *4*, 1186-1195.
(68) Thouless, M. D.; Jensen, H. M. *J. Adhesion* **1992**, *38*, 185-197.
(69) Gent, A. N.; Kaang, S. J. *Journal of Adhesion* **1987**, *24*, 173-181.
(70) Gent, A. N.; Hamed, G. R. *Journal of Applied Polymer Science* **1977**, *21*, 2817-2831.
(71) Kinloch, A. J.; Lau, C. C.; Williams, J. G. *International Journal of Fracture* **1994**, *66*, 45-70.
(72) Moidu, A. K.; Sinclair, A. N.; Spelt, J. K. *Journal of Testing and Evaluation* **1995**, *23*, 241-253.
(73) Moidu, A. K.; Sinclair, A. N.; Spelt, J. K. *Journal of Testing and Evaluation* **1998**, *26*, 247-254.
(74) Gent, A. N.; Kaang, S. J. *Appl. Polym. Sci.* **1986**, *32*, 4689-4700.
(75) Wan, K. T. *Journal of Adhesion* **1999**, *70*, 197-207.
(76) Dannenburg, H. *J. Appl. Polym. Sci.* **1961**, *5*, 125-134.
(77) Williams, M. L. *J. Adhesion* **1972**, *4*, 307.
(78) Gent, A. N.; Lewandowski, L. H. *J. Appl. Polym. Sci.* **1987**, *33*, 1597.
(79) Lai, Y. H.; Dillard, D. A. *J. Adhesion Sci. Technol.* **1994**, *8*, 663-678.
(80) Napolitano, J.; Chudnovsky, A.; Moet, A., J. *J. Adhesion Sci. Technol.* **1988**, *2*.
(81) Chang, Y. S.; Lai, Y. H.; Dillard, D. A. *J. Adhesion* **1989**, *27*, 197-211.
(82) Allen, M. G.; Senturia, S. D. *J. Adhesion* **1988**, *25*, 303-315.
(83) Allen, M. G.; Senturia, S. D. **1989**, *29*, 219-231.
(84) Dillard, D. A.; Bao, Y. *J. Adhesion* **1991**, *63*, 253-271.
(85) Wan, K. T.; Breach, C. D., J. Adhesion, 66, 183-202 (1998). *J. Adhesion* **1998**, *66*, 183-202.
(86) Wan, K. T. *Int. J. Adhesion & Adhesives* **2000**, *20*, 141-143.
(87) Tsunou, C.; Sproat, E. A.; Lai, Y. H.; Shephard, N. E.; Dillard, D. A. *J. Adhesion* **1997**, *60*, 153-162.
(88) Moidu, A. K.; Sinclair, A. N.; Spelt, J. K. *J. Adhesion* **1998**, *65*, 239-257.
(89) Malyshev, B. M.; Salganik, R. L. *Int. J. of Fracture Mechanics* **1965**, *1*, 114-128.
(90) Wan, K. T.; Mai, Y. W. *Int. J. of Fracture Mechanics* **1995**, *74*, 181-197.
(91) Wan, K. T.; DiPrima, A.; Ye, L.; Mai, Y. W. *J. of Matl. Sci.* **1996**, *31*, 2109-2116.
(92) Wan, K. T. *J. Adhesion* **1999**, *70*, 209-219.
(93) Wan, K. T.; Liao, K. *Thin Solid Films* **1999**, *352*, 167-172.
(94) Liao, K.; Wan, K. T. *Journal of Composite Technology and Research* **2001**, *23*, 15-20.
(95) Blackman, B.; Dear, J. P.; Kinloch, A. J.; Osiyemi, S., J. Mater. Sci. Lett.,10, 253 (1991). *J. Mater. Sci. Lett.* **1991**, *10*, 253.
(96) Pocius, A. V. *Adhesion and Adhesives Technology*; Hanser/Gardner Publications, Inc.: Cincinnati, 1997.
(97) Kinloch, A. J. *Adhesion and Adhesives: Science and Technology*; Chapman and Hall: New York, 1987.
(98) Park, T.; Dillard, D. A.; Ward, T. C. *J. Polym. Sci. Part B-Polym. Phys.* **2000**, *38*, 3222-3229.
(99) Chaudhury, M. K.; Whitesides, G. M., Langmuir, 7, 1013-1025 (1991). *Langmuir* **1991**, *7*, 1013-1025.
(100) Adamson, A. W.; John Wiley and Sons, Inc.: New York), pp 41 (1990), 1990; p 41.
(101) Herr, D. E.; Nikolic, N. A.; Schultz, R. A. *High Performance Polymers* **2001**, *13*, 79-100.

(102) Lefebvre, D. R.; Elliker, P. R.; Takahashi, K. M.; Raju, V. R. *Journal of Adhesion Science Technology* **2000**, *14*, 925-937.
(103) Gledhill, R. A.; Kinloch, A. J.; Shaw, S. J. *Journal of Adhesion* **1980**, *11*, 3-15.
(104) Walker, P. *Off. Dig.* **1965**, 1561.
(105) Brewis, D. M.; Comyn, J.; Cope, B. C.; Maloney, A. C. *Polymer* **1980**, *21*, 1477.
(106) Cognard, J. *International Journal of Adhesion and Adhesives* **1988**, *8*, 93.
(107) Kawasaki, T.; Motoie, K.; Kamata, H.; Miura, T.; Arakita, Y. *Journal of the Society of Materials Science (Japan)* **1990**, *39*, 1292.
(108) Brewis, D. M.; Comyn, J.; Raval, A. K.; Kinloch, A. J. *International Journal of Adhesion and Adhesives* **1990**, *10*, 247-253.
(109) Lefebvre, D. R.; Takahashi, K. M.; Muller, A. J.; Raju, V. R. *Journal of Adhesion Science Technology* **1991**, *5*, 201-227.
(110) Bowditch, M. R.; Hiscock, D.; Moth, D. A. *International Journal of Adhesion and Adhesives* **1992**, *12*, 164.
(111) Cognard, J. *Journal of Adhesion* **1994**, *47*, 83.
(112) Malyshev, B. M.; Salganik, R. L. *International Journal of Fracture Mechanics* **1965**, *1*, 114-128.
(113) Wan, K. T.; DiPrima, A.; Ye, L.; Mai, Y. W. *Journal of Materials Science* **1996**, *31*, 2109-2116.
(114) Wan, K. T. *Journal of Adhesion* **1999**, *70*, 209-219.
(115) Henderson, S. L.; Ward, T. C. *Journal of Adhesion* **2003**, *79*, TBA.
(116) Weast, R. C.; Astle, M. J., Eds. *CRC Handbook of Chemistry and Physics*, 60th ed.; CRC Press Inc.: Boca Raton, 1980.
(117) Eichstadt, A. E. In *Material Science and Engineering*; Virginia Tech: Blacksburg, 2002.
(118) Gurumurthy, C. K.; Kramer, E. J.; Hui, C. Y. *International Journal of Fracture* **2001**, *109*, 1-28.
(119) Weiderhorn, S. M.; Fuller Jr, E. R.; Thomson, R. *Met. Sci.* **1980**, *14*, 450-458.
(120) Lawn, B. R. *J. Mats. Sci.* **1975**, *18*, 469-480.
(121) Lane, M. W.; Snodgrass, J. M.; Dauskardt, R. H. *Microelectronics Reliability* **2001**, *41*, 1615-1624.
(122) Curley, A. J.; Jethwa, J. K.; Kinloch, A. J.; Taylor, A. C. *Journal of Adhesion* **1998**, *66*, 39-59.
(123) Ritter, J. E.; Huseinovic, A. *Journal of Electronic Packaging* **2001**, *123*, 401-404.
(124) Lane, M. W.; Snodgrass, J. M.; Dauskardt, R. H. *Microelectronics Reliability* **2001**, *41*, 1615-1624.
(125) Thouless, M. D.; Jensen, H. M. *Journal of Adhesion Science and Technology* **1994**, *8*, 579-589.
(126) J. W. Hutchinson, Z. S. *Advances in Applied Mechanics* **1992**, *29*, 63-191.
(127) Wan, K. T.; Guo, S.; Dillard, D. A. *Thin Solid Films* **2003**, *425*, 150-162.
(128) Wiederhorn, S. M. *Journal of the American Ceramics Society* **1967**, *50*, 407.
(129) Gurumurthy, C. K.; Kramer, E. J.; Hui, C. Y. *International Journal of Fracture* **2001**, *109*, 1-28.
(130) Shen, C. H.; Springer, G. S. *Journal of Composite Materials* **1976**, *10*, 2-20.
(131) O'Brien, E. P.; Reboa, P. F.; Field, M.; Pullen, D.; Markel, D.; Ward, T. C. *International Journal of Adhesion and Adhesives* **2003**, *23*, 335-338.
(132) Hedvig, P. *Dielectric Spectroscopy of Polymers*; John Wiley and Sons: New York, 1977.

(133) McCrum, N. G.; Read, B. E.; Williams, G. *Anelastic and Dielectric Effects in Polymeric Solids*; John Wiley and Sons: New York, 1967.
(134) D'Amore, A.; Kenny, J. M.; Nicolais, L.; Tucci, V. *Polymer Engineering Science* **1990**, *30*, 314.
(135) Senturia, S. D.; Sheppard, N. F. *Advances in Polymer Science* **1986**, *80*, 1.
(136) Day, D. R.; Shepard, D. D.; Craven, K. J. *Polymer Engineering and Science* **1992**, *32*, 524-528.
(137) Nairn, B. J.; Dickstein, P. A.; Plausinis, D. J.; Spelt, J. K. *J. Adhesion* **1995**, *48*, 121-136.
(138) Affrossman, S.; Banks, W. M.; Hayward, D.; Pethrick, R. A. *Proc. Instn. Mech. Engrs. Part C* **2000**, *214*, 87-102.
(139) Rammelt, U.; Reinhard, G. *Progress in Organic Coatings* **1992**, *21*, 205-226.
(140) Company, H., 5950-3000 ed.; Hewlett-Packard Company: USA, 1994.
(141) Rammelt, U.; Reinhard, G. *Progress in Organic Coatings* **1992**, *21*, 205-226.
(142) Murray, J. N. *Progress in Organic Coatings* **1997**, *31*, 255-264.
(143) VanWesting, E. P. M.; Ferrari, G. M.; Wit, J. H. W. D. *Corrosion Science* **1994**, *36*, 957-977.
(144) Sekine, I. *Progress in Organic Coatings* **1997**, *31*, 73-80.
(145) Brasher, D. M.; Kingsbury, A. H. *Journal of Applied Chemistry* **1954**, *4*, 62.
(146) Aldrich, P. D.; Thurow, S. K.; McKennon, M. J.; Lyssy, M. E. *Polymer* **1987**, *28*, 2289.
(147) Pathmanathan, K.; Johari, G. P. *Polymer* **1988**, *29*, 303.
(148) Fodor, J.; Hill, D. A. *Macromolecules* **1992**, *25*, 3511-3520.
(149) Amiruden, A.; Thierry, D. *Progress in Organic Coatings* **1995**, *26*, 1-28.
(150) McIntyre, J. M.; Pham, H. Q. *Progress in Organic Coatings* **1996**, *27*, 201-207.
(151) vanderWel, G. K.; Adan, O. C. G. *Prog. Org. Coat.* **1999**, *37*, 1-14.
(152) Vine, K.; Cawley, P.; Kinloch, A. J. *Journal of Adhesion* **2001**, *77*, 125-161.
(153) Nguyen, T.; Byrd, E.; Bentz, D.; Lin, C. *Progress in Organic Coatings* **1996**, *27*, 181.
(154) AbdelWahab, M. M.; Crocombe, A. D.; Beevers, A.; Ebtehaj, K. *International Journal of Adhesion and Adhesives* **2002**, *22*, 61-73.
(155) Hulden, M.; Hansen, C. M. *Progress in Organic Coatings* **1985**, *13*, 171-194.
(156) Lefebvre, D. R.; Dillard, D. A. *Journal of Adhesion* **1999**, *70*, 119-138.
(157) Lefebvre, D. R.; Dillard, D. A.; Dillard, J. G. *Journal of Adhesion* **1999**, *70*, 139-154.
(158) Francis, L. F.; McCormick, A. V.; Vaessen, D. M.; Payne, J. A. *Journal of Materials Science* **2002**, *37*, 4717-4731.
(159) Parera, D. Y. *Progress in Organic Coatings* **1996**, *28*, 21-23.
(160) Funke, W.; Negele, O. *Progress in Organic Coatings* **1996**, *28*, 285-289.
(161) Perera, D. Y.; Eynde, D. V. *Journal of Coatings Technology* **1987**, *59*, 55-63.
(162) Dillard, D. A., 2001.
(163) T. Park, D. A. D. **to be published**.
(164) Yaniv; Ishai. *Polymer Engineering and Science* **1987**, *27*.
(165) Weitsman, Y. *J. Composite Materials* **1977**, *11*, 378.
(166) Cowie, J. M.; Harris, G. S.; McEwan, I. *Journal of Polymer Science, Polymer Physics* **1997**, *35*, 1107.
(167) Kinloch, A. J. In *Adhesion and Adhesives: Science and Technology*; Chapman and Hall: New York, 1987; pp 26-34.
(168) Emig, G.; Popovska, N.; Edie, D. D.; Rhee, B. *Carbon* **1995**, *33*, 779-782.

(169) Springer, G. S., Ed. *Environmental Effects on Composite Materials*; Technomic Publishing Company: Westport, 1981.
(170) Senturia, S. D.; Garverick, S. L.: United States Patent # 4,423,371, 1983.
(171) Garverick, S. L.; Senturia, S. D. *IEEE Transaction on Electron Devices* **1982**, *ED-29*, 90-94.
(172) Sheppard, N. F.; Day, D. R.; Lee, H. L.; Senturia, S. D. *Sensors and Actuators* **1982**, *2*, 263-274.
(173) Senturia, S. D.; Sheppard, N. F. J.; Lee, H. L.; Day, D. R. *Journal of Adhesion* **1982**, *15*, 69-90.
(174) Jachowicz, R. S.; Senturia, S. D. *Sensors and Actuators* **1981/82**, *2*, 171-186.

Vita

Emmett O'Brien was born, but was not raised, in Beirut, Lebanon in 1971. He is an American. He is trying to get a job at NIST through the University of Connecticut, but is experiencing a quagmire of red tape and dropped balls. Today he learned an important life lesson: Do not trust an expert, unless you are sure that he or she is indeed an expert. He is also very busy at the time of this writing.